THE DESIGN AND DEVELOPMENT OF FAST PULSED POWER SUPPLIES USING TRANSMISSION LINE TRANSFORMERS

Colin Richard Wilson

A Thesis Submitted for the Degree of PhD
at the
University of St Andrews

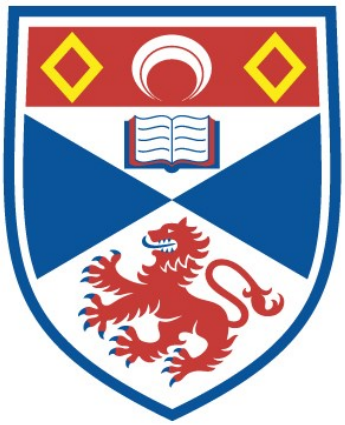

1992

Ph.D Thesis

The Design and Development of Fast Pulsed Power Supplies Using Transmission Line Transformers.

by Colin Wilson.

University of St Andrews, Fife, Scotland , KY16 9SS.

ProQuest LLC.
789 East Eisenhower Parkway
P.O. Box 1346
Ann Arbor, MI 48106 – 1346

Declarations

I, Colin Richard Wilson, hereby certify that this thesis has been composed by myself, that it is a record of my own work, and that it has not been accepted in partial or complete fulfilment of any other degree or professional qualification.

Signed : .. ..

I hereby certify that the candidate has fulfilled the conditions of the Resolution and Regulations appropriate to the Degree of PhD.

Signed : .....

Acknowledgments.

I would like to acknowledge my co-workers, Andy Brown and Andy Erickson for their contribution to the work presented in chapters 3 and 5. I also wish to thank my supervisor Paul Smith for his support and guidance during this work.

Abstract.

This thesis is concerned with the development of Transmission Line Transfomer (TLT) pulsed power supplies and the generation of fast risetime (>50ns), good quality, high repetition-rate voltage pulses for flash x-ray preionisors and other applications. It explains the principle of the TLT and reports on two TLT pulsed power supplies that have been built. The first, or prototype, produced output voltage pulses with risetimes of 50ns and durations of 200ns and was used to power a flash x-ray preionisation source for a mercury bromide laser. The second, a 50kV, 100Ω device, was built as part of a wider research program concerned with the development of space based pulsed power supplies. The development of ceramic tile technology is also described and the relevant electrical, mechanical and thermal properties of some barium titanate tiles given; it is then shown how ceramic tiles can be used to construct compact pulse generators for TLT systems. Finally, the subject of nonlinear dielectric pulse sharpening is introduced and pulse sharpening in a delay line ladder network containing air-core inductors and non-linear capacitors is demonstrated. It is then explained how these lines can be used to improve the output risetime of a TLT.

CONTENTS

INTRODUCTION.

The subject of pulsed power technology (PPT)[1] is a relatively new field of study concerned with the generation and application of fast risetime, short duration electrical pulses of high energy. Its origins probably date back to the early insulation test studies of the 1920s and the development of the high voltage impulse generator such as that reported by Marx[2] in 1924. The original circuit, and the subsequent improvements made to it by Goodlet,[3] Miner[4] (1926) and Peek[5] (1929), appear in Marx's book[6] on HV generating techniques published in 1941 and the review article on impulse generator design by Bouwers[7]. It is from these techniques that the subject of pulsed power can be said to have evolved.

This evolution appears to have been hastened when the second world war* produced a competitive climate to research. This resulted in the rapid development of radar[8,9], the Randell and Boot cavity magnetron oscillator[10], the hydrogen thyratron, the Blumlein[11] circuit, the lumped element Pulse Forming Network (PFN) and new magnetic materials. By 1945, radar modulators were available that could operate at duty ratios of 0.002 and output power levels of 1MW (the Model 9 Pulsar)[12].

---

* See "Pulse Generators", Glasoe and Lebacqz. Dover Publications Inc. New York. (1948).

Immediately after the war pulsed power progressed hand-in-hand with the development of radar. The 1950 Hydrogen Thyratron Tube Conference[13,14] which was established to address the problems associated with the design and development hydrogen thyratrons for radar modulators, provides evidence of this. During the 1950s the applications area of this conference began to occupy an increasingly large proportion of the proceedings and by 1956[15] the term modulator was included in the conference title. It was perhaps during this period that pulsed power began to emerge as a separate field of study.

The next notable development occurred in the early 1960s when J.C. Martin (Aldermaston, UK) designed a new generation of e-beam machine that could produce currents of hundreds of kiloamps and electron energies of many MeV[16-19]. These generators, which utilised fast pulse forming networks, transmission line techniques and non-incandescent (cold) cathodes, quickly became "tools of the trade" in many areas of scientific research, including flash x-ray generation[20], radiography[21], plasma physics[22], microwave generation[23], particle accelerators. They also enabled multigigawatt $C0_2$[24,25,26] lasers to be built and the first excimer laser to be realised[27-33]. These lasers were studied in great depth during the 1970s and as a result the design of the associated hardware became an important application areas for pulsed power*. For example, at the 12th Modulator Symposium Conference[34] approximately 35% of the papers were dedicated towards developing burst mode switches for $C0_2$ lasers.

---

* See "Pulsed Power for Lasers" 1988 and 1989. Proc IEEE. SPIE Conference Proc. Anaheim. Ca. USA.

In the same year the "International Pulse Power Conference" (IPPC)[35] was established. This has provided an additional platform for the presentation and discussion of new and innovative ideas and the conference proceedings a useful record of the trends in research that have occurred since 1976; these proceedings show that pulsed power is now a technology that is fundamental to many areas of science and industry. Pulsed high power gas discharge lasers are, for example, used extensively for material processing, lithography, cutting, drilling, welding and photochemical processes[36]. In the medical profession they are revolutionising the treatment of many illnesses[37] and are making possible new surgical techniques including corneal sculpting, laser angioplasty, photoradiative therapy (PRT) and cosmetic surgery; they are also providing improved diagnostic techniques for the identification of diseased tissue[38]. In the manufacturing industry pulsed power is needed to provide radiation to sterilise certain foods and the increasing reliance on space based technology has created a demand for pulsed power supplies that are compact, lightweight and extremely reliable[39,40,41]. At the high peak power end of the field, Inertial Confinement Fusion (ICF) continues to require large scale pulsed power systems to generate short pulse, high power laser or light ion beams to heat and compress a Deuterium-Tritium fuel pellet to the required densities and temperatures. The Nova[42] ICF facility at Lawrence Livermore National Labs, for example, is a Nd:Yag solid state laser that consists of a 58 MJ capacitor bank and produces over 100TW of laser power at 1.065μm. The Aurora[43] KrF laser at Los Alamos, which is e-beam pumped and driven by two pulse charged water filled pulse forming lines, can produce a current density of $20A/cm^2$ in a laser cavity of dimensions 1m x 1m x 2m and output energies of 10kJ at 248nm. Also notable is the PBFA[44] light ion accelerator in Sandia National Labs; this is a 4 MV 3.5MJ machine capable of

producing peak power levels of 100TW, a figure that is illustrative of the state of the art of peak pulsed power generation.

Looking further ahead, it seems probable that PPT will continue to play a fundamental role in many areas of scientific research throughout the next decade. As a result, there is a need for the pulsed power scientist to maintain the current momentum in the field by developing improved pulsed power systems that can operate at higher performance levels. In an effort to meet some of these demands, and from an analysis of present day pulsed power requirements, it has become apparent that there is a need for an efficient, fast*, type of pulsed power supply that can produce nanosecond pulse risetimes at voltage levels of hundreds of kV. This thesis is concerned with developing these power supplies. Its 7 chapters cover the following subject matter :-

Chapter 1 :- This chapter examines one application area of pulsed power, namely, x-ray preionisation. It reviews x-ray preionisation sources, discusses their electrical requirements and highlights the short comings of their pulsed power supplies. This illustrates the need for a type HV generator that can produce fast risetime, high quality voltage pulses at kilohertz repetition-rates.

Chapter 2 :- This chapter introduces the transmission line transformer (TLT) voltage generator. It describes a number of TLT circuit designs and shows

* The terms "fast" and "slow" are a reference to the bandwidth of the system. In this thesis, fast refers to risetimes less that 50ns.

that a TLT can often improve upon the performance of these conventional forms of HV generation.

Chapter 3 :- This brings together the subject matter covered in the previous two chapters by describing a 100kV TLT based pulsed power supply that was used to drive a flash x-ray generator and preionise a mercury bromide laser. An assessment of the pulsed power supply is also provided.

Chapter 4 :- This chapter describes an investigation that developed compact distributed ceramic tile transmission lines to replace water PFLs and PFNs in TLT pulse generators.

Chapter 5 :- Here a ceramic tile Blumlein circuit is described as well as a second 150kV TLT generator.

Chapter 6 :- This examines how the risetime of the output pulse from a TLT can be improved using a pulse sharpening circuit. A number of these circuits are described and a new development, the non-linear dielectric line introduced.

Chapter 7 :- This is a conclusion and summary. It provides a brief resume of the work and discusses a number of other interesting circuits; it also highlights a number of specific areas that may be worthy of further investigation.

References.

1). T.A.Weil ; "Looking Back, Looking Forward", Proc. Power Modulator Symposium, Seattle, (1986).

2). E.Marx; "Versuuche uber Prufung von Isolatorem mit Spannungsstossen", Electrotech. Z., **45**, p 652 (1925).

3). B.L. Goodlet ; British Patent No. 344 862.

4). D.F. Miner ; "Surge Generating Equipment", Electric Journal, No.**23**, p596, (1926).

5). F.W. Peek ; "Dielectric Phenomenon in HV Engineering", p 145, Mc-Graw-Hill Book Co., New York. (1922).

6). E. Marx ; "Hochspannungspraktikum", Julius Springer, Berlin. (1941).

7). A. Bouwer ; "Elektrishe Hochspannungen", Julius Springer, Berlin. (1941).

8). Mermill I. Skonik ; "Introduction to Radar Systems", Mc Graw-Hill, (1980).

9). G.J.Sonnenberg ; "Radar and Electronic Navigation", London, (1970).

10). A.A.H. Boot and J.T. Randell ; "The Cavity Magnetron", J. Inst. Electr. Engin., Vol. 93, pt 111A, pp 928-958, (1946).

11). Blumlein. A.D ; British Patent No. 589 127, October (1947).

12). Glasoe and Lebacqz; "Pulse Generators", Ch.5, New York Dover Publications Inc., (1948).

13). Minutes of "The Hydrogen Thyratron Tube Conference (1950)", Extracts from the Conference Records of the Power Modulator Symposia, University Buffalo, (1986).

14). Minutes of "The Hydrogen Thyratron Tube Conference (1953)", Extracts from the Conference Records of the Power Modulator Symposia, University Buffalo, (1986).

15). Abstracts from "The Hydrogen Thyratron Tube Conference, (1956)". Extracts from the Conference Records of the Power Modulator Symposia, University Buffalo, (1986).

16). J.C.Martin ; "Nanosecond Pulse Techniques", Report No. SSWA/JCM/704/49, Aldermaston, England.

17). H Frieschmann ; "High Current Electron Beams", Physics Today, May (1975).

18). J.C.Martin et al ; "LARK", Report No. SSWA/TS/755/99. Aldermaston, England.

19). J.C.Martin ; "Pulsed Charged Line for Laser Pumping", Report No. SSWA/JCM/732/373. Aldermaston, England.

20). Rudolf Germer ; "X-ray Flash Techniques. Review article", J.Phys.E. Sci. Instrum. Vol.12, (1979).

21). P.D.A. Chapney and P.W. Spence ; Proc. Flash X-ray Symp, New York : Am. Soc. Non-destructive Testing, (1977).

22). L.E. Bryant ; Proc. Flash X-ray Symp, New York, Am. Soc. Non-destructive Testing, (1977).

23). M.W.Wu et al ; "Pulsed High Power Microwaves from a Virtual Cathode Reflex Triode", Proc 6th Pulsed Power Conference, Arlington, (1989).

24). J.T. Verdeyeden ; "Laser Electronics", Ch. 8, Englewood Cliffs Books, N.J. (1981).

25). J.C.Martin ; "Pulsed Charged Line for Laser Pumping", Report No. SSWA/JCM/732/373. Aldermaston, England.

26). M.C. Richardson et al ; "A High Power TEA $C0_2$ Laser", Presented at the Symp. High Power Molecular Lasers, Quebec, May (1972).

27). Basov ; IEEE J . Quant. Electron., **QE-2**, p354, (1966).

28). F.G.Houtermanns ; Helv. Phys. Acta., p933. (1960).

29). C.H.Rhodes ; "Excimer Lasers", Topics in Applied Physics, Vol **30,** Springer Verlag Berlin Heidelberg series, (1984).

30). Basov et al ; JETP Lett. **12**, p329, (1970).

31). M.H.R.Hutchinson ; "Excimers and Excimer Lasers", Appl. Phys., **21,** pp 95-114, (1980).

32). M.J.Shaw ; "Excimer Lasers", Prog Quant Electron, Vol 6, pp 3-54. Pergamon Press Ltd.

33). J.J.Ewing ; "Rare-Gas Halide Excimer Lasers", Physics Today, May (1978).

34). Proc 12th Power Modulator Symposium. Extracts from the Conference Records of the Power Modulator Symposia, University Buffalo, (1986).

35). "Proc. 1st IEEE International Pulsed Power Conference", Lubbock, Texas, (1976).

36). 25th Aniversity Industry Guide, Laser Focus World, Jan, (1989).

37). M.Moretti ; "Lasers in Medicine", Laser Focus World, p63, March (1989).

38). Kazuhiko Atsumi ; "New Frontiers in Laser Medicine and Surgery", International Congress Series, **609**, (1983).

39). A.K.Hyder et al. ; "Prime Power for High Energy Space Systems". Available form the author.

40). W.G. Dunbar and D.L.Schweickkart ; "Effects of Breakdown Threshold for Power Components Exposed To the Natural and Induced Space Enviroments", Available from the author.

41). Auburn University ; Space Power Institute Prospectus, Auburn Univ. Texas, (1989).

42). K. Whitham et al. "NOVA. Pulse Power Design and Operational Experience". SPIE, Proc. Pulsed Power for Lasers Conference, Vol.735, p12, (1987).

43). D.C. Cartwright et al ; "Excimer Lasers Could be the Laser of Choice for the Next Generation ICF", Laser Focus World, p103, March, (1990)

44). B.N.Turman et al ; "PBFA 2. A 100 TW Pulsed Power Driver for the Inertial Confinement Fusion Program", Proc. 5th IEEE Pulsed Power Conf., (1985).

CHAPTER 1.

Preionisation and the Pulsed Power Requirements of a Flash X-ray Generator.

1.0. Introduction

Since the development of the first laser systems there has always been a close association between laser technology and pulsed power, from the early flashlamp modulators that were required to excite the first ruby lasers to the design and development of e-beam generators for the pumping of large volume gas lasers. As this reliance on pulsed power continues to increase so does the demand for more reliable pulsed power systems.

This opening chapter illustrates one aspect of high power gas discharge laser operation that is dependent on pulsed power technology, namely x-ray preionisation. It begins by explaining what preionisation is and why it is necessary to produce a homogeneous glow discharge in a high pressure gas. It then outlines the advantages of using x-rays as oppose to uv photons as the ionising radiation, describes the design, principle of operation and electrical requirements of a cold cathode flash x-ray source and explains why these requirements are difficult to satisfy using the pulse transformer, the Marx generator or the pulse charged pulse formimg line. This then leads to the introduction of the transmission line transformer in chapter 2.

1.1. Background Information. Scaling Pulsed Electric Discharge Lasers to High Power Levels.

Of the many different techniques that are available to pump a laser gas, by far the most widely used is electric discharge excitation[2]. Its effectiveness was probably first demonstrated when the continuous wave CO_2 gas laser was successfully developed by Patel in 1964[3]. Leonard (1965[4]) and Frieberg and Clark (1968[5]) were among the first people to try to scale this type of laser using pulsed high power discharge circuits and higher gas pressures. These attempts were, however, only partly successful because at pressures above 60 Torr free electrons cannot diffuse into the bulk of a laser gas and develop into a glow discharge. Instead, they form a localised avalanche and a "wake" of positive ions known collectively as a primary streamer.

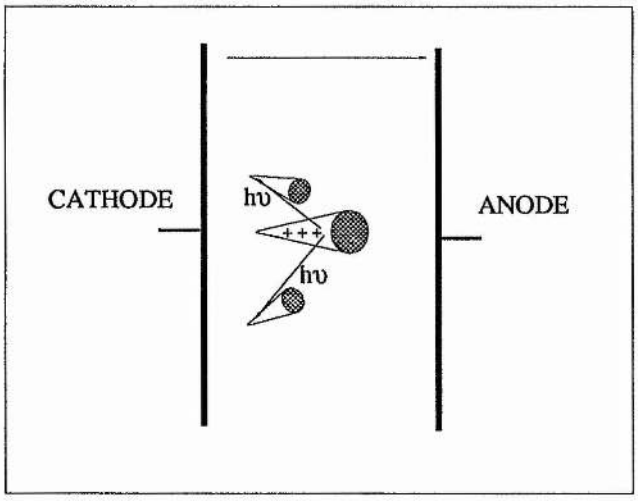

Fig 1.1.1 :- Diagram showing streamer breakdown initiated by a single primary avalanche.

The wake of a streamer produces strong local field gradients and electron collisions generate secondary streamers by photo-ionisation (see figure 1.1.1). When these local field gradients are strong enough to cause secondary streamers to converge with the primary streamer, an arc is formed. An arc cannot pump a laser effectively because, being localised, it provides a non-uniform gain medium and a poor quality laser pulse.

In order to operate a high pressure gas laser it is necessary to suppress arc formation. In some early laser systems, such as that developed by Beaulieu[6], this was achieved using resistively ballasted parallel pin electrodes and discharge voltage pulses shorter than the arc formation time. This technique, however, produces conical discharges and poor quality laser pulses. In other systems[8], better results were obtained by exposing the laser gas to uv light prior to the application of the discharge pulse. The uv was produced using a simple capacitor discharge pulsed power circuit and a spark-array; the technique is called preionisation[9,10].

Preionisation works because ionising radiation produces high energy primary electrons by photo-electric absorption and secondary electrons by collisional ionisation. If these electrons are distributed uniformily throughout a laser gas with a minimum preionisation density, n_0, they increase the number of streamers formed. This reduces the field gradients produced by the positive ions, inhibits the convergence of secondary streamers and produces a homogeneous discharge (see figure 1.1.2).

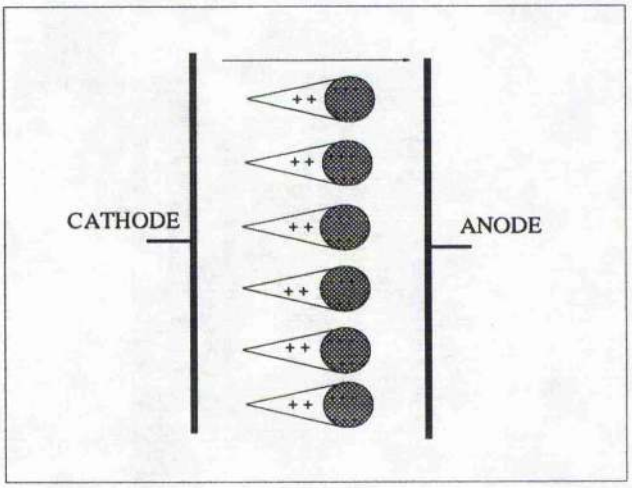

Fig 1.1.2 :- Schematic diagram showing one row of simultaneously formed primary avalanches propagating uniformly towards the anode.

1.2. The Minimum Preionisation Electron Density.

It is important to be able to calculate the minimum preionisation density because this determines the required radiation intensity and ultimately the specifications of the pulsed power supply. In the analysis developed by Palmer[9], n_0 is calculated by making the following assumptions :-

1). The lateral extent, r, of a primary streamer having propagated a distance z in a laser gas with a mean free path of λ is given by :-

$$r^2 = z\,\lambda. \qquad 1.2.1.$$

2). The electric field, E_r, produced at the surface of a streamer is : -

$$E_r = e N_e / 4 \pi \varepsilon_0 r^2. \qquad 1.2.2.$$

where :-

$$N_e = \exp(\alpha z). \qquad 1.2.3.$$

and α is the First Townsend coefficient, e the electronic charge and ε_0 the permittivity of free space.

3). Secondary streamers are attracted to the primary streamer when the space charge field, E_r, becomes comparable to the discharge field, E_0.

4). $n_0^{-1/3}$ can be taken as a measure of the separation of the primary streamers, r : $(n_0)^{-1/3}$ as the smoothness of the local field and $r > (n_0)^{-1/3}$ as the condition that ensures that these streamers overlap at the critical stage of the discharge i.e. after propagating a distance z_{crit}.

Assumptions 1, 2 and 3 enable z_{crit} to be calculated. It is given by equation 1.2.4.

$$\alpha z_{crit} = \ln(4\pi\varepsilon_0 E_0 \lambda / e) + \ln z_{crit}. \qquad 1.2.4.$$

Assumption 4 allows n_0 to be introduced into the analysis via equation 1.2.5 :-

$$n_0^{-1/3} < (\lambda z_{crit})^{1/2} \qquad 1.2.5.$$

This condition ensures that the primary streamers overlap and smooth the space charge fields before they have propagated a distance z_{crit}. For a $C0_2$ gas laser

operating with breakdown parameters of $\lambda = 10^{-3}$cm and $\alpha = 10\text{cm}^{-1}$, $n_0 = 10^4$ electrons cm^{-3}, a figure consistent with experimental observations.

Lavatter and Lin[10] have developed this analysis further and have shown that the preionisation electron density is also dependent on the voltage risetime of the discharge pulse across the electrodes, the total gas pressure, the various electro-chemical properties of the gas mixture which govern the net rate of change of the First Townsend Coefficient and the recombination coefficient of the gas because electro-negative species can quickly attach themselves to the preionisation electrons. When recombination dominates the time dependent electron density is given by :-

$$\frac{dn_0}{dt} = S(t) - k_a N_a n_0. \qquad 1.2.6.$$

where S(t) is the production rate of the preionisation electrons, k_a is the rate coefficient for electron attachment to the attaching species of density N_a [11].

Application of equation 1.2.6 shows that n_0 is greater in rare-gas-halide lasers* than $C0_2$ lasers. This has also been verified by experiment. The XeF laser system developed by Levatter and Lin[12,13] operated at 6 bar pressure and required an initial electron density of 10^5-10^7 electrons cm^{-3}. Sumida et al.[14,15] have reported on a KrF laser that required electron densities of the order of of 10^8 electrons cm^{-3} and Tallman and Bigio[16] investigated the output energy and spatial uniformity of a XeCl discharge laser as a function of preionisation electron

* See reference 33.

density; they found that a minimum electron density of 10^6 electrons cm^{-3} is sufficient to adequately preionise this type of laser.

1.3. Preionisation Techniques

As gas laser technology has advanced over the last twenty years, so many different pulsed power circuit designs have evolved to generate the ionising radiation and satisfy these preionisation requirements. Early $C0_2$ and excimer laser systems were, for example, preionised using ultraviolet radiation produced from spark arrays or surface or corona discharges[17,18]. Such techniques are still used extensively in commercial laser systems primarily because the associated pulsed power circuitry is relatively simple to design, can operate at modest repetition rates and fit neatly inside a laser cavity. Uv preionisation is, however, only effective over relatively short distances, approximately 10cms in a CO_2-N_2-He gas laser at 1 bar pressure[19]. This means that the pulsed power circuit has to be located in the immediate vicinity of the active region where it can contaminate the laser mix; it also means that uv radiation cannot preionise large volume lasers.

More recently there has been a tendency to use x-rays as the ionising radiation because these have a larger mass penetration power[20-23]. For example, the e-fold intensity attenuation distance of 200-keV photons in pure Xe, Kr, Ar and Neon at 1 atms is 5, 13, 50 and 110m respectively[24]. This means that they preionise more uniformly and the generator can be isolated from the laser cavity using a nickel plated aluminium window. This is particularly important when the gas mix is corrosive because then the operational lifetime of any form of "internal" preionisation circuit is drastically reduced.

1.4. The General Design of a Flash X-ray Preionisation Source.

X-ray preionisation sources can be conveniently divided into two separate classes depending on the method used to produce the electron-beam. The first class of device, namely the thermionic diode, operates by heating a metallic cathode to high temperatures (>1000°K depending on the metal) in a high vacuum environment. The electrons are liberated from the filament when the thermal energy of the electrons exceeds the work function of the metal. This enables them to escape into the surrounding medium where they are accelerated by the application of a large electric field. The current density, J Acm^{-2}, is given by the Richardson-Dushman equation :-

$$J = 60.2\ T^2 \exp\{-eW/\ kT\}. \qquad 1.4.1.$$

where W is the work function of the material, k the Boltzmann constant, T the temperature and e the electronic charge.

Thermionic devices, including thoriated tungsten and dispenser cathodes, are not often used for preionisation because they require high vacuums and large heater powers and they can only produce small currents over limited areas. For example, the thermionic emitter used by Tallman and Bigio[25] in a XeCl laser system required an accelerating voltage of 60kV and 50 Watts of low voltage AC power. This produced a filament temperature of 1000^0C and a total current of 20A, or a current density of $0.34A/cm^2$ at the x-ray anode. Similarly the device developed by van Goor et al[26], which used a Philips scandate cathode and an accelerating voltage of between 60kV - 80kV, produced a current density of

360A/cm^2. This, however, was only over a very small area, approximately 0.11cm^2.

A better way to preionise a gas is to use a cold cathode x-ray source because this can produce a higher currents over a larger area (Kline and Denes[27], Levatter and Lin[28], Sumida et al[29], Steyer and Voges[30], Taylor[31] and the thesis by Osborne[32]). It consists of a pulsed power supply, an e-beam diode that can be evacuated to pressures of 10^{-5} - 10^{-6} Torr and a high Z anode foil (see figure 1.4.1).

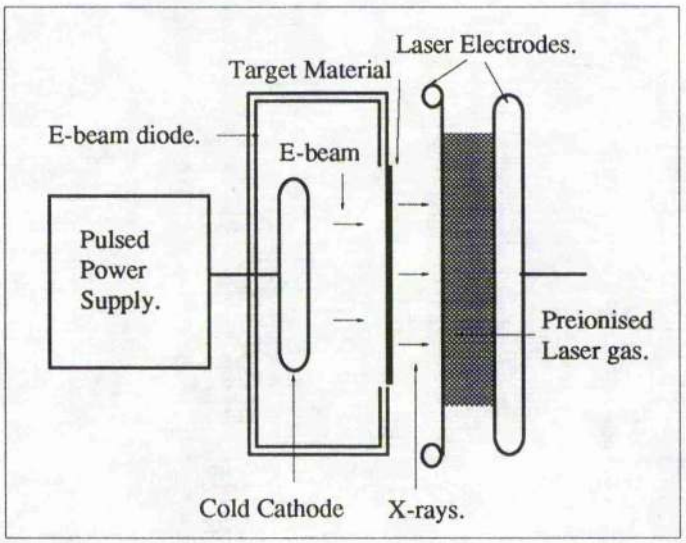

Fig 1.4.1:- Schematic diagram of a flash x-ray generator [33].

The pulsed power supply is required to produce high gross fields at the micro-protrusions on the surface of a cold cathode, which is usually a razor blade or a pin array [34-37]. Field enhancement at the surface of these microprotrusions

magnifies this field by 10 - 1000 times and this establishes the conditions necessary for a field emitted current to flow. This current generates a "cathode vapour" by evapourating material from the electrode surface. Electron bombardment of this vapour then produces ions that increases the local field strength and produces a massive increase in current. This current raises the temperature of the micro-protrusions by Joule heating until, at a certain critical temperature, they explode. The material ejected from this explosion forms a plasma which expands outwards, traverses the diode cavity at a velocity of approximately 2×10^6 cm/sec and becomes the principle electron emitter. The current it produces is space charge limited and for accelerating voltages less than 500kV is given by the Child-Langmuir relation :-

$$I = 2.34\ A\ \frac{V^{3/2}}{d^2}\quad \text{Amps.} \qquad 1.4.2.$$

where d is the anode cathode separation in cm, I the current in Amps and A the cathode area.

The x-radiation is produced when the electrons from this plasma are decelerated as they strike the high Z anode foil, which is usually made from tanatalum. The production efficiency, the mean and average x-ray energy and cut-off wavelength are given by equations 1.4.3 - 1.4.6 :-

$$\text{Conversion Efficiency, } C = 1.4 \times 10^{-4} V_0 Z \qquad 1.4.3.$$

$$\text{Mean Photon Energy, } E_{mean} = eV_0 / 2 \qquad 1.4.4.$$

$$\text{Peak Photon Energy, } E_{peak} = 2eV_0/3 \qquad 1.4.5.$$

$$\text{Cut-off wavelength, } \lambda_{min} = h\,c\,/\,e\,V_0\,. \qquad 1.4.6.$$

In these equations, h is Plancks constant, c the velocity of light, e the electronic charge and V_0 the accelerating potential[34].

If the electrons have enough energy to displace electrons in the target atoms, then characteristic line radiation will be superimposed on the Bremsstrahlung spectrum. The intensity I of this line radiation can be calculated using the corresponding excitation voltage for the target element , V_c, and the formula :-

$$I = k\,(V_0 - V_c)^n \qquad 1.4.7.$$

where k is a constant and n lies between 1.5 and 2 [35].

1.5. The Electrical Requirements of an X-ray Preionisation Source.

In order for x-ray preionisation to be effective, the e-beam diode must be able to produce a current pulse that has a duration, uniformity, current density and energy sufficient to produce the required x-ray dose and preionisation electron density in the laser gas. A survey of available literature[36-41] has shown that this can be achieved and the x-ray generator satisfy the preionisation requirements of most high pressure gas discharge laser systems if the pulse power supply can establish the following operating conditions :-

The Operating Voltage :- The operating voltage of the e-beam diode must produce fields of 10^7 Vm^{-1} for field emission to occur and to maximise the "beam utilisation efficiency", η [42]. This is defined as the ratio of the absorbed energy per unit volume of the laser gas to the energy of the e-beam electrons per unit surface area of the anode target in the e-beam generator.

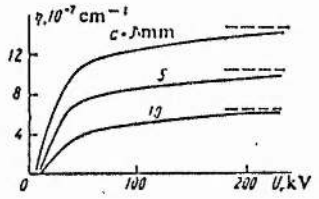

Fig 1.5.1:- Plot of the variation of η for Nitrogen at 1 atms, different accelerating voltages and polyethylene dividers[42].

Figure 1.5.1 shows how η varies as a function of the accelerating voltage for nitrogen gas and a number of polyethylene dividers of different thicknesses. Below 50kV it drops significantly because lower energy x-rays are absorbed more easily in the dividers. Above 50kV η is a weak function of V because the increase in the number of x-rays that can propagate through the dividers, is off-set by a fall in absorption in the gas.

The actual operating voltage of a pulsed power supply must be above the "knee" of this curve, the actual value being determined by technical problems associated with insulation. In most x-ray generators a voltage of 100kV is adequate.

Pulse Risetime :- In order provide uniform preionisation of a laser gas it is necessary that the number of emission sites per unit length of the cathode are maximised. The number of emitting sites is determined by the voltage, the geometry, the cathode material, the condition of the micro-structure and the dV/dt [43]. The dV/dt is one of the prime concerns of the circuit designer.

When any large cold cathode x-ray generator is operated there is a variation in the voltage, σ, at which field emission begins to occur because some micro-protrusions are sharper than others. This means that some sites begin to emit before others, the time difference, ΔT, being given by :-

$$\Delta T = \sigma V \left[\frac{dV}{dt}\right]^{-1} \qquad 1.5.1.$$

To produce a large number of sites per unit length of cathode it is necessary that the gross field on the cathode remain at or above $10^7 Vm^{-1}$ for a length of time ΔT. ΔT must therefore be alot less than the resistive phase of the diode, a condition that is usually met by maximising the dV/dt of the voltage pulse. A survey of the available literature has shown that effective e-beam generation can be obtained with values of 6kV/ns[27-32]. This means that voltage risetimes of at least 17ns are required for an x-ray generator operating at 100kV.

The Current Density at the x-ray window :- The output impedance of the x-ray pulsed power supply must be low enough to produce the current density required to produce the specified x-ray dose in the cavity. It has been

shown that a currrent density of $1Acm^{-2}$ is sufficient for the preionisation of most types of laser[33].

The Pulse Duration :- The duration of the x-ray pulse must be sufficient to provide the required x-ray dose and as large a "window" in which to operate the discharge circuit. Previous x-ray generator designs have shown that a pulse duration of 200ns is sufficient for an operating voltages of 100kV[33].

Other Requirements :- A flash x-ray generator requires a good quality voltage pulse with a well defined risetime, fall time and flat top to provide a definite "on" and "off" period. A low jitter is desirable because this simplifies the timing of the preionisation and discharge circuits. The repetition-rate requirement of the generator depends on the application but research is, at present, attempting to operate certain gas lasers, such as the rare-gas-halides, at kHz repetition rates in order to provide the average power levels required for many industrial, medical and military applications.

1.6. Limitations of Conventional Pulse Generating Techniques in X-Ray Preionisation Sources.

Of the three most commonly used pulse power supply designs that are used in x-ray preionisation sources the first generates the necessary voltage level using a a pulse transformer[43,44]. The second uses the Marx generator[45,46], the third a pulse charged, high speed pulse forming line. This section takes a brief look at each of these methods, discusses their limitations and shows how they make the electrical requirements of a x-ray preionisation source difficult to satisfy in practice.

The pulse transformer :- Many x-ray pulsed power supplies use a HV pulse transformers[47,48] to step the voltage up from a capacitor discharge circuit or PFN. They were originally developed by Martin during the 1960s and are capable of generating voltages of 3MV. One particular type is shown in figure 1.6.1.

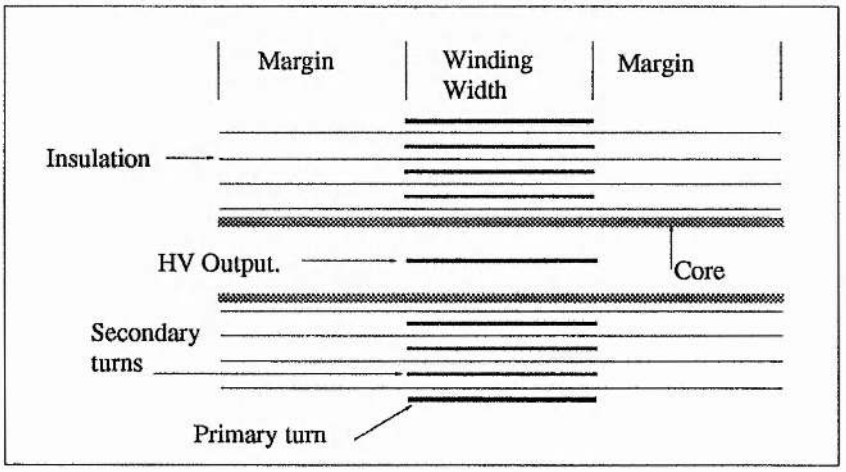

Fig 1.6.1 :- Diagram showing the construction of a Martin Type HV pulse transformer.

Its general design is different from that of a low power transformer because high voltage levels preclude the use of magnetics. The conductors, which are made from copper sheet separated with a thin layer of insulating plastic, are wound onto an air core which is usually made of perspex. In most cases the low voltage primary is located on the outside of the secondary and the high voltage output in the centre of the assembly. The large fields generated at the edges of the

windings are graded with a conducting liquid so the transformer has to be housed in a water tight vessel (not shown).

To see why it is difficult to satisfy the electrical requirements of a flash x-ray generator with a pulse transformer it is necessary to evaluate it's high and low frequency response using the equivalent circuit shown in figure 1.6.2. This has been obtained by referring the secondary circuit elements to the primary circuit. R_1 represents loss in the primary and secondary windings, L_1 the leakage inductance, L_2 the magnetising inductance and C_1 the inter-turn capacitance and primary and secondary winding capacitances. R_2 is the referred value of the load resistance.

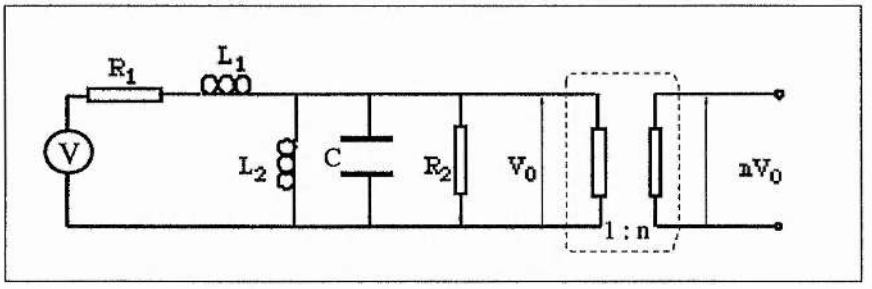

Fig 1.6.2 : - The equivalent circuit of a pulse transformer with the secondary circuit referred to the primary.

The high frequency response is determined from the high-frequency equivalent circuit obtained by approximating L_2 to an open circuit since, at the frequencies of interest, $\omega L_2 >> 1/\omega C$ and $\omega L_2 >> R_2$. The roots of the resulting transfer function are:-

$$s = -\frac{2\pi}{T} k \pm j\frac{2\pi}{T}(1 - k^2)^{1/2} \qquad 1.6.1.$$

where

$$a = \frac{R_2}{R_1 + R_2} \quad ; \quad T = 2\pi(L_1 C a)^{1/2} \quad \text{and} \quad k = \left(\frac{R_1}{L_1} + \frac{1}{R_2 C}\right)\frac{T}{4\pi}$$

Note that three different responses are possible depending on whether the pulse transformer is critically damped (k=1), underdamped (k<1) or overdamped (k>1). The critically damped case gives the fastest risetime without overshoot :-

$$\frac{V_0}{aV} = 1 - \left(1 + 2\pi\frac{t}{T}\right) \exp\left(-2\pi\frac{t}{T}\right) \qquad 1.6.2.$$

This can be simplified to give an expression for the 10 - 90% risetime, t_r [49]:-

$$t_r = 3.33\,(L_1 C a)^{1/2}. \qquad 1.6.3.$$

The low frequency response is determined by solving the network equations of the corresponding low frequency equivalent circuit obtained by neglecting the leakage inductance and the shunt capacitance (since $\omega L_1 < R_1$ and $\omega L_2 < 1/\omega C$). This analysis, which can be found in reference 49, gives :-

$$V_0 = aV \exp\left[-\frac{R\,t}{L_2}\right] \qquad 1.6.4.$$

where $R = R_1R_2/(R_1+R_2)$ and $V_0 = aV$ at t=0.

For small values of Rt/L_2 the exponential may be expanded to give the familiar expression for the pulse droop for a pulse of duration t_p:-

$$L_2/R=10t_p. \qquad 1.6.5.$$

This can be re-written as :-

$$10t_p=L_1/(1-K)R_2. \qquad 1.6.6.$$

since the leakage inductance of a pulse transformer is related to the magnetising inductance by the equation $L_1=(1-K)L_2$. K is the flux linking coefficient.

The form of equation 1.6.6 shows that fast pulses can only be achieved at the expense of the pulse duration. This limit on their operational range can be problematic when designing a flash x-ray generator of the type described because the combined requirement of a 17ns pulse risetime and 200ns duration with negligible droop is difficult to achieve. When this is the case it is necessary to operate at voltage levels higher than are required in order to produce the required rate of rise of voltage at the cathode and higher energy x-rays (higher energy x-rays are needed to generate the minimum preionisation electron density with a

reduced pulse duration). This situation is, in general, undesirable because higher voltages increase insulation problems and shorten the life of circuit components.

The Marx generator :- The second commonly used form of voltage multiplication used in x-ray pulsed power supplies is the Marx generator. This is a device that stacks the voltage on capacitors by charging them in parallel and switching them in series using spark-gaps. A 4-stage Marx generator shown in figure 1.6.3.

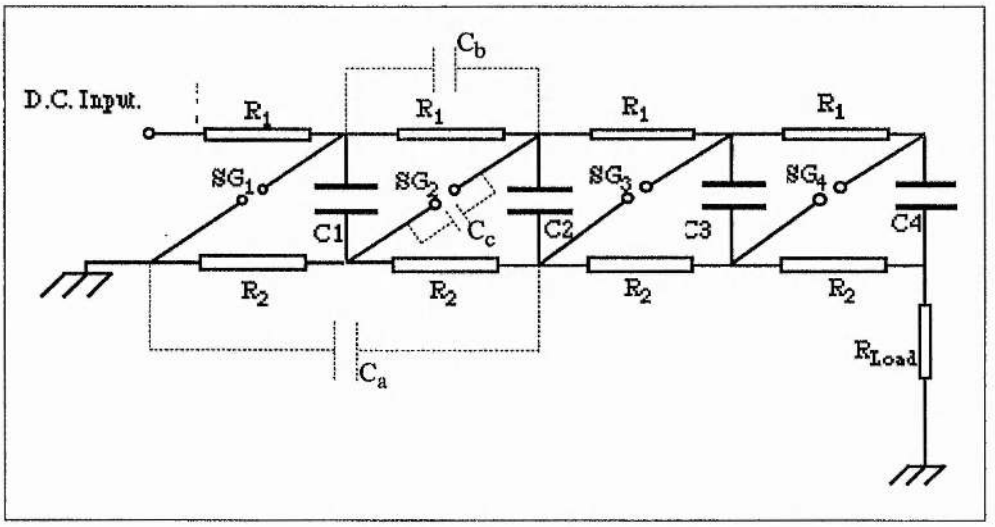

Fig 1.6.3 :- Circuit diagram of a 4-stage Marx Generator showing the Stray Capacitance associated with the 2nd-stage. C_a, C_b and C_c represent the stray capacitance between the 2nd-stage and ground, between the Marx capacitors and the spark-gap respectively.

It is operated by triggering the first spark gap, SG_1. This switches the voltage, V_{charge}, across C_1, overvolts SG_2 and raises the potential on C_2 to $2V_{charge}$. The process is repeated at the 2nd, 3rd and 4th stage. This produces an output pulse V_{out}, equal to $4V_{charge}$, with a risetime given by the appropriate time constant.

In practice the operation of a Marx is degraded by the divider formed by stray capacitance between each stage and the ground plane, adjacent stages, and across the spark-gaps (only those at the second stage are shown in figure 1.6.3). This divider increases the output risetime because it discharges through the charging resistors with an RC time constant[50], an effect that gets progressively worse higher up the Marx. The risetime is also increased by self inductance in the spark-gaps, capacitor connections and feeds. When this inductance dominates, the output pulse risetime is given by :-

$$t_p = 2.2\ L_{MARX}/R_L. \qquad 1.6.7.$$

where L_{MARX} is the total self inductance in the Marx generator and R_L the load resistance.

The Marx generator has a well established track record in the pulsed power field, and certain specialist devices have produced output risetimes of 10ns in certain high impedance loads. It is, however, unwieldly in construction, has a limited operational voltage range, produces pulses with no well defined leading, trailing edge and flat-top and is unable to operate at high repetition rates.

The Pulse Charged PFL :- One way of producing a good quality pulse with a fast risetime is to use a Marx generator or pulse transformer to pulse charge a pulse forming circuit, see figure 1.6.4. [51,52]. This fast section is switched across the load using a HV closing switch, usually a spark-gap.

The problem with these circuits is that they (i) cannot be made to operate at high repetition-rates because there is no reliable, repetitive, fast closing switch yet available that can operate at potentials of a few hundred kV (ii) they are difficult to insulate because a large part of the system is charged to the full output potential of the power supply (iii) they are physicaly large and bulky since water and insulating plastics, which are the only suitable PFL dielectrics capable of operating at these voltages, have a low permittivity, ε_r. For example a water line capable of producing a 200ns pulse has to be over 3.3m in length.

1.7. The Aims of this Thesis.

It is the aim of this thesis to develop a pulsed power supply that does not suffer from the problems inherent in these voltage generating systems. This pulsed power supply uses a transmission line transformer, or TLT, to step-up the voltage from a PFL or Blumlein circuit. As will be seen, a TLT is constructed from distributed transmission lines, has no first order limit on their high frequency response, can produce fast, good quality voltage waveforms and operate at high repetition-rates.

1.8. Summary of Chapter 1

This chapter has provided a degree of background information concerning preionisation and the pulsed power requirements of x-ray preionisation sources.

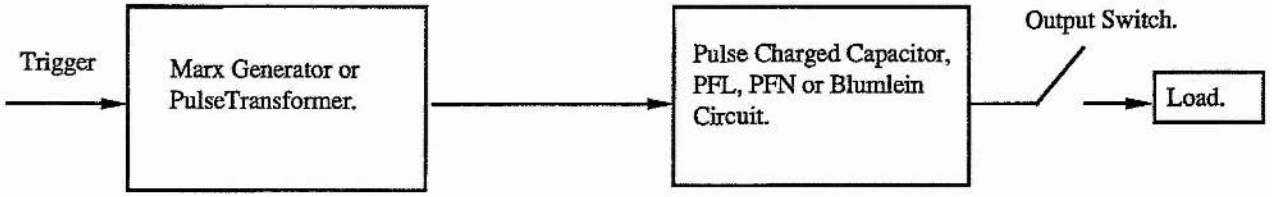

Disadvantages.

(i) No reliable repetitive closing switch yet available at potentials of a few hundred kV.

(ii). Large part of the system is charged to the full output potential of the pulsed power supply.

(iii) Physically bulky and heavy.

(iv). Double switching.

Figure 1.6.4 :- Traditional Approach Includes using a Marx Generator or Pulse Transformer to Pulse Charge a Fast Section.

It has explained why it is difficult to construct conventional HV generators that can satisfy these requirements and shown that a new design of pulsed power supply is required. The following chapter introduces this pulsed power supply.

References.

1). A Brown ; Ph.D. Thesis. Univ. St. Andrews. (1988).

2). Smith and Sorokin ; "The Laser", p 229, McGraw-Hill Physics and Quantum Electronics Series. (1966).

3).C.N.K. Patel et al ; Appl. Phys. Lett., Vol. 7, pp 290-292, Dec. (1965).

4). D.A.Leonard ; Proc. IEEE (Corresp.), Vol. 51, pp 1785-1786, Dec. (1963).

5). R.J.Frieberg and P.O.Clark ; IEEE J.Quant. Electron., Vol. Q.E.-8, pp 882 -892, Dec. (1972).

6). A.J.Beaulieu ; Appl. Phys. Lett., Vol. 16, pp 504-505, June (1970).

7). A.K.Laflamme ; Rev. Sci. Instrum., Vo 41, pp 1578-1581, Nov. (1970).

8). H.M. Lamberton and P.R. Pearson ; Electron. Lett., Vol 7, pp. 141-142, Mar. (1970).

9). A.J.Palmer ; Appl. Phys. Letts. Vol 25, No.**3**, p138, Aug. (1974).

10). J.I.Levatter and Shao-Chi-Lin ; J.Appl. Phys. 51(**1**), p 210. Jan. (1980).

11). H Shields ; "X-ray Preionisation Technology for High Pressure Gas Discharge Lasers", Proc. Pulsed Power for Lasers 2, SPIE Vol. 1046, (1989).

12). J.I.Levatter and Shao-Chi-Lin ; J.Appl.Phys. **51**, p210, (1980).

13). J.I.Levatter and Shao-Chi-Lin ; Appl.Phys.Lett. **34**, p505, (1979).

14). S.Sumida et al ; J.Appl.Phys. **52**, p2682, (1981).

15). L.E.Kline and L.J.Denes ; J.Appl.Phys. **46**, p1567, (1975).

16). C.R.Tallman and I.J.Bigio ; Appl.Phys.Lett. **42**, p149, (1983).

17). K.A.Laurie and M.M. Hale ; IEEE J.Quant. Electron.(Corresp.) Vol.10, pp 65-71, Jan (1972).

18). _____ ; IEEE J.Quant. Electron. (Corresp.), Vol Q.E.-7., pp 530-531. Nov. (1971).

19). O.R.Wood ; Proc. IEEE., 62, p355. (1974).

20). Lin and J Levatter. Appl. Phys. Lett. , 34(**8**). April (1979).

21). H.Shields and A.J.A.Alcock ; Optics Communications, Vol 42, No **2**, p128. (1982).

22). K.Jamaram and A.J.Alcock ; J.Appl.Phys. 58(**5**). p. 1719. (1985).

23). H.Shields et al ; Appl. Phys. B., B(**31**), pp. 27-35. (1983).

24). Sha-Chi-Liu and J.F.Levatter, "X-ray Preionisation for Electric Discharge Lasers", Appl. Phys. Lett., 34(**8**), (1979).

25). C.R.Tallman and I.J.Bigio ; Appl. Phys. Lett. No**42**, p149, Jan. (1983).

26). F.A.van Goor and W.J.Witterman ; SPIE Conference. Proc. 3rd Pulsed Power for Lasers, (1991).

27). L.E.Kline and L.J.Denes ; J.Appl. Phys. No.46, p1567, (1975).

28). J.I.Levatter and S.C. Lin ; Rev. Sci. Instrum. No.**52**, p1651. Nov. (1981).

29). S Sumida et al ; J.Appl. Phys. Lett. No. **52**, p 2682. (1981).

30). M.Steyer and H.Voges ; Appl. Phys. Lett. No. **42**. p149. (1987).

31). R.S. Taylor ; Appl. Phys. B. **41**, pp1-24. (1986).

32). M.Osborne ; Ph.D. Thesis., Imperial College, Univ. of London, (1985).

33). H Shields ; "X-ray Preionisation Technology for High Pressure Gas Discharge Lasers", Proc. Pulsed Power for Lasers 2, SPIE Vol. 1046, (1989).

34). Equations 1.4.3 - 1.4.6; Radiation Dosimetry ; Ch.1. G.J. Hire and G.L Bronwell. (Academic New York. 1956).

35). P Krehl ; "Analytical Study on the maximum Bremsstrahlung and K Series Production Efficiencies of Flash X-ray Tubes", Rev Sci. Instrum. 57(**8**). p1581. Aug. (1986).

36). Parker et al ; J. Appl. Phys. Vol. 45, No. 6, (1974).

37). R.Germer ; "X-ray Flash Techniques", J.Sci. Instrum., Vol. 12, (1979).

38). S. Loyd et al ; "500kV Rep-Rate Electron Beam Generator". Proc. 7th Pulsed Power Conference. (1989).

39).P.Krehl ; Rev. Sci. Instrum. 57, p1581-1589. (1986).

40). A.V.Kozyrev et al ; Sov.J.Quant. Electron., 14(**3**), p 356. March. (1984).

41). J.C.Martin ; "Multichannel Railgaps." Notes, AWRE, Aldermaston, England.

42). A.V.Kozyrev et al ; Sov.J.Quant. Electron., 14(**3**), p 356. March. (1984).

43). J.H.Smith ; "Simplified Pulse Transformer Design", Electronic Enginnering, p. 551, Nov. (1957).

44). " Pulse Transformers", Ch.6. "High Speed Pulse Techniques".

45). F.S.Edwards ; "The Development and Design of High Voltage Impulse Generators", Proc. IEE., Vol 98 p155, (1951).

46). "The Power Behind the Pulse", Optical Spectra, Dec, (1976).

47). J.C.Martin *et al*, "High Voltage Pulse Generating Transformer", Patent No. 510 481. July 15th. (1969).

48) J.C.Martin ; "Lark" Report No. SSWA/TS/755/99, Aldermaston, England.

49). Millman and Taub ; "Pulse Digital and Switching Waveforms", International Student Edition. McGraw-Hill Inc. (1965). Chapter 3, p 64.

50). W.L.Willis ; "Pulse Voltage Circuits", Los Alamos Lecture Notes. p19, October (1980).

51). I.G.Kaprinkov and K.A.Stankov ; J.Phys.D, Appl. Phys., **20** (1987).

52). J.C.Martin ; "Pulse Charged Line for Laser Pumping", Report No. SSWA/JCM/732/373. AWRE, Aldermaston, England.

CHAPTER 2.

Transmission Line Transformers.

2.0. Introduction.

This chapter introduces the Transmission Line Transformer voltage generator. It explains its principle of operation, demonstrates its high efficiency and excellent frequency response and shows that it can often perform better than conventional voltage generators. This work is supplemented by Appendices A and B. These develop a TLT equivalent circuit, solve the resulting network equations and derive a general transfer function that can be used to provide a mathematical framework upon which the design of future TLT generators can be based.

2.1. The Transmission Line Transformer.

There are three basic types of TLT, the Darlington circuit, the stacked Blumlein circuit and the stacked transmission line generator. Each is discussed briefly below.

The Darlington Circuit :- The Darlington circuit[1,2,3] was originally developed by Sidney Darlington at Bell Laboratories. The general circuit, which is shown in figure 2.1.1, is constructed from N transmission line sections, each with an equal transit time t_p and impedance Z_N given by :-

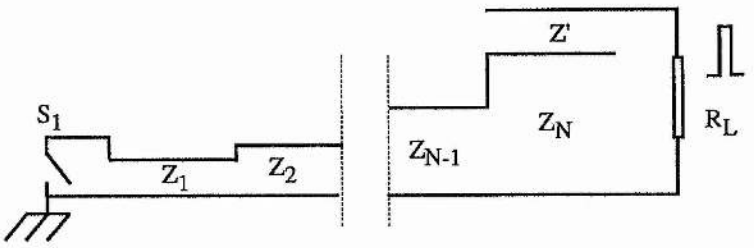

Fig 2.1.1 :- A circuit diagram of the Darlington Circuit.

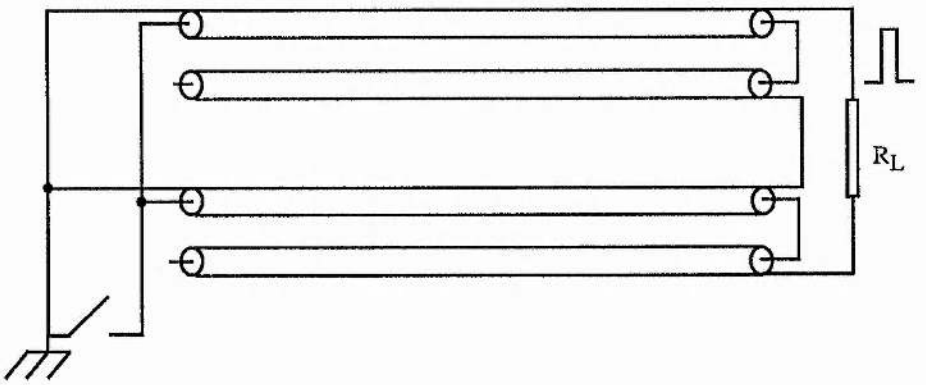

Fig 2.1.2 :- Circuit diagram of a stacked Blumlein Generator using coaxial cable.

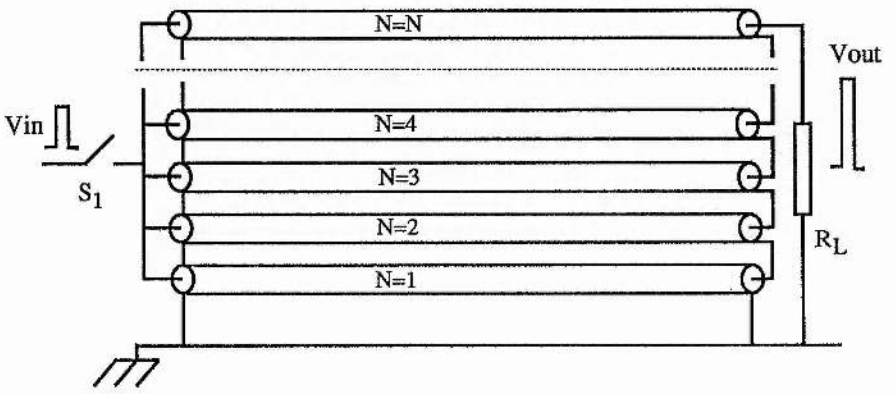

Fig 2.1.3 :- Circuit diagram of an N-stage Stacked Line Generator.

$$Z_N = \frac{N(N+1)Z_1}{2} \qquad 2.1.1.$$

where Z_1 is the impedance of the first section.

At the end of the line there is a separate section of impedance Z' :-

$$Z' = \frac{(N+1)Z_1}{2} \qquad 2.1.2.$$

and this is connected to the matched load R_L :-

$$R_L = \frac{(N+1)^2 Z_1}{2} \qquad 2.1.3.$$

The Darlington circuit is operated by closing the primary switch S_1 and launching a discharge wave, V_0, along the line. This wave is amplified and partially reflected at each impedance discontinuity. If the impedances of the lines are as given by equation 2.1.1, then the reflections cancel out amongst themselves and the discharge wave accumulates all the stored energy in the line. This energy appears as an output pulse with an amplitude of :-

$$V_{out} = \frac{-(N+1)V_0}{2} \qquad 2.1.4.$$

and duration equal to $2t_p$.

Although Darlington circuits are occasionally used in large custom-built e-beam accelerators[4,5] they are difficult to construct in the laboratory because (i) HV coaxial cable is not available with the appropriate characteristic impedance values (ii) each successive stage has to be more heavily insulated because the amplitude of the pulse increases as it travels towards the load (iii) the inter-connections between stages degrades the risetime and (iv) the output pulse duration cannot be varied because it is set by the propagation time of the transmission lines.

Stacked Blumlein Generators :- Stacked Blumlein generators are really hybrids of the N=1 Darlington circuit and stacked Transmission Line Transformer discussed below. Their principle of operation is illustrated by the two stage circuit shown in figure 2.1.2. The output of the lower Blumlein circuit is used to raise the potential of the upper one and produce a voltage of pulse of $2V_0$ across the matched load. These types of generator have been used by Cogan et al. to drive an x-ray generator and Somerville for voltage breakdown tests [6,7], so they are a tried and tested technique. However, being a Darlington circuit, they can only produce output pulses with a fixed duration.

Stacked Transmission Line Transformers :- The stacked Transmission Line Transformers, or TLT, is not a new idea. It was originally used to provide an impedance match between different circuit components and generate fast pulses for nuclear instrumentation in the 1950s. It is discussed in the book "Millimicrosecond Pulse Techniques" by Lewis and Wells[8] (1957) and in the papers by Winningstad[9] and Matick[10,11]. Its potential as a pulsed power generator has, however, only been briefly assessed by Fitch and Howell[12] in the

paper "The Principles of High Voltage Generation" published in 1964. Recently, it appears to have drifted into obscurity.

The general form of the N-stage stacked line TLT is shown in figure 2.1.3. The initial voltage waveform is produced by a pulse generator which is usually a matched Blumlein circuit. The TLT is constructed by connecting N distributed transmission lines in a series/parallel configuration. These have a characteristic impedance, Z_0, a propagation delay time, t_d, and a combined input and output impedance of Z_0/N and NZ_0 respectively. The uppermost line is connected to the matched resistive load, R_L, which must equal NZ_0.

The TLT generator is operated by discharging the pulse generator into the TLT thereby propagating a voltage pulse, V_0, along each transmission line; the propagation delay, t_d, of this pulse is given by $3.3(\varepsilon_0\varepsilon_r\mu_0\mu_r)^{1/2}l$, where l is the length of each line and ε_r and μ_r the relative permittivity and permeability of the dielectric. At the output of each line the pulse sees a load that consists of R_L and the remaining N-1 primary lines that are connected in series. This impedance mis-match produces a reflected and transmitted wave, V_R and V_T, with amplitudes :-

$$V_R = V_0\left[\frac{R_L + (N-2)Z_0}{R_L + NZ_0}\right] \qquad 2.1.5.$$

and

$$V_T = 2V_0\left[\frac{[R_L + (N-1)Z_0}{R_L + NZ_0}\right] \qquad 2.1.6$$

V_T is dropped across the N-1 primary lines and the load resistance R_L. When the contribution from the other N-1 lines are added, a voltage of NV_T is generated at the load and $V_T(N-1)/(2N-1)$ across the transmission lines. The later is opposite in polarity to the reflected waves so both cancel out.

Stacked line generators are probably the best type of TLT for moderate pulsed power systems because they can be used to construct a pulsed power supply of the type shown in figure 2.1.4. This design is desirable because (i) it is easier to insulate since the transmission lines are only stressed to the charge voltage of the PFL and only the output of the Nth line reaches full volts (ii) the initial voltage waveform can be generated at relatively low voltages, typically at the 30kV level, using standard tried and tested HV equipment such as the thyratron switch (iii) it has the potential of being a reliable design that can operate at high repetition rates because of the low tanδ of the dielectric (iv) it can have an almost all "solid state" construction and a variable output voltage that is determined by the DC charging unit (v) it can be easily constructed from standard 50Ω coaxial cable (vi) the pulse length can easily be varied because this is determined by a separate circuit, the pulse generator and (vii) it is capable of extremely fast risetimes because there is no first order limit to its high frequency response. The loss in risetime that does occur is primarily due to the skin-effect in the transmission lines and to a lesser extent the conductance of the dielectric and radiation. The output risetime is therefore determined by the step response of the cable, and this is given by :-

$$V_{out}(t) = V_{in}\left[1 - \mathrm{erf}\frac{1K}{4 Z_0 t^{1/2}}\right]. \qquad 2.1.7.$$

Improved Type of Pulsed Power Supply Using a TLT Voltage Generator.

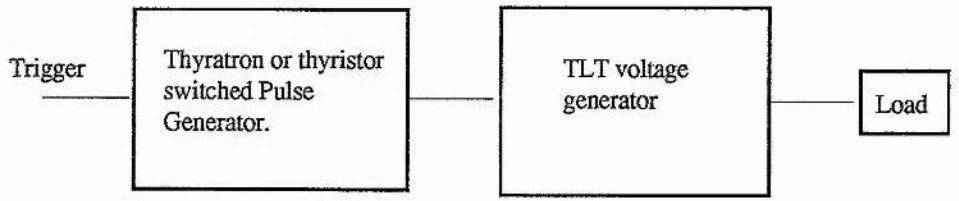

Advantages :-

1). Switched by long life, repetitive switches, eg the thyratron.

2). Output connectiona at the load reach full volts.

3). Continuously variable output voltage.

4) A stacked line TLT can generate fast, good quality pulses.

Fig 2.1.4 :- An improved pulsed power supply design based on the TLT voltage generator.

where V_{in} is the amplitude of the input step, t the time after the propagation delay, l the length of the cable; K is given by the equation :-

$$K = \frac{1}{2\pi r}\left[\frac{\mu}{\delta}\right] \qquad 2.1.8.$$

r and δ being the conductor radius and conductivity and μ the permeability of the dielectric.

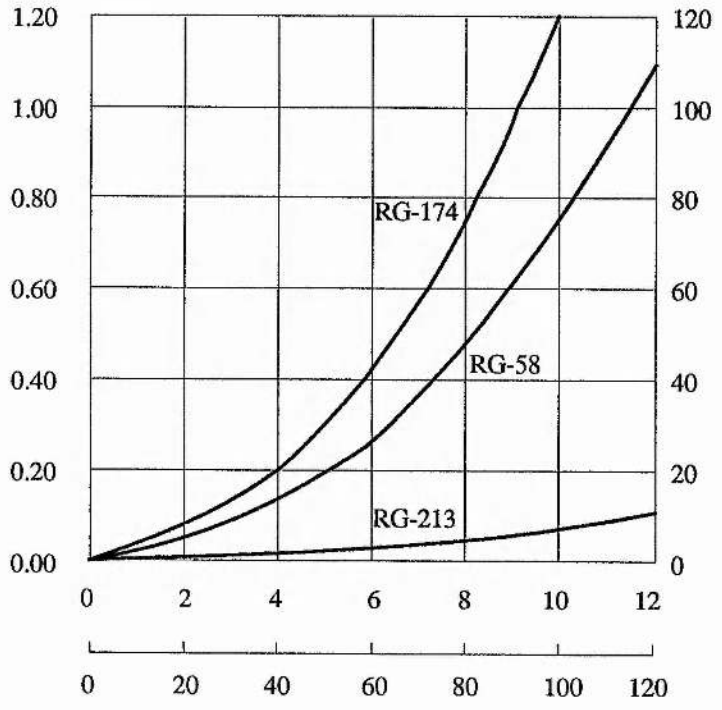

Fig 2.1.5 :- Plot of output risetime vs cable length for common solid-poly cables[13].

Figure 2.1.5 is a graph that shows this equation in a more convenient form. It implies that a TLT constructed from 10m lengths of RG-213 should be capable of producing 10% - 90% risetimes of under 3ns.

2.2. The Secondary Mode. The Effect of a Transmission Line above the Ground Plane.

The theory of a stacked transmission line device is actually more complicated than the previous description suggests because two related effects perturb the output pulse. Firstly, the self inductance of the outer cable of a stacked line shorts the pulse generator and this produces pulse droop. Secondly, the self inductance and stray capacitance couples to form a secondary transmission line to the ground plane. Secondary lines appear at every stage except the first and they :-

1). Act as a shunt to the output of the preceding stage. They therefore reduce the amplitude of transmitted voltage pulse, V_T, and the gain of a TLT.

2). Support a secondary mode (SM) of propagation. In the 2-stage TLT shown in figure 2.2.1 a SM is excited between the outer cable of line 2 and the ground plane. It propagates from the stacking point, **A**, towards the input end of the TLT, **B**, (where it is totally reflected) and back to **A**. This second reflection reduces its amplitude and produces a step in the output pulse. The length of the step is equal to the two way transit time of the SM and more steps are produced on succeeding round trips.

To demonstrate these effects, circuit 2.2.1 was constructed from two 3m lengths of 50Ω coaxial cable. It was matched into a 100Ω resistive load and used

to step up a 200ns, 30V pulse from a PFL with an output impedance of 25Ω. The output pulse produced when the PFL was operated into a 25Ω load is shown in figure 2.2.2 and that from the TLT in figure 2.2.3. Note how the secondary line has reduced the amplitude of the output pulse from 60V to 55V and the gain from 2 to 1.83; note also the stepping superimposed on the L/Z_0 voltage decay. The secondary mode steps are approximately 20ns in length, which is equal to the two way transit time of the SM propagating along a 3m transmission line in air.

2.3. Suppression of the Secondary Mode.

To construct a practical TLT system it is necessary to suppress the effect of the SM. This can be achieved using long cable runs because this introduces extra self inductance that increases the L/Z_0 decay time and produces a secondary mode round trip-time greater than the output pulse duration, i.e. :-

$$2T_2 > t_p. \qquad 2.3.1.$$

Figure 2.3.1 shows a 4-stage TLT circuit that was constructed using this technique. The four 20m transmission lines, **A**, were wound on top of each other on a plastic air cored former **B** with line N=1 at the bottom and line N=4 at the top. **C** and **D** are the input and output connections respectively. The initial voltage pulse was produced using a PFL that was switched with a mercury wetted relay. The output pulse produced by this system is shown in figure 2.3.2. It had a risetime of about 15 - 20ns and there was no droop present. The system gain was 3.3.

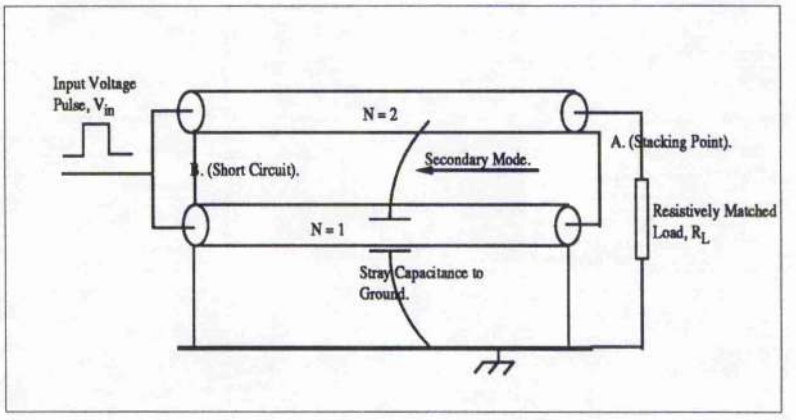

Fig 2.2.1 :-Diagram showing the principle of a 2-stage TLT.

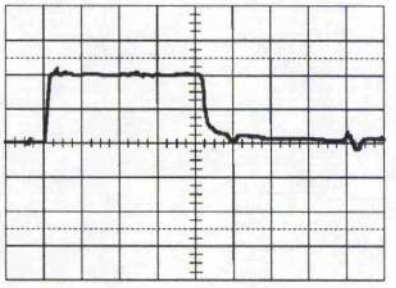

Fig 2.2.2 :- Output waveform from the

PFL into a matched resistive load. 15V/div; 50ns/div.

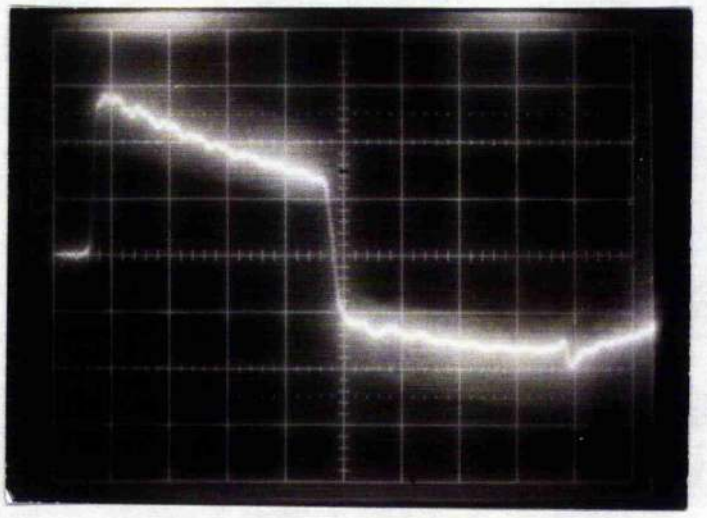

Fig 2.2.3 :- Output waveform from the 2-Stage

TLT Test Circuit. 20V/div; 50 ns/div.

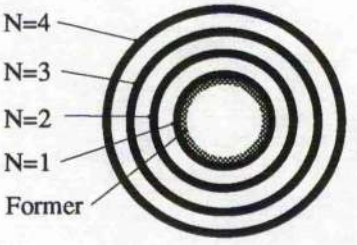

Fig 2.3.1 :- This shows a diagram of the construction of a mutually wound TLT and a completed device : **A** - the primary lines, **B** -- Plastic Former, **C** input terminals, **D-** output terminals.

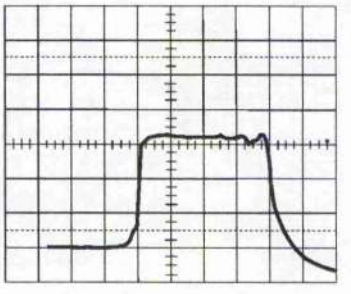

Fig 2.3.2 :- Output pulse of 4-stage TLT at low voltage. 20v /div : 50ns/div.

It is also possible to reduce the effect of the SM by maximising both the SM impedance, $Z_2 = (L/C)^{1/2}$, and the propagation delay time, $T_2 = (LC)^{1/2}$. This is achieved by winding the stacked lines inductively. The amount of self inductance that is required on the Nth stage of a TLT is given by equation 2.4.2 :-

$$L_{(\text{Line N})}/(N-1)Z_0 = 10t_p \qquad 2.3.2.$$

If equation 2.3.2 is satisfied then there is no noticeable droop on the output pulse.

Figure 2.3.3 shows the design of a 4-stage magnetically isolated TLT. The PFL, which was constructed from four 20m lengths of coaxial cable, was switched using a mercury wetted relay. Each stage of the TLT comprised of four 5 m lengths of coaxial cable each wound loosely on an F5 magnetic toroid. These toroids had an area core factor of $15mm^2$, a magnetic path length of 100mm and enabled self inductances of over 500μH to be produced on the 2nd, 3rd and 4th stages of the TLT. The TLT was terminated by 200Ω resistive load.

Figure 2.3.4 shows the input and output pulses. The risetime of the input pulse, which had an amplitude of 20V, was limited to 25ns by the mercury wetted relay. The output pulse risetime was identical so there was no loss in the TLT itself. There was no visible droop on the output pulse, which had a peak voltage of just under 80V. The corresponds to a system gain of 3.85 and a TLT efficiency of over 90%.

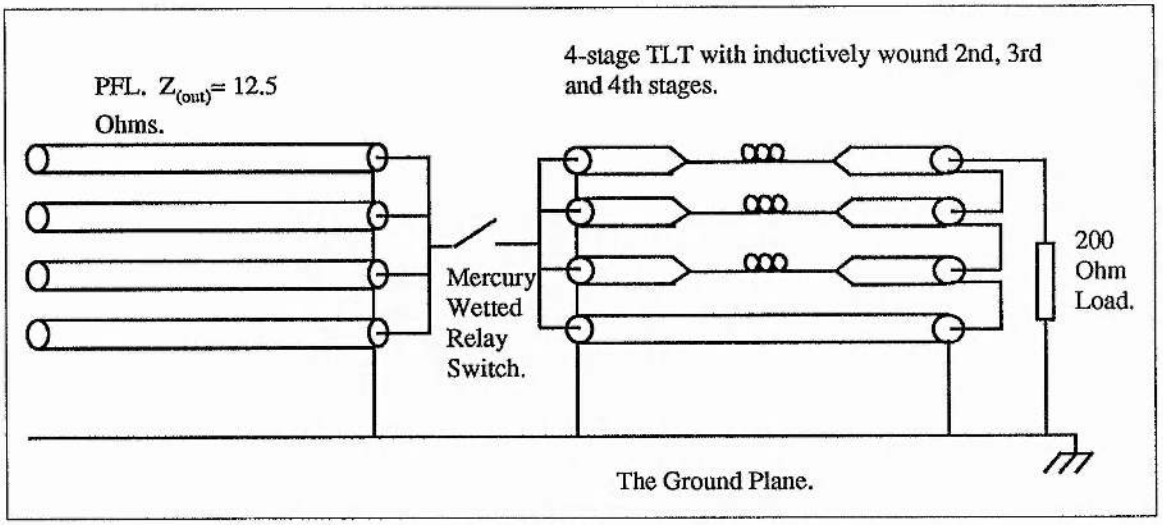

Fig 2.3.3 :- Circuit diagram of the 4-stage TLT. The PFL consisted of four 20m lengths of coaxial cable and could produce an input pulse of 200ns duration. The output of the TLT was matched into a 200 Ohm load.

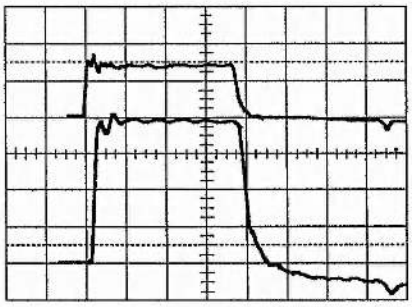

Fig 2.3.4 :- Output waveform of a 4-stage magnetically isolated TLT using F5 magnetic cores. The improvement in the response of the TLT is clearly evident.Input pulse (upper trace) 20V (channel not calibrated). Output 20V/Div : 50ns/div.

2.4. Operational Limits of the TLT.

A magnetically isolated TLT like that just described can, in general, perform better than a mutually wound one because magnetic materials enable higher secondary mode impedances to be achieved, shorter cable lengths to be used (this produces faster pulses) and higher winding inductances to be obtained (this is necessary for long pulse durations). For example, figure 2.1.5 and equation 2.1.2 reveal that the minimum risetime and maximum pulse duration that can be produced from a 5m length of transmission line with a self inductance of 500μH is 1ns and 300ns respectively. This represents a risetime to pulse duration ratio of 300 which is adequate for preionisation purposes. High voltage magnetically isolated TLTs are, however, difficult to construct because 30kV coaxial cable is relatively inflexible and difficult to wind on a magnetic core of any practical size. One way round this problem is to use strip transmission lines although these are more lossy and are prone to breakdown. A strip transmission line TLT system is described in chapter 5.

In contrast, a mutually wound TLT tends to require longer cable runs than its magnetically isolated counterpart and this makes it physically large, heavy and slower. In addition, the condition that the output pulse duration must be less than the two way transit time of the secondary mode means that it is difficult to produce pulse lengths much greater than 200ns. It is, however, a design that is well suited for used in an x-ray preionisation source because, as the following chapter will reveal, it can be readily scaled to high voltage levels.

2.5. Summary of Chapter 2.

This chapter has explained the principle of operation of the TLT, described a 4-stage mutually wound and magnetically isolated design and demonstrated their performance potential using a number of low voltage circuits. This has shown that both are capable of satisfying the electrical requirements of a flash x-ray preionisation source.

References.

1). G.N.Glasoe and J.V.Lebacqz "Pulse Generators", p 464. Dover Publications (1965).

2). I.Smith ; "A novel Voltage Multiplication Scheme Using Transmission lines", Proc. 15th IEEE Power Modulator Symposium, (1982).

3). I. Smith ; "Principles of the Design of Lossless Tapered Transmission Line Transformers", Proc 7th IEEE Pulsed Power Conference, (1989).

4). A.I. Pavlovskii et al ; Sov. Phys.-Dolk., 20, p441, (1975).

5). I.D.Smith ; "Ultra Relativistic Electron Beam Sources for the ARA", PIFR - 1103, Oct. (1978)

6). Coogan et al ; Proc &th IEEE Pulsed Power Conf., (1989).

7). I Sommerville et al ; "An Efficient Stacked Blumlein HV Pulse Generator", Meas. Sci. Tech., **1**. p865, (1990).

8). T.A.D.Lewis and F.H.Wells ; " Millimicrosecond Pulse Techinques", London, Pergamon, 1959, Ch.3, pp. 109 -111.

9). C.N.Winningstad; "Nanosecond Pulse Transformers", I.R.F. Trans. Nuc. Science, March, (1959).

10). R.E.Matick ; "Transmission Line Pulse Transformers", Proc. IEEE., Vol. 56, No.**1**, p 47, (1969).

11). _____ "Comments on Transmission Line Transformers for Pulse Applications", Proc. IEEE Lett. p 994, August (1972).

12). R.A. Fitch and V.T.S. Howell ; Proc. IEEE., **111**, p 849, (1964).

13). T.Dreher ; "Cabling Fast Pulses, Don't Trip on the Steps", The Electronic Engineer, p71, Aug., (1969).

CHAPTER 3

Construction and Performance of a HV TLT Pulsed Power Supply, a Flash X-ray Generator and the Preionisation of a Mercury Bromide Laser.

3.0. Introduction.

This chapter brings together the material presented in chapters 1 and 2 by describing a flash x-ray generator that was driven by a TLT based pulsed power supply. It begins by first outlining some of the general features of this generator. It then describes the pulsed power supply in detail, with the emphasis placed on the TLT, the Blumlein circuits, the thyratron switches and the performance of the x-ray generator when used as a preionisation source for a mercury bromide laser system.

3.1. General Outline of the Flash X-ray Generator.

The design strategy for the x-ray generator was to construct a device with a pulsed power supply that satisfied the electrical requirements given in chapter 1. This necessitated the use of TLT technology. The circuit diagram of the pulsed power supply is shown in figure 3.1.1. It was simply a scaled up version of the mutually wound TLT circuit described in the previous chapter and comprised two parallel, DC charged lumped element Blumlein circuits, each switched with a CX

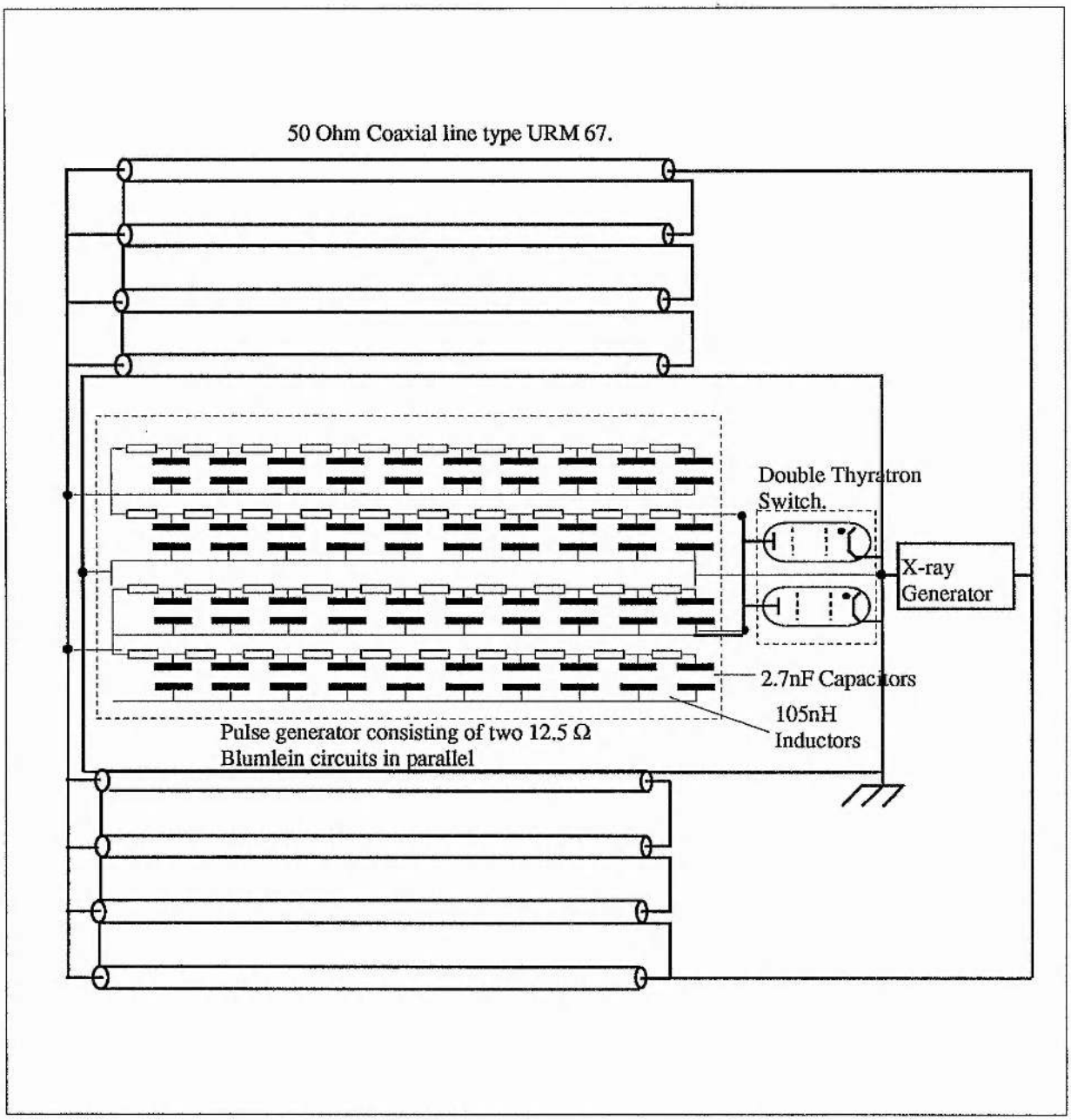

Fig 3.1.1 :- Circuit diagram of the x-ray generator. The PFN in the centre of the diagram was constructed as two 12.5 Ω Blumlein circuits in parallel. Each individual Blumlein circuit was switched using a CX 1685 Hydrogen Thyratron. and matched to two TLTs . These were connected to the e-beam diode. Details of the charging circuit, the thyratron grid drive circuits and the thyratron trigger unit have been omitted for clarity.

1685 hydrogen thyratron and each designed to operate into a 12.5Ω load. These produced output pulses with a 50ns risetime, 230ns duration and an amplitude of 30kV. The TLT voltage generator comprised two parallel 4-stage TLTs with a combined input and output impedance of 6.25Ω and 100Ω respectively. They were constructed according to the mutually wound 4-stage TLT design using 50Ω HV coaxial cable type URM 67. The TLTs stepped the voltage pulse up to 100kV when operated into a 100Ω matched resistive load. The pulsed power supply as a whole was operated under oil and housed in an earthed metal box located directly behind the vacuum chamber of the x-ray generator. This can be seen in photograph in figure 3.1.2.

The e-beam diode and tantalum foil anode were located in the vacuum chamber visible in the foreground of this photograph. Also visible is the rotary/diffusion pump and a nitrogen cold trap that were used to evacuate it to 10^{-4} - 10^{-5} Torr. Figures 3.1.3 - 3.1.4 show the cathode assembly. It was "in-line", and similar in design to that used by Smith and Osborne in their large volume, x-ray preionised XeCl laser system[1]. The HV connection from the two TLTs was located at the end of the low inductance coaxial feed, **A**. This was, in turn, connected to a cathode feed, **B**, by a sliding contact. This contact allowed the cathode assembly to be removed from the vacuum chamber for maintenance purposes and for adjustment of the anode/cathode spacing. Insulation between feeds A and B and the vacuum chamber was provided by a field grader constructed from a series of perspex insulators, each chamfered at a 45^0 angle and each sandwiched in between two aluminium rings. Cathode feed **B** was connected to a stainless steel cathode support plate, **C**, which had dimensions of 100cm x 10cm x 0.5cm. This contained a bracket that held the field-emitter, **D**, which was constructed from an

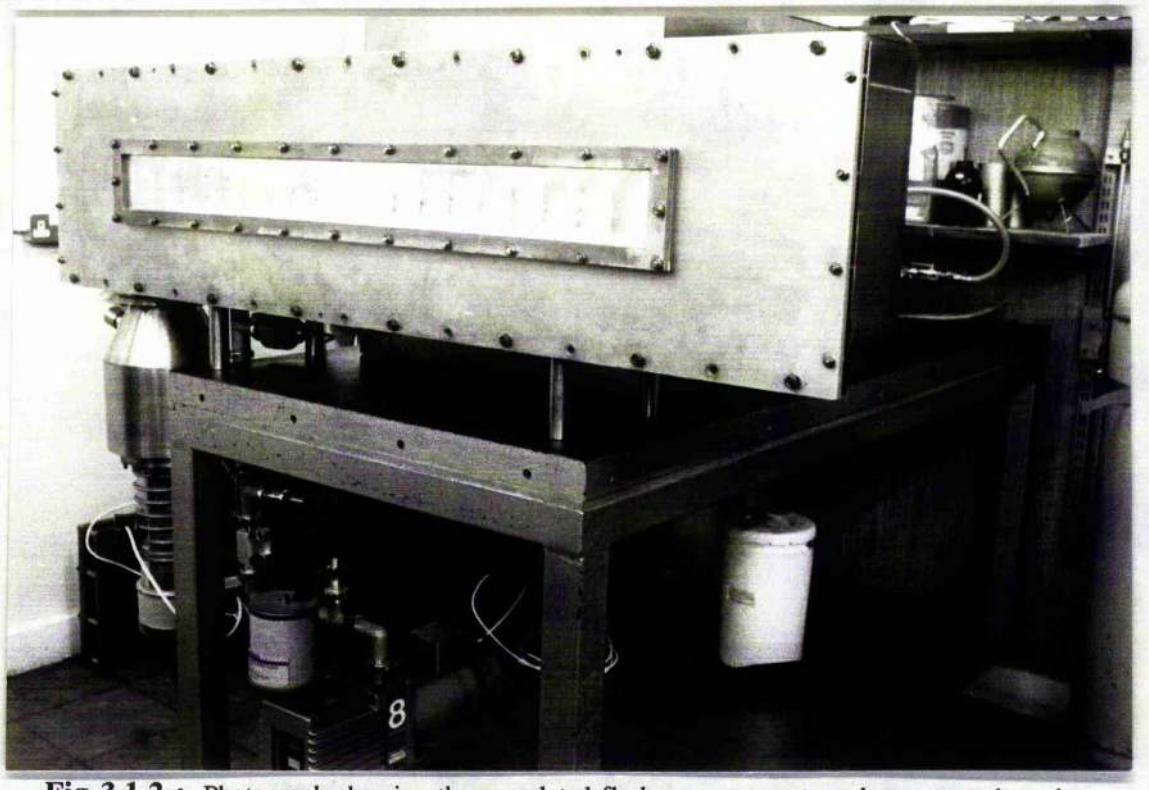

Fig 3.1.2 :- Photograph showing the completed flash x-ray generator when mounted on the movable metal table. The TLT pulsed power supply is located the earthed metal tank positioned behind the x-ray generator, which is in the foreground. The aluminium window is visible on the front plate and the rotary and diffusion pumps can be seen to the left of the photograph.

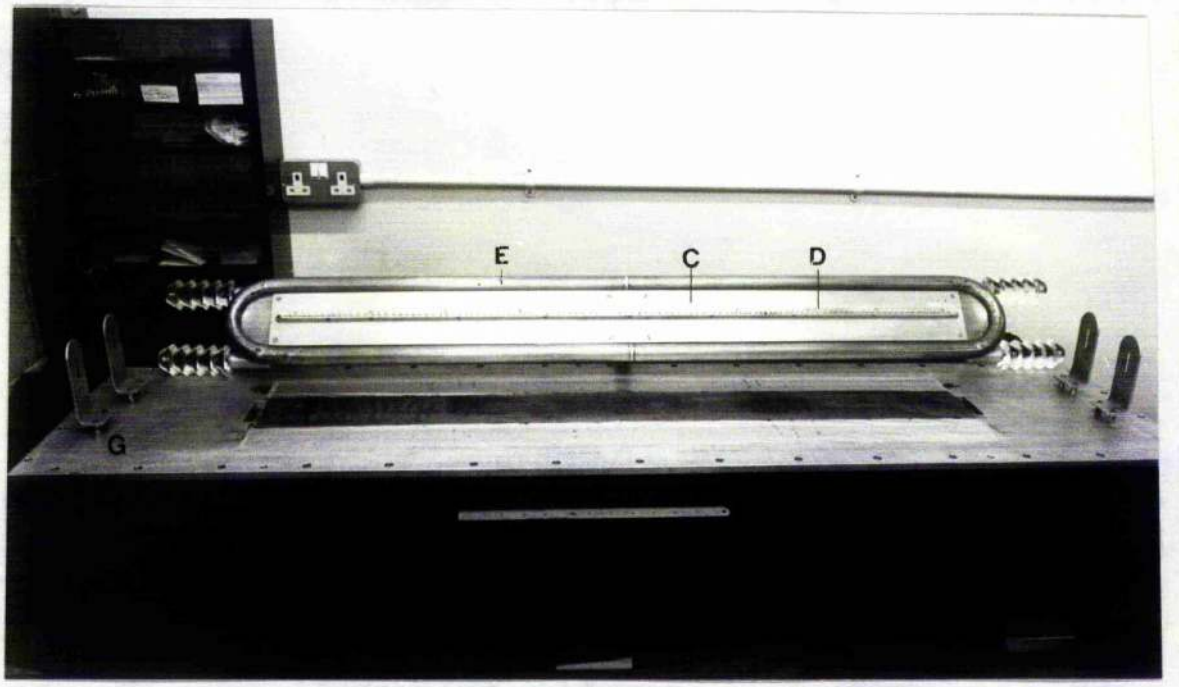

Fig 3.1.3 :- Photograph showing the cathode field emitter resting on the front plate of the x-ray generator, **G**. The pin array, **D**, which consisted of over 100 pins spaced 1cm apart, can be seen running along the length of the cathode support plate **C**. The copper tubing, **E**, that encircles **C** is the race track. The perspex insulators and sliding brackets that hold the cold cathode in position can also be seen. **F** is the tantalum foil anode.

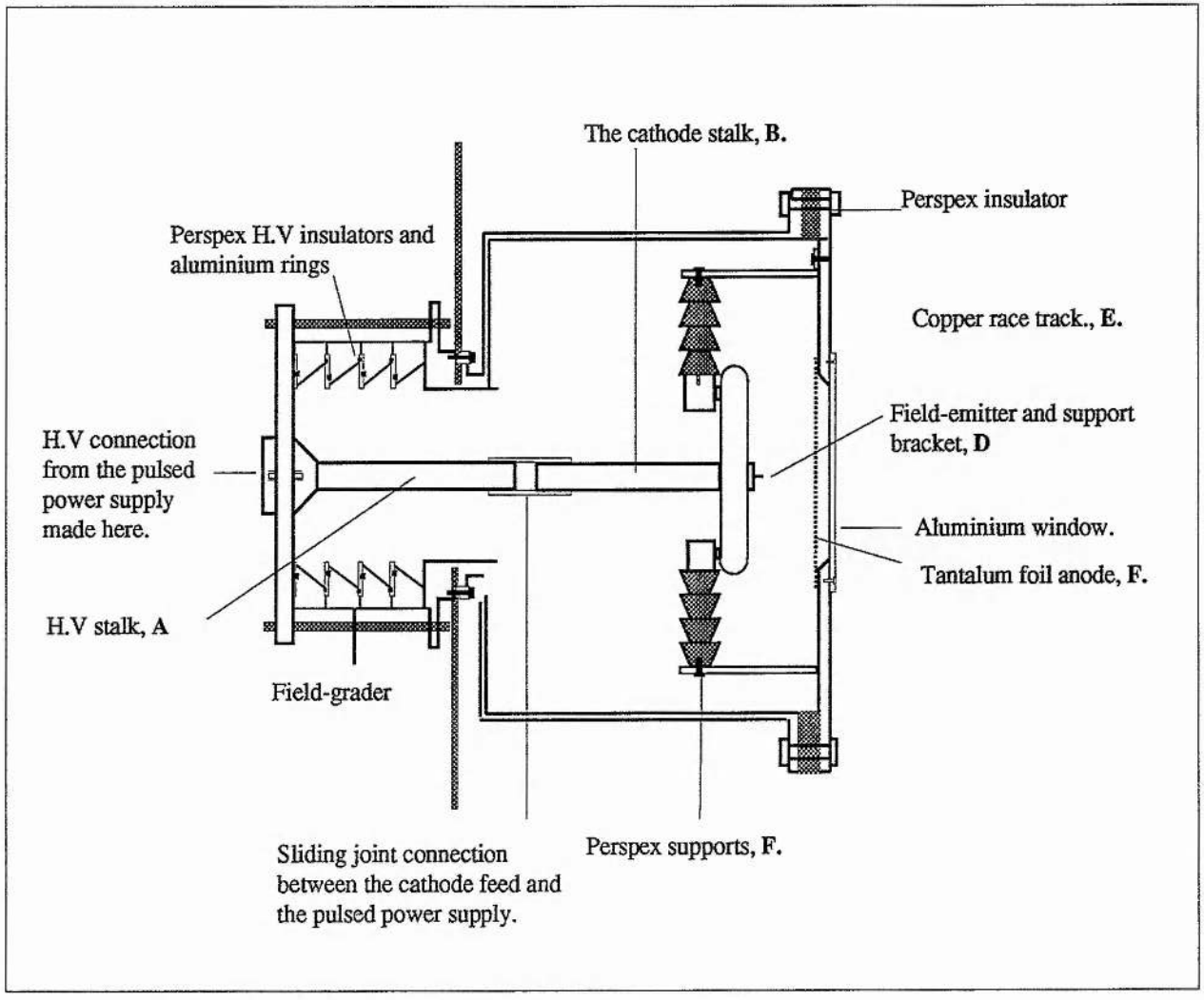

Figure 3.1.4 :- Schematic diagram of the e-beam diode .

array of 100 pins each spaced 1cm apart. The copper tubing, **E**, that surrounded C is called a "race track" and this reduced any field enhancement at the edge of the cathode support plate and focused the electron beam. The anode, **F**, which was made from 7μm of tantalum foil backed with aluminium foil, was electrically connected to the front plate of the x-ray generator window, **G**, with a silver loaded epoxy adhesive. The four perspex supports, which can clearly be seen at the ends of the copper race track in photograph 3.3, were used to connect the cathode assembly to the front plate with a sliding screw bracket. This bracket enabled the anode/cathode (A-K) spacing, and hence the diode impedance, to be carefully controlled. The x-ray window was constructed from a 100 cm x 8 cm x 0.1 cm aluminium plate and a Habachi style grill. This grill prevented the aluminium from flexing due to the pressure differential between the vacuum chamber and the atmosphere.

Details of the Pulsed Power Supply.

3.2. The Blumlein Circuit.

It is difficult to produce a lumped element Blumlein circuit that can operate into 6.25Ω* load because this is less than the low impedance limit imposed by the self inductance in the capacitor leads and other inter-connections. Consequently, the voltage pulse was produced paralleling two 12.5Ω circuits together (see figure 3.2.1). These were each constructed from 20 LC stages using 105nH air-cored inductors and TDK type K105 capacitors rated at 2.7nF at 35kV. These

* For the capacitors used the required inductance for this line was 28nH. This was difficult to achieve, even using parallel plate inductors.

capacitors are made from strontium titanate, which is a polar dielectric material whose permittivity remains constant over the stipulated operating voltage range. The capacitors were DC charged to 30kV using a Hartley Measurements capacitor charging unit (200J/s) and a 100kΩ high power wirewound charging resistor. When fully charged they stored a total of 48.6 Joules.

3.3. The Thyratron Switch.

It was decided to switch the Blumlein circuits with hydrogen thyratrons because these are highly reliable long life devices with good switching characteristics and, unlike the spark-gap, they can operate without an external gas supply. The particular thyratron used was the CX 1685. This is a deuterium filled tetrode device originally designed for use in $C0_2$ gas laser systems. It is constructed from glass, has dimensions of 213mm x 65mm and contains an x-ray shield that screens the user from x-ray emission from the 10 cm long molybdenum anode stem. The maximum voltage it can be operated at is 35kV and the fastest it can switch is 80kA/μs. Further information concerning these thyratrons can be found in the manufacturers preamble, which is reproduced in Appendix C.

Design of the Thyratron switch :- In order to produce a uniform electron beam field at the cold cathode field emitter the voltage pulse had to have a dV/dt of at least 6kV/ns or a risetime of 17ns. This meant that each Blumlein circuit had to be switched at 282kA/μs. 3 and 4 CX 1685s thyratrons are required to produce this rate of rise of current but only two were available at the time of construction. This limited the output risetime to about 60ns and meant that a degree of non-uniformity in the x-ray flux had to be tolerated. These two thyratrons were

connected to the Blumlein circuits using low inductance feeds, the earth return to the cathode flange being made from aluminium sheet. The heater and reservoir circuits were operated at 12A at 6.3V and 2A at 6.8V using a simple mains transformer without any form of regulation. Operating the reservoir voltage at this level sets the thyratron breakdown voltage at the operational voltage of the circuit. This is necessary to obtain the maximum switch performance.

Details of the Thyratron Trigger Unit :- The CX 1685 can be triggered using a DC primed or pulse primed circuit. For DC priming grid 1 must be supplied with a current of 10 to 150mA from a DC source of about 100V[3]. In addition, a hold-off voltage of -150V is required on grid 2 to prevent any high energy electrons produced by thermionic emission at the cathode and/or field emission from the grids from switching the tube prior to the application of the trigger pulse to grid 2 (prefire). Under these biasing conditions the tube is switched by applying a 200 - 1000V voltage pulse to grid 2.

Pulse priming simplifies these requirements because only a single drive pulse and negative DC bias is required. However, the trigger unit must have an output impedance less than 250Ω and the trigger pulse an amplitude of over 500V. This particular approach was used to switch both thyratrons and a diagram of the trigger unit used is shown in figures 3.3.1. A brief explanation of how it works is presented below.

The -150V hold-off bias voltage was obtained by rectifying and smoothing the output of the centre tapped transformer, T_3, which was connected to the secondary windings of the output transformer, T_4. The output voltage pulse was

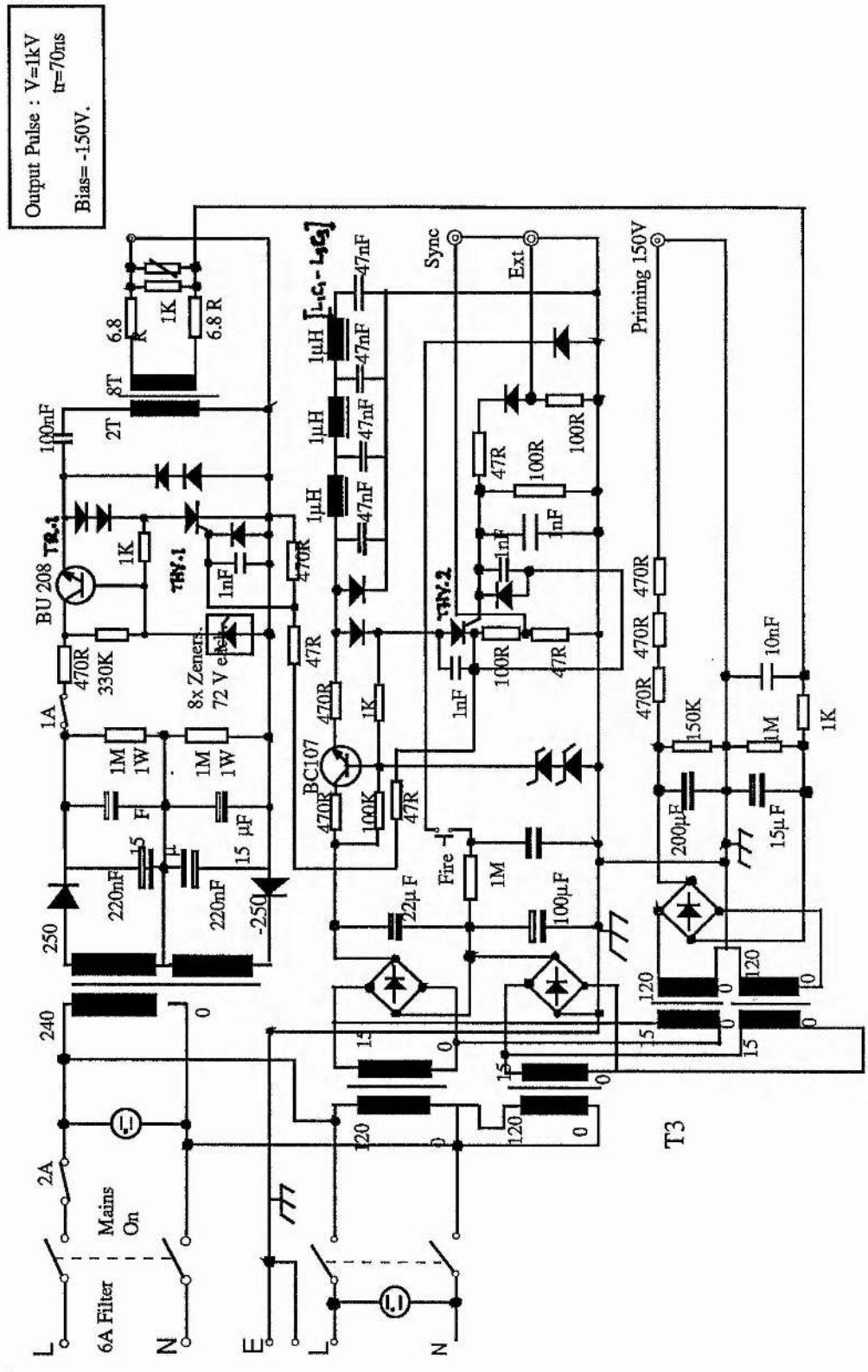

Fig 3.3.1 :- Thyratron Trigger Circuit.

produced by switching the charge voltage on the 100nF capacitor, C_1, across the primary of the 1:4 step-up transformer T_4 using a thyristor switch, THY1. THY1 was in turn switched by discharging a 3-stage PFN (components L_1C_1, L_2C_2 and L_3C_3) using a second thyristor, THY2. Since C_1 was initially charged to about 300V, the trigger unit was capable of producing an output voltage pulse of 1kV, with a risetime of 100ns into a matched load of 70Ω. Transistor TR1 was required to isolate THY 1 from the charging circuitry to prevent "latch-up".

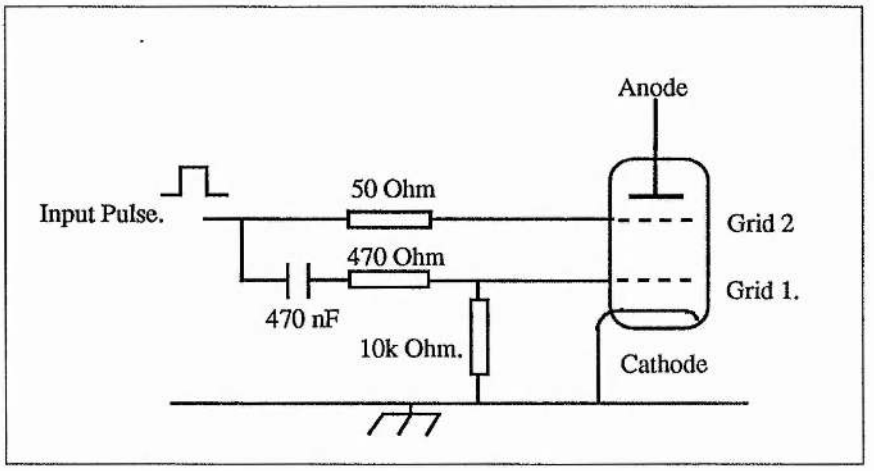

Fig. 3.3.2 :- Details of the thyratron grid drive circuitry.

The trigger pulse from the trigger generator was fed to the thyratrons using two lengths of coaxial cable. These lengths were different because they had to compensate for the different anode delay times, t_a, of the two tubes. This is the time it takes for a thyratron to conduct current after the gas has broken down in the grid region. Compensation was achieved when the propagation delay time, t_p, plus the anode delay time, t_a, was the same for both thyratrons. The coaxial cable

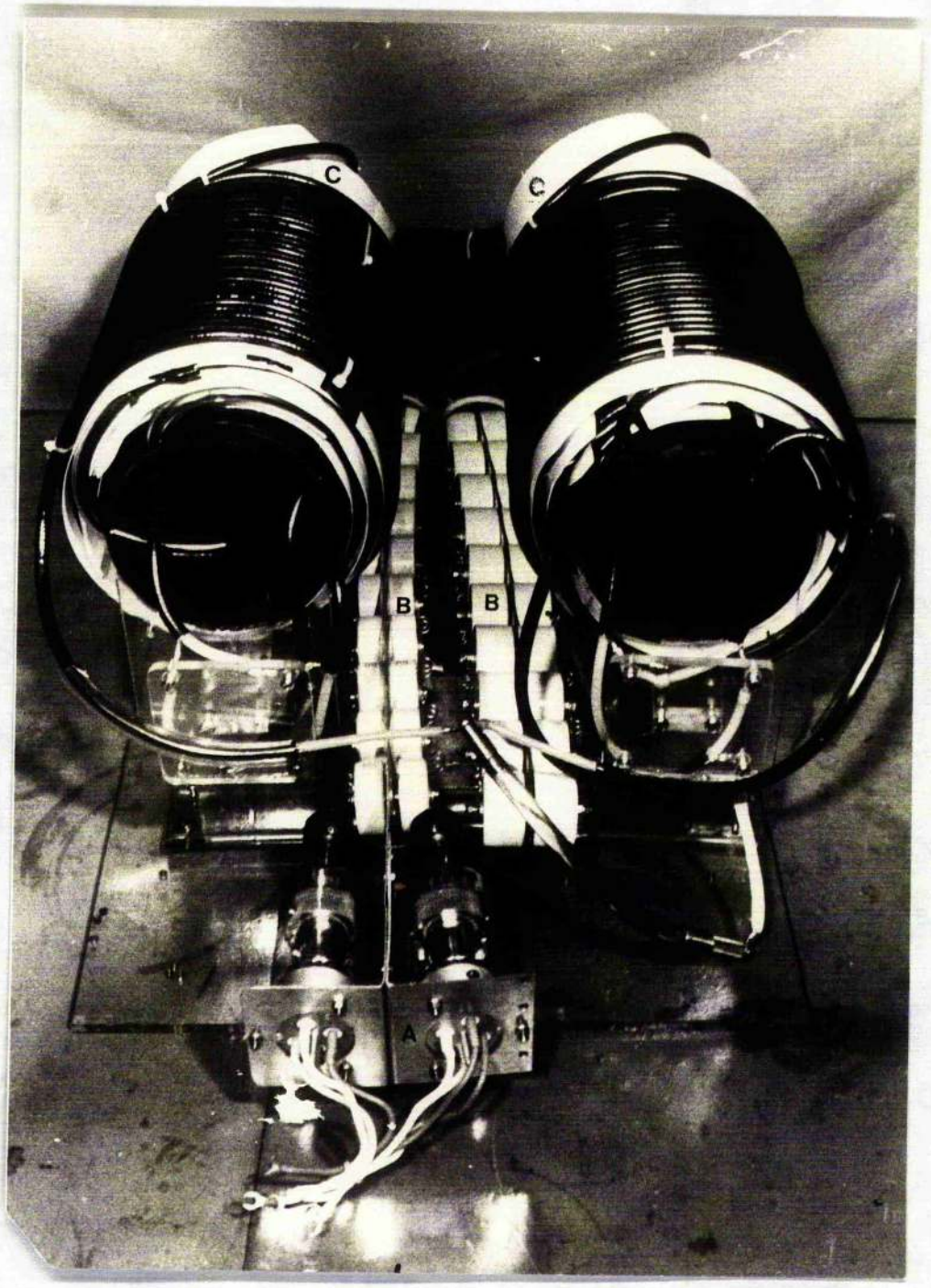

Fig 3.4.1 :- Photograph showing the front view of the pulsed power supply shortly before final assembly. The two thyratrons are situated at the front of the photograph (**A**). The two Blumlein circuits (**B**) lie inbetween the two TLTs (**C**). The individual stages that comprise the TLT can be seen inbetween the Mylar insulation.

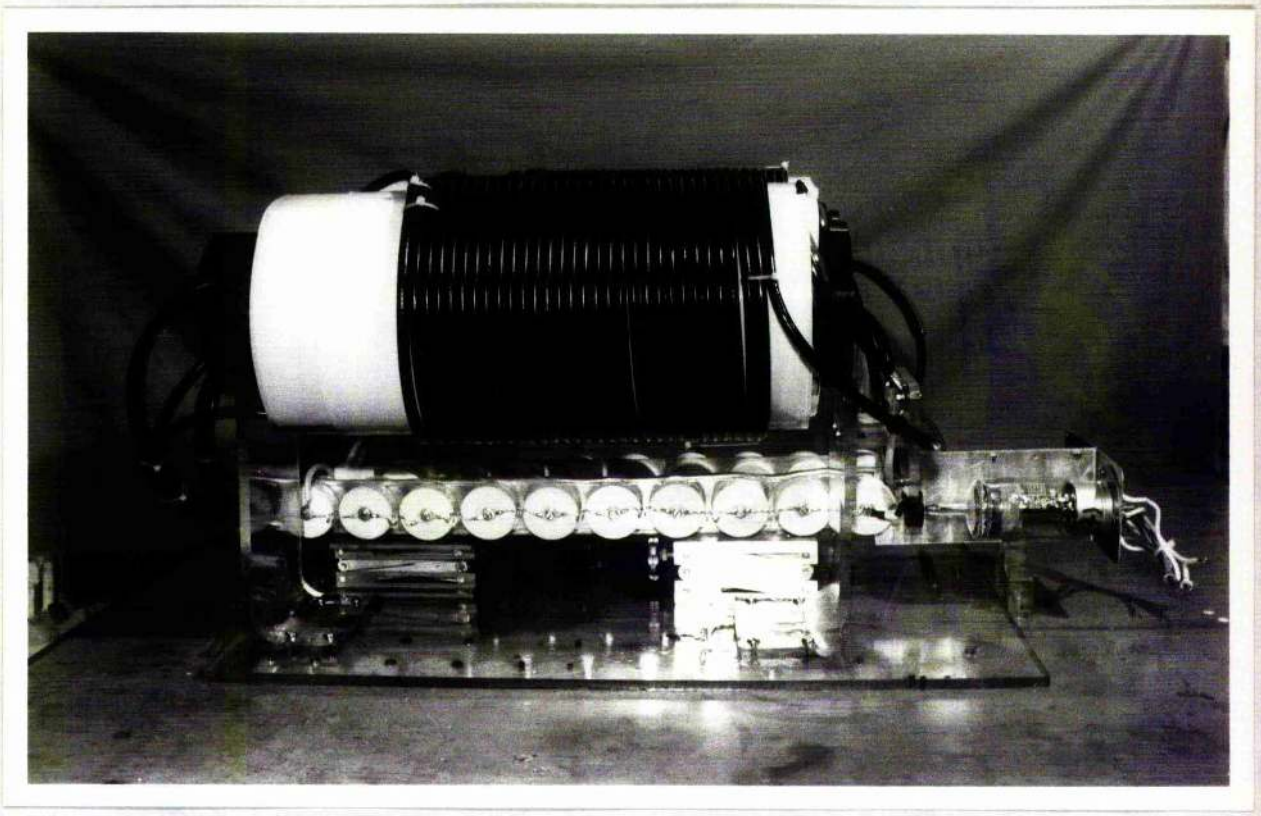

Figure 3.4.2 :- Side view of the TLT pulsed power supply. The two Blumlein circuits are supported on labjacks because this photograph was taken shortly before final assembly.

was terminated by the grid drive circuits. These were just 470Ω/10kΩ resistive voltage dividers and 470nF, 1.5kV polypropylene capacitors. The capacitors isolated grid 1 from the DC bias.

3.4. Assembly of the TLTs and the Pulsed Power Supply.

The HV TLTs used in the pulsed power supply were constructed in almost the same way as the low voltage mutually wound ones described in section 2.4. The former was simply a 6" x 25" piece of plastic piping that had been cleaned and smoothed to remove any sharp edges. It was wrapped in a 750μm thick layer of Mylar insulating film. The first stage of the TLT was assembled by winding a 25m length of the HV coaxial cable, type URM 67, carefully on top of this Mylar with a uniform pitch. The last 18" length of this cable was threaded through two holes that had been drilled at either end of the pipe and pulled tight. These served as "anchor points" i.e. they prevented the cable from working loose after assembly. The TLTs were completed by adding layers of Mylar in between the windings of the 2nd, 3rd and 4th stage cables. The finished TLTs can be seen in the photographs of the pulsed power supply in figures 3.4.1 and 3.4.2. They were supported on two perspex supports and their input terminals connected directly to the outputs of the Blumlein circuits. The thyratron heater and reservoir transformers and the grid drive circuits have been omitted for clarity but were positioned to the left of the Blumlein circuits.

3.5. Performance of the Pulsed Power Supply.

When the pulsed power supply was tested, it was operated in air at 1Hz (the limit of the charging unit) and into a 100Ω copper sulphate resistive load. The voltage waveforms it produced were measured at the input and output of the TLT

with copper sulphate voltage probes and a Tektronix 519 oscilloscope. The 519, which was used consistently throughout the work described in this thesis, is an ideal instrument for fast high voltage work for a number of reasons. Firstly, the vertical deflection system, which contains no pre-amplifier, is designed along transmission line principles and is capable of measuring extremely fast risetimes, down to 0.3ns. Secondly, it is a valve driven instrument so small transients induced in the circuits by electromagnetic pick-up have little effect on it's operation.

Figures 3.5.1 and 3.5.2 show the input and output voltage waveforms produced during testing.

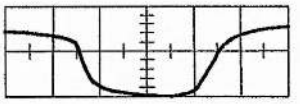

Fig 3.5.1:- Input pulse waveform to the TLT. 20kV/Div ; 100ns/Div.

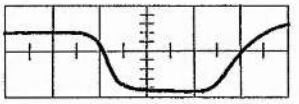

Fig 3.5.2:- Output waveform from the TLT into 100Ω load. 75kV/Div ; 100ns/Div.

At the full charge voltage the output pulse from the Blumlein circuit, shown in figure 3.5.1, had an amplitude of 28kV, a risetime of about 50ns and a duration

of 230ns. The pulse at the 100Ω load was identical except it had an amplitude of 94kV, corresponding to a gain of 3.3. This gain could be varied by altering the charging voltage and the pulse duration by changing the number of stages in the Blumlein circuit. The 125ns delay between the pulse risetimes was caused by the propagation delay through the transmission lines.

The Design of the Flash X-ray Generator.

3.6. Assembly and Operation of the Flash X-ray Generator. Diagnostics.

The x-ray generator that incorporated the TLT pulsed power supply was mounted on a movable metal table so that it could be accurately aligned with a laser cavity or used as an independent test facility. Before the x-ray generator was first used it was necessary to (i) coat the cathode assembly with a solution of 50% diffusion pump oil and 50% acetone to suppress field emission on all the non-emitting sites (ii) condition the field emitter by firing the generator until there was no noticable jitter on the cathode voltage signal when viewed on the 20ns/division time base on the 519 (ii) optimise the x-ray generator. This was achieved by varying the anode cathode spacing (and hence the diode impedance) until a peak cathode voltage of 100kV and a maximum x-ray dose was obtained. These dose readings were made using Quartz Fibre dosemeters (R.A.Stephen, calibrated to measure 0-200mR) positioned at the far left (position 1), the far right (2) and the centre (3) of the x-ray window. They were cross checked with a Vinton Instruments Model 37D3 ionisation chamber. The uniformity of the x-rays across

the window was measured using an x-ray fluorescent screen* and a video camera. This set-up was particularly useful because the video could be paused at the point of fluorescence and the variation in intensity across the x-ray window compared with the absolute measurements obtained using the dosemeters. No measurements were made to detect line radiation because at voltages around the 100kV level any L radiation produced is immediately reabsorbed in the tantalum foil anode and the spectrally integrated intensity of the K radiation is at least 2 orders of magnitude less than that of the continuous spectrum[7]. The voltage measurements were made using a standard copper sulphate voltage probe and a 519 oscilloscope.

Results :- In this particular system optimum performance was achieved with an A-K spacing of 38mm. The cathode voltage is shown in figure 3.6.1.

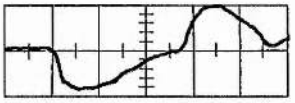

Fig 3.6.1 :- Voltage Pulse across the e-beam diode. 100 ns/div; 113 kV/div.

To analyse this waveform it is convenient to divide it into three distinct time intervals, 0 - 50ns, 50ns - 250ns and 250ns - 500ns.

0 - 50ns :- During this period the field emitted current was generated, the micro-protrusions on the pin array cathode vapourised and the plasma formed.

* These contain a number of rare earth elements activated with terbium and they fluoresce in the visible part of the spectrum when excited by x-rays.

No detectable current flowed because the diode impedance is high during field emission[4]. The peak voltage on the cathode after 50ns was over 90kV.

50ns - 250ns :- Space charge limited current flow and plasma expansion occurred during this time interval. This resulted in a fall in the diode impedance and cathode voltage. Steyer[5] has shown that this impedance varies as :-

$$Z(t) = K\, t^{-\alpha} \qquad 3.6.1.$$

where α is between 2 and 3.

The diode response time, t_{diode}, or the time interval between the application of the voltage pulse and the space charge limited current flow is dependent on many factors including the dV/dt of the voltage pulse, the cathode material, the field, and the output impedance of the pulsed power supply. Attempts were made to measure it using a current viewing resistor in the x-ray generator but the resulting waveform was swamped by noise and provided no useful information.

250ns - 500ns :- The voltage reversal that occurred after 250ns was due to the negative voltage step at the end of the voltage pulse.

The x-ray dose produced by the x-ray generator is plotted as a function of distance in figure 3.6.2.

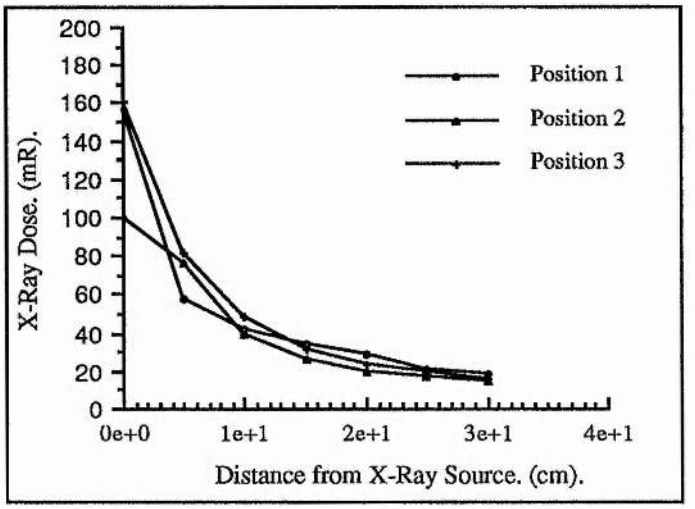

Fig 3.6.2 :- Plot of x-ray Attenuation in air at 3 different positions on the x-ray window. The shot to shot reproducibility of the integrated x-ray dose, measured over 100 shots was to within 7%.

Note that the dose at the surface of the x-ray window was less at position 2 than at 1 and 3. This was in accordance with the visual results obtained with the fluorescent screen and was probably a consequence of the low dV/dt that was produced by the pulsed power supply. Note also that the x-ray dose appears to become more uniform with distance from the generator. This is because the x-rays were scattered as they propagated through the air. Brown[6] and Steyer and Voges[7] have shown that this fall in x-ray intensity varies as $1/r^n$ where r is the distance from the x-ray window. N is equal to 0.5 or, at distances greater than 15cm, 1.2. No x-ray flux were detected at distances greater than 2m from the generator.

3.7. Performance of the Flash X-ray Generator as a Preionisation Source.

The x-ray generator was used to operate a mercury bromide laser[6] with an active region that measured 5 cm x 3.5 cm x 100 cm. Since mercury bromide is a solid at room temperature, it was necessary to enclose the laser in an oven and operate it at a temperature of 200^0C. The closest the x-ray generator could be positioned to the laser with the oven in position was 25cm. At this distance the dose in the active region was 5mR, sufficient for the preionisation for this type of laser.

During operation the variation in the output energy from the laser was measured as a function of x-ray dose by varying the amplitude of output voltage from the pulsed power supply from a few kilovolts up to the maximum output voltage. This would have been difficult to do with a Marx generator type pulsed power supply. The two photographs shown in figures 3.7.1 and 3.7.2 show the laser discharge taken with an x-ray dose of 0 and 5mR in the laser cavity (i.e. with and without preionisation). The x-rays suppressed streamer formation and produced a uniform glow discharge and a peak output pulse energy of 710mJ per shot (pulse width 92ns FWHM). This represented an energy extraction efficiency of 0.5 J/litre at an overall efficiency of 1.5%. This is the second largest energy output that has been achieved from a discharge pumped mercury bromide laser system to date. A more detailed analysis of the results from the point of view of the laser performance is given in reference 6.

Fig :- 3.7.1 :- Photograph showing the discharge from the mercury bromide laser without x-ray preionisation. The individual streamers are clearly visible.

Fig 3.7.2 :- Photograph of a high pressure glow discharge. The photograph was taken immediately after that shown in figure 3.7.1, but with x-ray preionisation. The dimensions of the discharge are 3.5 cm x 3.5 cm.

3.8. Comment on the Performance and Design of the Pulsed Power Supply.

An analysis of the mutually wound TLT has shown that it can produce pulse risetimes of 8ns at high repetition-rates, the limit being determined by heating caused by loss in the transmission line dielectric. This performance level was not achieved because of the limitations of the pulse generator. Most TLTs have a low input impedance because of the N^2 impedance transformation and a fast, high repetition rate low impedance pulse generator requires powerful capacitor charging units and a high dI/dt switch. In this circuit, the pulse generator had to be matched into 6.25Ωs even though the load impedance was 100Ω and the 200J/s capacitor charging unit and CX 1685 thyratrons were only capable of producing a 1Hz repetition-rate and pulses with a 60ns risetimes. This risetime was further limited by the Blumlein circuits. Any LC network has a limited bandwidth because the linear phase response, β, changes from 0 to π and attenuation coefficient, α, increases from 0 as the frequency components of a propagating wave approach a cut-off frequency, f_c (see figure 3.8.3).

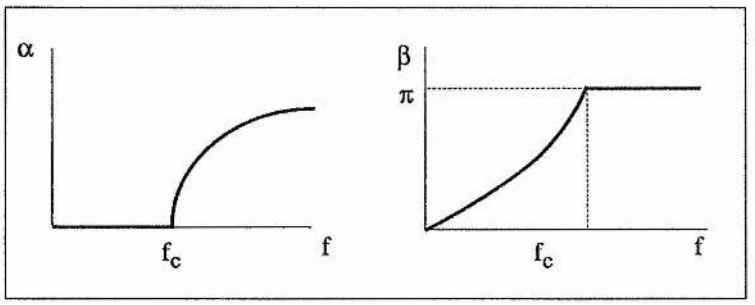

Fig 3.8.1 :- Variation of attenuation coefficient, α, and the linear phase response, β, in a lumped element transmission line [8].

This cut-off frequency is given by[8] :-

$$f_c = 1/2\pi(LC)^{1/2}. \qquad 3.8.1.$$

and the minimum output risetime by[9]: -

$$t_r = (N\,L\,C)^{1/2} \qquad 3.8.2.$$

For Blumlein circuits constructed with values of L =105nH and C= 2.7nF the minimum 10 - 90% risetime that is possible is 53ns. This figure, which is in agreement with the experimental results, illustrates two important points. Firstly, there is no use using a switch that can produce pulses faster than the bandwidth of the line and secondly, distributed lines are required to produce pulses fast enough to determine the risetime limit of a TLT.

The large physical size and weight of the pulsed power supply was a consequence of two features of the design, the need to parallel two Blumlein circuits and the heavy mechanical construction of the coaxial transmission lines. Smaller pulse generators can be built using high permittivity ceramic tiles and TLTs using lightweight striplines. A ceramic tile Blumlein circuit and a stripline TLT is described in chapters 4 and 5.

3.9. Summary Of Chapter 3.

This chapter has described the construction of a 100kV pulsed power supply that incorporated a mutually wound TLT. It has explained how the TLT was constructed and shown that it was able to accurately reproduce an input pulse

waveform at the output and produce a gain of 3.3. It has also shown that it can be used in an x-ray generator for the preionisation of a mercury bromide laser.

References

1). M.Osborne ; Ph.D Thesis, Imperial College London, Chapter 2, (1985).

2). A.Brown and P.W.Smith ; "Multi-Paralleled Thyratron, Repetitively Pulsed Power Supply for a High Power Gas Lasers", Proc. Seveteenth Modulator Symposium, Seattle, June, (1986).

3). E.E.V. Data Book ; E.E.V. Ltd, Chelmsford, England.

4). Parker et al. ; J.Appl. Phys., Vol. 45, No.6, (1974).

5). M.Steyers ; J. Phys. D.; Appl. Phys., **23**, (1990).

6). A.Brown ; Ph.D Thesis, Univ. St. Andrews, (1988).

7). M. Steyer and H. Voges ; Appl. Phys. Lett., No. **42**, p149, (1987).

8). B.I.Bleany and B.Bleany ; Electricity and Magnetism, p264. Oxford Univ. Press. (1976).

9). A.R.Owens and G.White ; "Generation of High Speed Waveforms Using Nonlinear Delay Lines", Proc. IEE, Vol. 113, No.11, (1966).

CHAPTER 4.

High Permittivity Ceramic Tiles for use in the Construction of Compact Pulse Generators for TLT Pulsed Power Supplies.

4.0 Introduction.

This chapter reports on an investigation that developed high permittivity barium titanate ceramic tiles for use in the construction of compact, low impedance pulse generators. It is included in this thesis because a compact pulse generator design can greatly reduce the size and weight of a TLT pulsed power supply.

4.1. Dielectric Materials for use in Pulse Generators.

In order to construct a compact, low impedance pulse generator it is necessary to use distributed transmission lines (PFNs have a relatively high impedance because of the inductance of the capacitor leads and other inter-connections; paralleling them makes the generator heavy and bulky and the extra circuit components reduces their reliability).

Probably the simplest and easiest way to construct a distributed transmission line is to use a parallel-plate geometry, the characteristic impedance, Z_0, and propagation delay time, T_D, of which is :-

$$Z_0 = \frac{377}{(\mu_r \varepsilon_r)^{1/2}} \frac{s}{w} \quad * \qquad 4.1.1.$$

and

$$T_D = 3.3\ \mu_r \varepsilon_r^{1/2} l \text{ ns.} \qquad 4.1.2.$$

where s the thickness of the dielectric, w the line width, l the length, ε_r the relative permittivity and μ_r the relative permeability of the dielectric that is used as the propagating medium for the electro-magnetic wave. If $\mu_r = 1$ (no magnetic materials) the dielectric must satisfy the following conditions :-

1). It must have a high relative permittivity to maximise the energy storage capability of the line at modest voltages and, because of the form of equations 4.1.1 and 4.1.2, keep its physical size to a minimum.

2). A high breakdown strength to enable it to be charged to the required potential, to reduce breakdown problems and keep the parameter s to a minimum.

3). Electrical properties that remain constant with variations in temperature, voltage, current, frequency and mechanical stress.

4). A low loss (small tanδ), exhibit no resonance points and have a constant permittivity over a large bandwidth (under such conditions the phase velocity will equal the group velocity at all frequencies of interest).

5). A high mechanical strength, a low conductivity and cost.

---

* This equation holds when s<<w.

There is no dielectric material available that can satisfy all these conditions, particularly when pulse durations of a few hundred nanoseconds are required. For instance, thin insulating films such as Mylar and Kapton[1,2] have a relative permittivity that is too low and water, with an ε_r of 80, has to be continuously de-ionised and de-aerated and even then a 200ns line can be over 3m in length! [3,4]. The reason why barium titanate tiles are of interest is because they can have a relative permittivity of several thousand, a feature that enables the dimensions of an equivalent water line to be reduced by a factor of about five.

4.2. Barium Titanate Ceramic Tiles* .

Figures 4.2.1 and 4.2.2 are photographs of some barium titanate tiles that have been prepared by a company called Morgan Matroc Ltd, Stourport, England and figure 4.2.3 shows the accompanying data sheet. They measure 7.5cm x 7.5cm x 2.5cm, weigh 805g and are made using a K2100 dielectric mix, 2100 being its low voltage, low frequency relative permittivity. They are square shaped and metallised on their upper and lower surface so they can be fitted together to form a neat compact transmission line.

4.3. Temperature Dependence of the K2100 Tiles.

The temperature dependence of ε_r is an important parameter because in low impedance, high repetition rate pulse generators any energy dissipated as loss in a dielectric produces heating. If ε_r is a strong function of temperature, it can

* Details concerning the properties of barium titanate can be found in references 5 to 10.

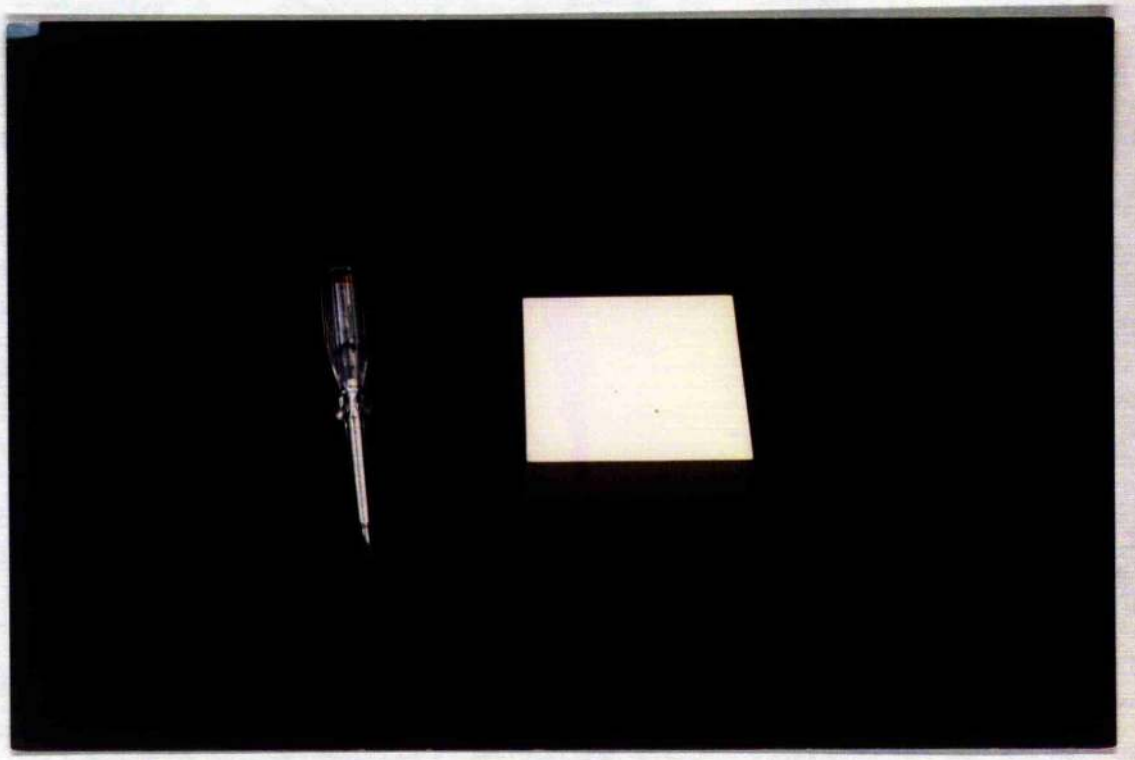

Figure 4.2.1 :- Photograph showing a single K2100 ceramic tile. It has dimensions of 7.5 cm x 7.5 cm x 2.5 cm.

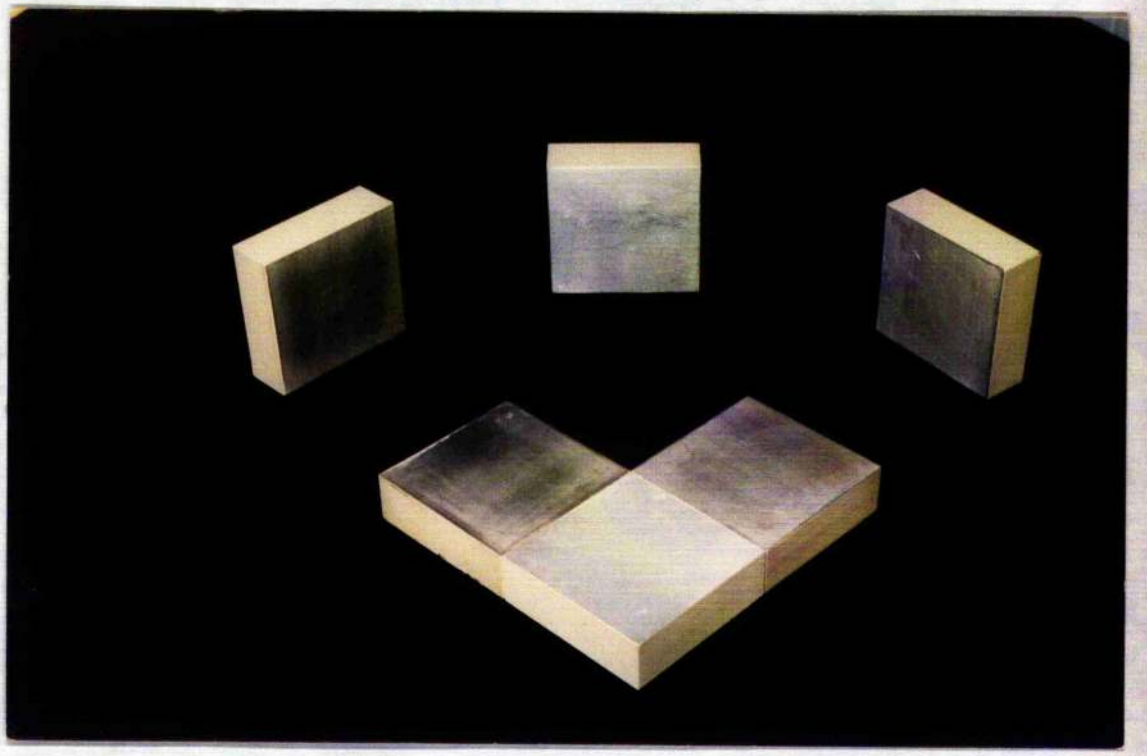

Figure 4.2.2:- Photograph showing a number of K2100 tiles.

Property.	Dielectric Type.	
	(K2100).	(K3500).
Colour	Yellow.	Brown.
Permittivity at 20^0C; 1kHz; 1V (10%).	2100.	4300.
" " 1MHz.	1900.	3900.
" " 50Hz; 0.35kV/mm.	3000.	5200.
Dissipation factor at 20^0C; 1kHz; 1V.	1.8%.	0.6%.
Insulation resistance at 20^0C; MΩ/μF[1].	500.	300.
Aging Rate ; 20^0C[2].	-2.5%.	-3.5%.
D.C dielectric breakdown strength; kV/mm.	8.	7.
Effect of an applied D.C stress of 2kV/mm on the incremental permittivity[3].	-25%.	-65%.
Permittivity/temperature characteristics; 1kHz (I.E.C 187 catorigisation)[4].	2B2.	2E4.
Flextural strength; Mpa.	120.	90.
Density; grams/cc.	5.6.	5.5.
Coefficient of linear expansion; (0^0C to 600^0C) p.p.m/^{0}C[5].	11.0.	10.9.

Figure 4.2.3 :- Comparison of the typical properties of the K2100 and K3500 dielectric materials.

Notes.

1). Product of a D.C insulation resistance and 1kHz capacity value for a given capacitor.

2).Loss capacitance value with time, expressed as a percentage over logarithmic decades of time. The figures of the permittivity quoted in the table are 100hrs (2 decades aged).

3).Applicable for test pieces 0.5mm thick.

4). 2B2 >10% variation from the 20^0C figure over the temperature range - 55^0C to 85^0C.

2E4 > +20% variation over the same temperature range.

5). Applicable to rods 5mm in diameter.

produce a change in the electrical properties of the pulsed power circuit with possibly serious consequences (e.g thermal runaway). Barium titanate tiles present a particular problem in this respect because they exhibit a dramatic change in ε_r at the Curie temperature, T_c.

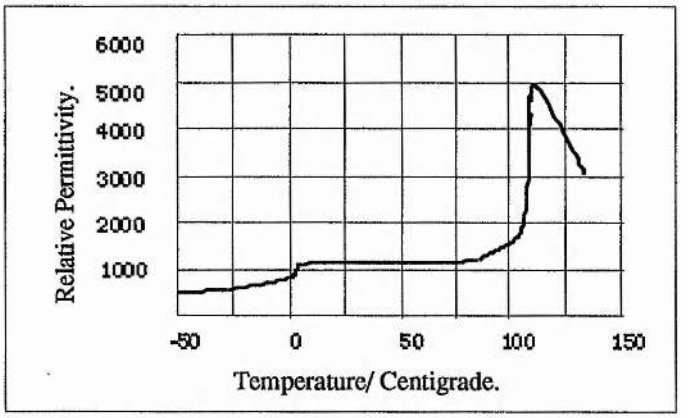

Fig 4.3.1 :-Temperature dependence of the relative permitttivity of $BaTi0_3$ (measured at 400 kHz; zero bias)[11].

The temperature/ε_r curve of pure $BaTi0_3$ shows this (see figure 4.3.1). Between 35^0C - 100^0C it has a tetragonal structure and an ε_r that remains constant at 1400. This is high because (i) the centre of charge in each unit cell is loosely bound; it can therefore be easily displaced from its geometric centre to form a dipole (ii) adjacent dipoles couple to form domains. Near T_c ε_r changes by 70% of its maximum value over 11^0C as it undergoes a transition to a Perovskite. Above T_c it is in the paraelectric phase and then ε_r varies according to the Curie-Wiess law :-

$$\varepsilon_r = \frac{C}{T - T_c} \qquad 4.3.1.$$

where C a constant that is dependent on the material, T the temperature (^{0}C) and T_c the Curie Temperature.

It is desirable to be able to taylor these thermal properties to meet the requirements demanded by a specific device application[12]. For example, a tile may be required to have a value of ε_r of over 3000 at a specified temperature of say 22^{0}C or, alternatively, a constant ε_r of 2000 over a temperature range of 0^{0}C - 100^{0}C may be required. Tailoring is achieved by adding certain modifying agents to the dielectric mix at the pre-milling stage during tile manufacture. For example[12], one percent of strontium can translate the permittivity peak by 4^{0}C down the temperature scale whereas 9% of calcium zirconate can broaden it out and give an ε_r of 7000 at 65^{0}C with a width of 60^{0}C at 70% of the maximum.

The effect modifying agents have can be seen by comparing the temperature/ε_r characteristics of pure barium titanate with that of a K2100 tile and another, the K3500 tile manufactured by the same company (see figures 4.3.2 and 4.3.3). Note that a K3500 tile has an ε_r of 4500 at 20^{0}C that falls fairly linearly with temperature, i.e. at 90^{0}C it is down by over 50%. This permittivity peak has been shifted to room temperatures so above 25^{0}C the tile is in the para-electric phase. In contrast, a K2100 tile peak has been both shifted to lower temperatures and broadened out. The result, a value of ε_r of over 2000 that remains constant to within 5% of this value up to 90^{0}C and a tile that fairly well suited for high

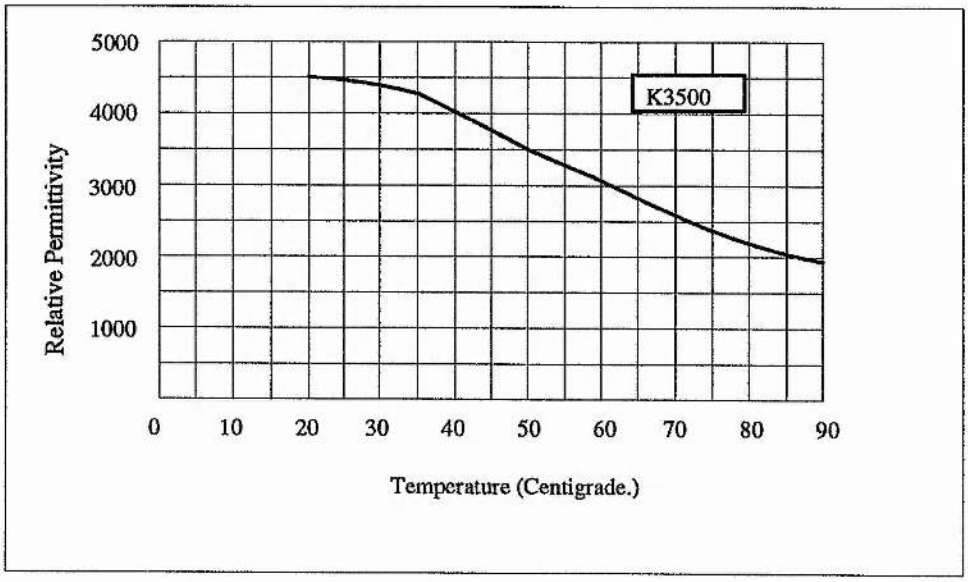

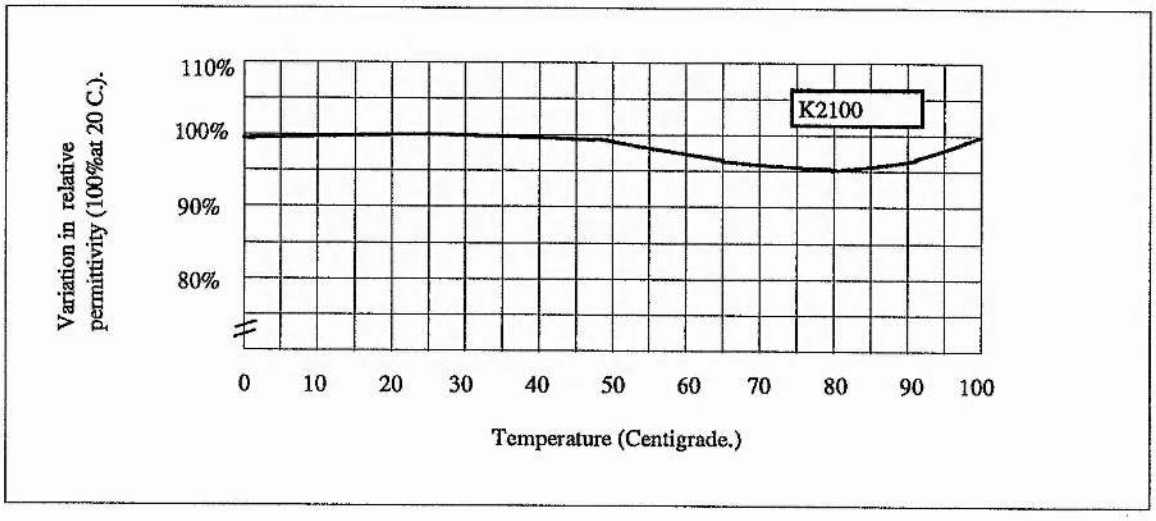

Figure 4.3.2 and 4.3.3. :- Temperature/ relative permittivity curves for K3500 and K2100 dielectric measured at 1 kHz, 1V/5V.

repetition rate pulsed power systems, or for applications where the ambient temperature may be subject to variations.

4.4. The Variation in Relative Permittivity due to Electrical Stress.

In most cases the relative permittivity of a $BaTi0_3$ tile falls with the electric field strength, E. Johnson[13] has shown that $\varepsilon_r(E)$ is approximately given by :-

$$\frac{\varepsilon}{\varepsilon_0} \approx \left[1+a\varepsilon_0^3 E^2\right]^{-1/3}. \qquad 4.4.1.$$

where a is a constant and E the applied DC electric field.

This effect has also been investigated by many other people. Devonshire[14], for example, has tried to explain it using a thermodynamic theory and Diamond[15] has attributed it to an induced ferroelectric state rather than domain processes. A discussion on the dependence of the permittivity of $BaTi0_3$ ceramics with applied electrical stress together with the influence of piezo-electric and anisotropy effects has also been published by Marutake and Ikeda[16] and Uchida and Ikeda[17]

There are two main reasons why the field dependence of the relativity permittivity is important. Firstly, if it is not a constant the velocity, v, of an electromagnetic wave, given by : -

$$v = \frac{1}{(\varepsilon_0 \varepsilon_r(E))^{1/2}} \qquad 4.4.2.$$

becomes amplitude dependent and this can can distort the pulse profile. The nature of this distortion depends on whether the tile is being used in a simple transmission line or a pulse generator. The difference matters. A transmission-line is initially uncharged and so a fall in permittivity with field produces a velocity of propagation that is faster at higher signal amplitudes than at lower ones. This sharpens up the leading edge and smears out the trailing edge. A pulse generator such as the Blumlein circuit is, on the other hand, initially charged and so the process is different, the trailing edge is sharpened.

The fall in ε_r with field can also produce "energy storage saturation", particularly when it is sufficient to offset the increase in stored energy produced by the rise in charge voltage. Matsumoto et al.[18] have investigated this effect by comparing the performance of some unspecified $BaTiO_3$ and $SrTiO_3$ capacitors in a CO_2 gas laser LC inversion circuit. This revealed that $BaTiO_3$ capacitors are sometimes inferior to the $SrTiO_3$ titanate ones because their relative permittivity can decrease by as much as 50% of the initial unstressed value at fields of 1.5kV/mm. The corresponding figure for the $SrTiO_3$ titanate capacitors was 1%. Ogura et al.[19] have made a similar study using a 2.6MV coaxial Marx type generator and they also conclude that nonlinear $BaTiO_3$ capacitors are unable to store energy as efficiently as $SrTiO_3$ capacitors at high voltages.

When choosing a tile for a given application it is important to have a prior knowledge of the field dependency of its relative permittivity. This can be easily measured using the circuit shown in figure 4.4.1.

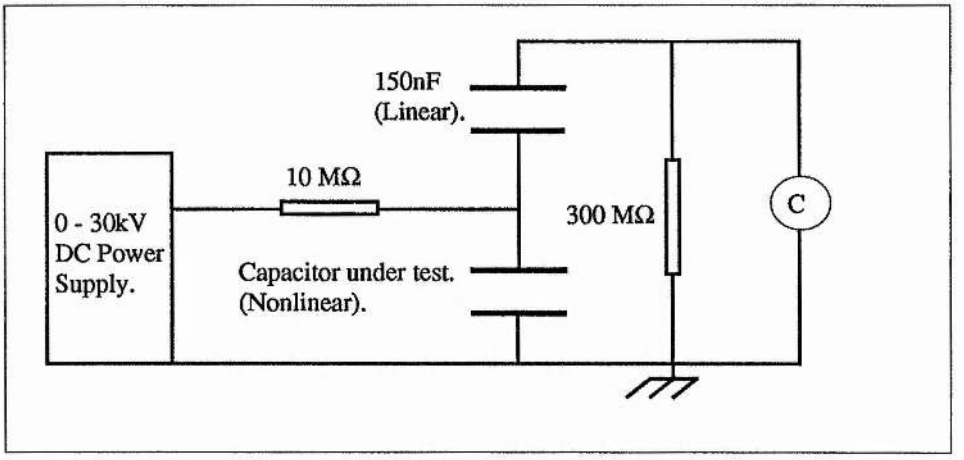

Fig.4.4.1 :- Circuit diagram of the test equipment used to determine the variation in the permittivity of the ceramic tiles with charge voltage.

Capacitor C_1 is a linear 50kV Maxwell HV capacitor rated at 150nF, the power supply a Wallis 0-30kV device and the digital capacitance meter an RS type CM 20A. This experiment measures the "differential capacitance" because the test voltage generated by the capacitance meter, v, is alot less than the DC charge voltage, V. This differential capacitance, $C_2(v)$, is determined by first measuring the total series capacitance, C_T, for charge voltages in the range of 0 - 30kV and then substituting the appropriate values in the equation :-

$$C_2(v) = \frac{C_1 C_T}{C_1 + C_T} \qquad 4.4.3.$$

When the K2100 and K3500 tiles were tested using this experimental arrangement, the following results were obtained (see figure 4.4.2).

When the K2100 and K3500 tiles were tested using this experimental arrangement, the following results were obtained (see figure 4.4.2).

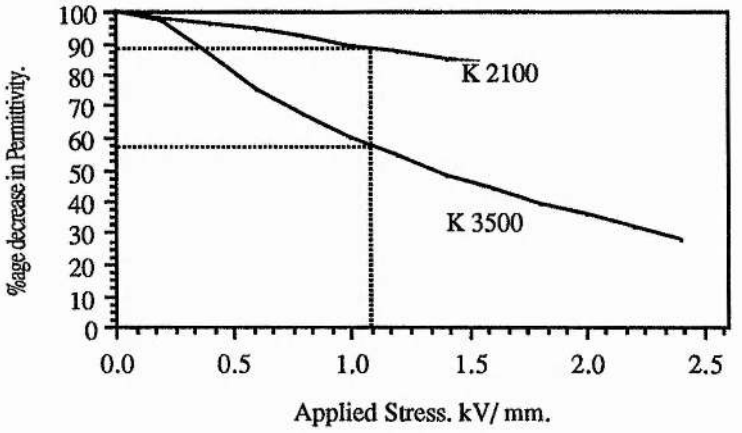

Fig 4.4.2 :- Plot of the %age decrease of the initial permittivity with applied D.C. stress. The %age decrease in the initial permittivity at 30kV is 88% and 57% for the K2100 and the K3500 dielectrics respectfully.

Note that the permittivity of the K2100 tiles falls off less rapidly that for K3500 tiles although its initial permittivity is alot less. The K2100 tiles have the added advantage of being more linear and are therefore more suited for use in a standard pulse generator and the others for pulse sharpening. Pulse sharpening is discussed further in chapter 6.

There is another way to determine the relative loss and nonlinearity of a tile. A Tower-Sawyer[20] circuit can be used to view the Polarisation verses Electric field hysteresis curve on an oscilloscope. The area of this loop is a measure of dielectric loss and the remnant polarisation and coercive field a measure of the

nonlinearity. Unfortunately, these curves cannot be given here because the technique had not been developed at the time. Details of the experiment can, however, be found in reference 21.

4.5. Determination of the Hold-off Potential. Experimental details.

The breakdown strength of the K2100 tiles, 8kV/mm, has been determined by the manufacturers; their flashover voltage has been measured using the simple circuit shown in figure 4.5.1[22].

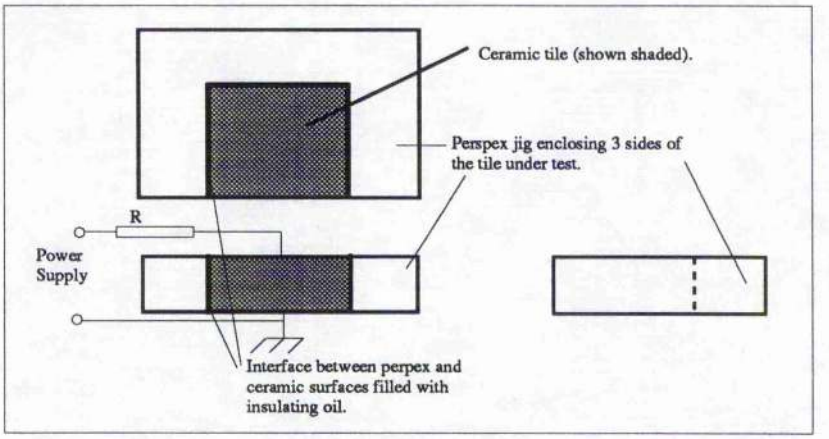

Fig 4.5.1 :- Experimental arrangement of the voltage hold-off circuit.

This consists of a perspex block that encloses three sides of a clean tile that has no cracks or raised or sharp areas along its edges. These sides of this tile are insulated by pouring castor oil in between the ceramic and perspex surfaces in order to localise the flashover site on the forth side. A 40kV capacitor charging unit charges the tile via a 100MΩ charging resistor until a flashover occurs. The flashover

voltage under oil has been measured using the same arrangement but without the perspex surround.

This experiment has shown that it is only possible to charge a tile to -22kV (0.88kV/mm). Above this a flashover occurs and a black conductive track is formed; this track is conductive and lowers the flashover voltage to -4kV (0.16kV/mm). When a tile is charged under oil the following is observed: (i) the oil around the electrode edge moves in a rapid, random, turbulent motion (ii) the maximum charge voltage that can be achieved is -25kV (iii) current flowing in the oil loads the circuit and, at charge voltages above -25kV, initiates breakdown (iv) a flashover again produces a black conductive track that lowers the charge voltage*.

The first important point to bear in mind when interpreting these results is that barium titanate tiles can produce extremely high fringing fields at the electrode edges, even at relatively low voltages[23,24,25]. According to Burgaev et al.[26], this field is given by :-

$$E = \frac{E_0 \varepsilon_r}{\left[\{\Delta\varepsilon_r/\delta\} + 1\right]}. \qquad 4.5.1.$$

where E_0, ε_r , δ and Δ are the magnitude of the initial field, the relative permittivity, the dielectric thickness and the gap spacing between the dielectric and the metal respectively (see figure 4.5.2).

---

* No polarity effects have detected because of the simple nature of the experiment.

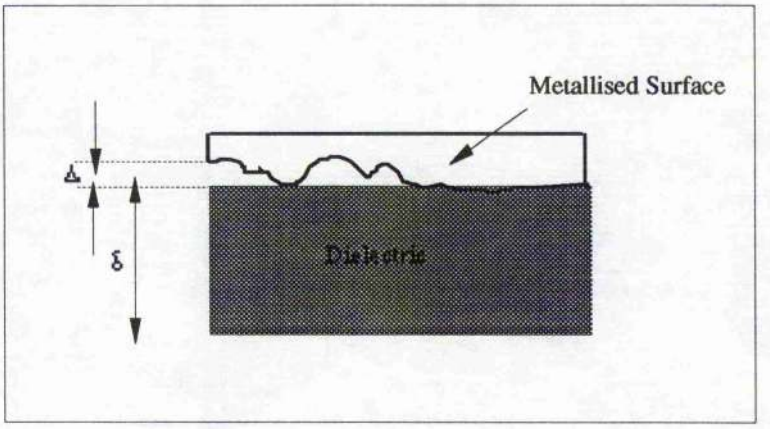

Figure 4.5.2 :- Hypothetical model of the electrode-dielectric contact.

Since Δ is very small the denominator in equation 4.5.1 is approximately equal to one and the fringing field enhanced by a factor equal to the permittivity of the material. With high permittivity materials such as a barium titanate tile, these fields can be as high as 10^7 Vm^{-1} at voltages as low as 20kV[27,28,29]. These high fields are primarily responsible for flashover at low voltages because they produce electrons by field emission. These electrons are scattered or attracted back to the tile surface where they liberate a greater number of secondary electrons and desorb gases by stimulated electron bombardment. Further bombardment ionises the resulting gases and this forms a plasma that spreads out to form a fully developed streamer discharge. The high temperatures developed in this streamer vaporises molecules from the ceramic surface and the surrounding medium. Some of these molecules adhere to the ceramic surface and form a black deposit. It is this deposit that lowers the flashover voltage of the tile.

When a tile is operated under oil, it appears that high fringing fields produce electrophoretic effects, i.e. they attract or repel the strongly polarised hydrocarbon molecules and other particles present that give up or accept charge from each electrode and produce a current that loads the circuit[30,31]. This current quickly leads to breakdown.

The above results mean, of course, that barium titanate tiles are best used pulse charged because it is difficult to suppress this flashover mechanism. For example, in commercially available HV doorknob capacitors the dielectric has to (i) have large stress relief plates brazed to it to grade the electric field at the triple junction and keep the field homogeneous (particles with higher than average permittivities can migrate to regions of high field strengths[32,33]) (ii) be encapsulated in a low permitivity compound[34].

4.6. PFL Fabrication using the Ceramic Tiles.

It is relatively straight forward to construct a pulse generator with barium titanate tiles. The one described in this section was used to calculate the tiles transit time and characteristic impedance.

Figure 4.6.1 shows the circuit. The pulse generator was a PFL* that comprised seven K2100 ceramic tiles that had previously been cleaned with tri-chloroethane. The connections between adjacent tiles were made by soldering copper bridging contacts onto the surface of adjacent tiles and placing a copper sheet along the top and bottom of the completed PFL. This sheet was covered with neoprene rubber

* Details concerning the operation of a PFL are given in Appendix D.

and clamped in place using two metal plates (see figure 4.6.2 and 4.6.3). R_L was a 2.5Ω copper sulphate resistive load and the switch, S_2, an edge-plane spark-gap of standard design with a self-breakdown voltage of 30kV. The completed assembly measured 55cm x 2.5cm x 7.5 cm, had a total capacitance of 29.4nF and could store 11.6 J at 30kV.

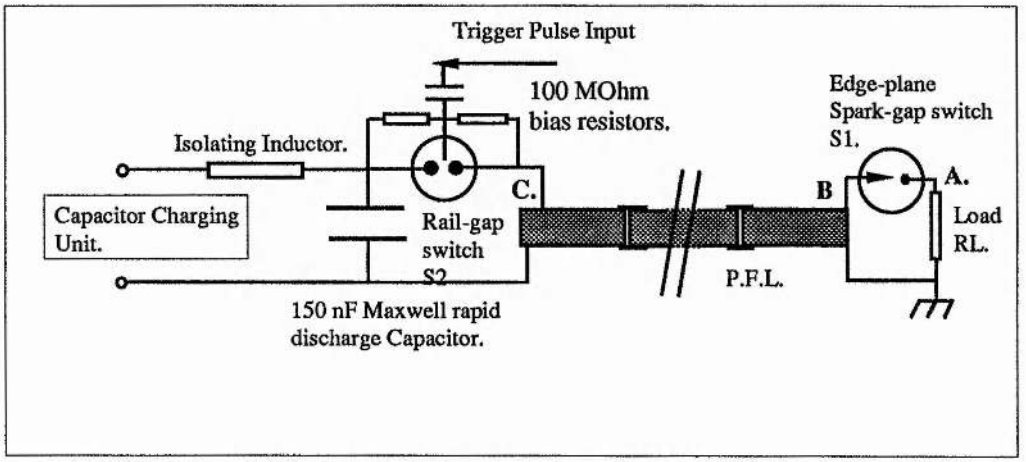

Figure 4.6.1 :- Circuit diagram of the PFL test circuit.

The tiles were pulse charged using a simple resonant circuit. The capacitor C_1 was a Maxwell 150nF, 50kV rapid discharge capacitor charged using a 40kV charging unit and a 10kΩ charging resistor. The resonant inductor, L_1, was equal to 4.1μH and the switch S_2 was a simple spark gap triggered using a -20kV voltage pulse from a separate HV generator. A 500Ω wirewound resistor (not shown) was connected in parallel with the PFL to dampen the waveform and discharge C_1 and the PFL should S_1 fail to close.

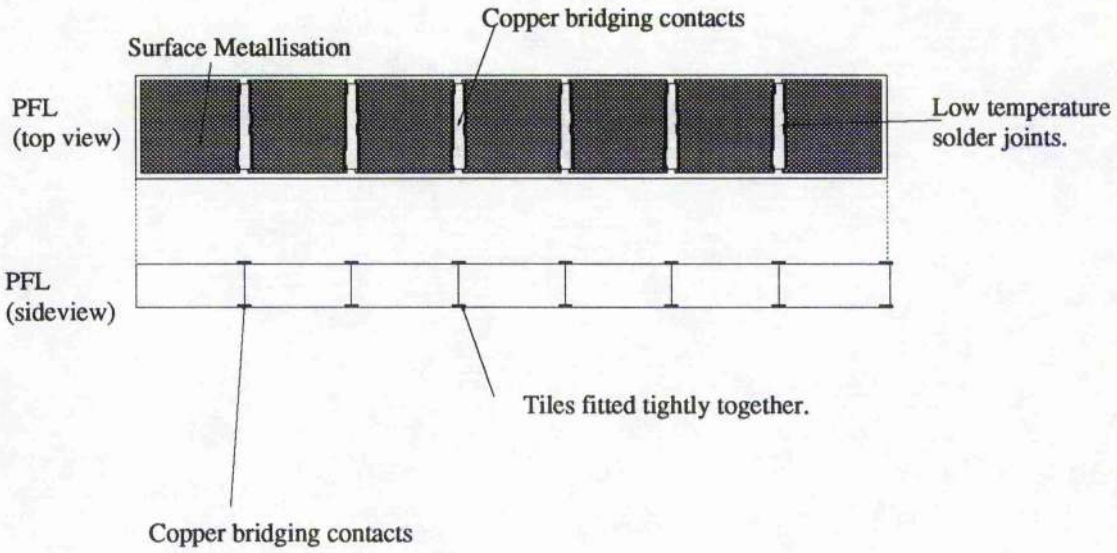

Fig 4.6.2 :- Diagram showing how the 7 tiles were connnected together.

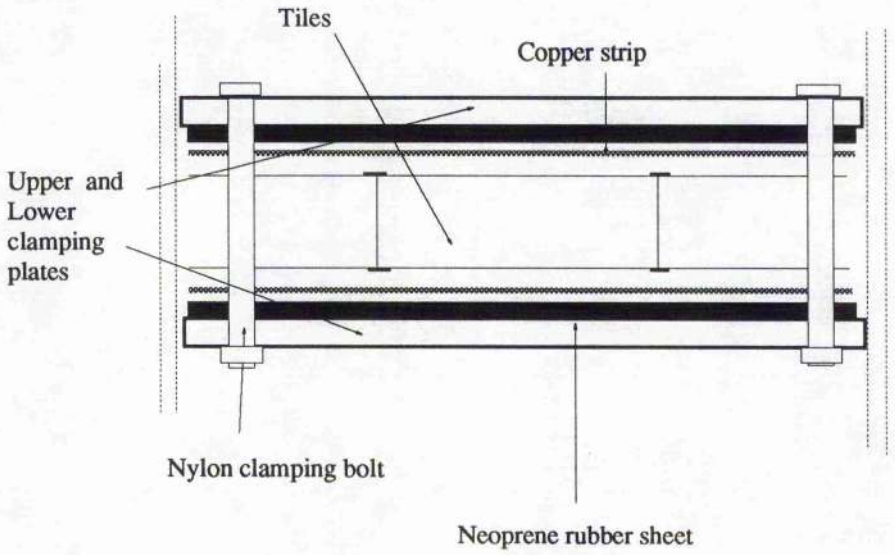

Fig 4.6.3 :- Cross section of the HV PFL.

Figures 4.6.4 shows the voltage at the switch, S_2, and the load, R_L, when C_1 was charged to 17kV. Each trace was obtained using a 519 oscilloscope and a copper sulphate voltage probe.

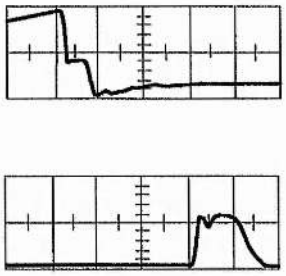

Figures 4.6.4 :- (Upper trace) Charging waveform on the PFL (200 ns/D;15 kV/D) and (Lower trace) voltage across the load. (100 ns/D;15 kV/D).

The voltage waveform on the upper trace is given by the familiar equation :-

$$v_{(C_2)} = V_0 \left[\frac{C_1}{C_1+C_2} \right] \{1 - \cos \omega t\}. \qquad 4.6.1.$$

and the charging time and peak gain by :-

$$T_{charge} = \pi \, (L_1 C_{eff})^{1/2} \qquad 4.6.2.$$

and

$$\text{Gain} = \frac{2C_1}{C_1 + C_2} \qquad 4.6.3.$$

where $\omega = 1/(LC_{eff})^{1/2}$, C_2 the capacitance of the PFL and $C_{eff} = C_1C_2/(C_1 + C_2)$.

For this circuit $L_1 = 4.1\mu H$, $C_1 = 150nF$ and $C_2 = 29.4nF$, $T_{charge} = 1.0\mu s$ and the gain = 1.7. These figures are in agreement with the experimental results.

The fall in voltage that occurs at the peak of this waveform, i.e after 1.0μs, is the point where S_1 closed and the output pulse appeared across the load. This pulse is shown in the previous traces. It had a risetime of 30ns, an amplitude of 15kV and a pulse duration of 130ns. The spike on the front of the pulse suggests that there was some stray inductance present either in the switch or the feeds and the lack of reflections show the load was matched to the PFL.

Implications of the results :- Although this was a relatively simple pulse generator, it established a number of important facts.

1). It showed that high permittivity ceramic tiles can be used without any edge control if they are pulse charged. It also showed that they can withstand the mechanical forces generated by the piezo-electric effect (this occasionally produces bulk breakdown or cracking in commercially produced capacitors[37]).

2). It established that the delay time and characteristic impedance of a single tile is 2.5Ω and 11ns respectively. This information was important because it

enabled other, more complicated pulse generators to be constructed quickly and simply.

3). Operating at higher voltage levels showed that the tiles could be pulse charged to at least 62kV. This has suggested that at 30kV the optimum tile dimensions of the tiles are: 7.5 cm x 3cm x 1 cm. These smaller tiles should bring about a further reduction in the size of a pulse generator.

4). Monitoring the risetime and fall time of the pulse and the variation in pulse shape revealed that the voltage falltime or tail on the pulse is affected by : dielectric loss, stray capacitance between adjacent tiles and the fall in relative permittivity with voltage (the "nonlinearity"). The fact that the nonlinearity produces an amplitude dependent velocity of a propagation eventually led to the development of the nonlinear dielectric (NLD) pulse sharpening line. This is discussed in chapter 6.

4.7. Summary of Chapter 4.

This chapter has demonstrated that barium titanate tiles can be used as dielectric material at or around the 30kV voltage level. It has done this by reporting on design and construction of a barium titanate tile PFL that produced 15kV voltage pulses with a 30ns risetime and pulse duration of 130ns. Smaller tiles, with a thickness more appropriate for use at the 30kV voltage level, should improve on this design and allow more compact pulse generators to be constructed.

Details have also been given concerning some of the important electrical, thermal and physical characteristics of the tiles. The temperature/permittivity

curve has been compared with a K3500 dielectric mix manufactured by the same company and this has shown that the K2100 dielectric mix has attractive thermal characteristics. The DC flashover electric field strength of the tiles has been measured, both in air and in oil, and found to be 0.88kV/mm and 1kV/mm respectfully. This low flashover voltage has been attributed to the large fringing fields that are produced at the edges of the electrodes. Under oil, these fields are sufficient to produce a discharge current that can load the charging circuit and quickly develop into an avalanche discharge. The permittivity/DC charge voltage characteristics have also been measured and this has shown that the dielectric constant of the K2100 mix decreases to 88% of it's unstressed capacitance at an electric field strength of 2.2 kV/mm. In contrast, the K3500 dielectric mix is down to 58% at the same level of stress.

References.

1). J.C. Martin ; "Pulse Charged Line for Laser Pumping", Research Note :- SSWA/JCM/723/373., Aldermaton, England, (1973).

2). N.C. Jaitly et al ; "HV Pulsed Performance of Advanced Dielectric Materials", 18th Power Modulator Symposium, South Carolina, (1988).

3). I.K. Kaprinkov and S. K. Stankov ; J. Appl. Phys. 20 (1987).

4). M.R. Osborne et al ; Optics Communications, Vol. 52(**6**), (1985).

5). W. J. Merz ; "Ferroelectricity", Progress in Dielectrics, No.(**4**), p.101, Heywards Books, Temple Press Books Ltd, London, (1965).

6). Lines and Glass ; "Principles and Applications of Ferroelectrics and Related Materials", Oxford University Press, Oxford, (1977).

7). C.Kittel ; "Introduction to Solid State Physics", Chapter 13, John Widey and Sons, 5th Edition, (1976).

8). A.D. Franklin ; "Ferroelectricity of $BaTi0_3$ Single Crystals." Progress in Dielectrics Heywards Books, Temple Press Books Ltd, London, (1965).

9). K.W.Ptessner and R.West ; "High Permittivity Ceramics for Capacitors." No(**2**), p165.

10). Phillipe Robert ; "Electrical and Magnetic Properties of Materials", Chapter 4, Artech House Materials Science Libraray, (1988).

11). S.Roberts "Dielectric and Piezoelectric Properties of Barium Titanate", Phys.Rev., No.12, June, (1947).

12). W.W.Coffen ; "The Effects of Minor Constituents in High Dielectric Constant Titanate Capacitors", Source unknown.

13). A.F. Devonshire ; Philos. Mag. Suppl. No. (**3**), p.85, (1954).

14). H. Diamond ; "Variation in the Permittivity with Electric Field In Perovskite-Like Ferroelectrics", J.Appl. Phys., Vol. 32, No.**5**, May, (1961).

15). M. Marutake and T. Ikeda ; J. Phys. Soc. Jpn., No.(**12**), p.233, (1957).

16). N. Uchida and T. Ikeda ; Jap. J. Appl. Phys., No.(**4**), p.867, (1965).

17). Kenneth M.Johnson ; "Variation of Dielectric Constant with Voltage in Ferroelectrics and it's Applications to Parametric Devices", J. Appl. Phys., Vol. 33, No. **9**, September, (1962).

18). Koji Matsumoto ; "Properties of Pulsed Gas Lasers Pumped by an LC Inversion Circuit made of $BaTi0_3$ and $SrTi0_3$ Series Ceramic Capacitors", Rev. Sci. Instrum., 51(**8**), pp.1046-8, (1980).

19). Tokihiko Ogura et al ; "Output Performance of the Coaxial Marx Generator Consisting of $BaTi0_3$ Series Capacitors", Rev. Sci. Instrum. 52(**2**), p.273-5, (1981).

20). J.C.Burfoot and G.W.Taylor ; "Polar Dieletrics and their Applications ", p.38, The McMillain Press Ltd, (1979).

21). C.Wilson et al ; "Pulse Shaping in Uniform LC Ladder Networks ", IEEE Trans . Elect. Devices, Vol.38, No.4, p.767, (1991).

22). J.C. Martin. Private Communication.

23). M. Akahane et al ; J. Appl. Phys., No. 44, p.2927, (1973).

24). P. H. Gleichauf. J.Appl.Phys. No. 22, p.535, (1951).

25). P. H. Gleichauf; J.Appl.Phys., No. 22, p.766, (1951).

26). S. P. Bugaev et al ; "Surface Brakdown in Vacumm on Barium Titanate", Soviet Physics-Technical Physics, Vol. 16, No. **9**, March, (1972).

27). Masao Akahane et al ; "Effect of Dielectric Constant on Surface Discharge of Polymer Insulators in a Vacuum", J.Appl. Phys., Vol. 44, No.**6**, June, (1973).

28). J.H.Mason; "Mechanisms of Deterioration and Breakdown by Surface Discharge", page 33, No.(**1**), Progress in Dielectrics Heywards Books, Temple Press Books Ltd, London, (1965).

29). K.Geissler et al ; "Intense Laser-Induced Electron Emission From Prepoled Lead-Lanthium-Zirconium-Titanate Ceramics", Appl. Phys. Lett., 56 (**10**), March, (1990).

30). W. F. Pickard; "Electrical Force Effects in Dielectric Liquids", No. (6), p.1, *Progress in Dielectrics*, Heywards Books, Temple Press Books Ltd, London, (1965).

31). J. A. Kok and M.M.G. Corby ; "Testing the Electric Strength of Liquid Dielectric or Insulating Material", Appli. Sci. Res., Section B, Vol. 6, p. 826, (1978).

32). G.McDuff; PhD Thesis, Chapter 4, Univ. St.Andrews, (1988).

33). G.J. Sloggett et al ; "Fringing Fields in Disc Capacitors", J.Phys. A, No. (**19**) (1986).

34). Ken Matsuda et al ; "Dielectric Breakdown of a Ceramic-Epoxy Resin Interface on a High Voltage Ceramic Capacitor", Proc. 21st Symp. on Elect. Insul. Mat., p.307. (1988).

CHAPTER 5

Compact, Repetitive Pulsed Power for Space Based Applications.

5.0 Introduction.

This chapter describes a second TLT system that was constructed to help assess whether stacked transmission line techniques have potential for high repetition-rate, space based pulsed power supplies. It begins by discussing the special requirements of space qualifiable pulsed power systems; it then gives a general overview of the TLT, together with a detailed description of the individual circuit components and an analysis of the appropriate results. Finally, the summary and conclusion discusses whether a TLT has potential for space deployment.

5.1. Space Based Pulsed Power Supplies.

Space based technology will become increasingly important in future years because of the wealth of information it provides for public services, scientific research and defense. Space based lasers and microwave sources can, for example, measure wind speeds, temperature profiles, trace gases and pollutants; they are also used extensively for communications, radiology, climatology, siesmology and lidar.

In order to operate this space based technology effectively it is necessary to use a pulsed power supply that can be transported into and operate in the harsh conditions of the space environment (a brief summary of the problems of

operating pulsed power supplies in space is given in figures 5.1.1 and 5.1.2). Such a pulsed power supply has to be lightweight, compact, reliable, capable of operating for over 10^8 shots and extremely well insulated since the space plasma produces breakdown voltages as low as 300V-400V; it also has to be constructed from materials that can withstand irradiation by uv, x-ray and gamma rays, chemical attack by atomic oxygen, bombardment by space particulates and other effects unique in space[1].

These combined requirements are difficult to satisfy using present state-of-the-art pulsed power technology. Consequently, it has become necessary for the Space Power Institute[2] (SPI), Auburn University, USA to initiate an international research program to attempt to provide a better understanding of the mechanisms that produce breakdown within the space environment, develop new circuit components, system architectures, advanced semiconducting and insulating materials, surface coatings that are resistant to chemical attack by atomic oxygen, radiation and bombardment by space particulates and thyratron switched TLT pulsed power supplies. These pulsed power supplies are being investigated because (i) thyratrons are, at present, the only switch technology that can operate reliably for more than 10^8 shots at the required repetition rates and power levels and (ii) a TLT may provide an effective way of generating fast voltage risetimes for the production of uniform e-beams for laser pumping, x-ray preionisation and microwave generation.

This chapter gives a brief overview of a second TLT pulsed power supply built as part of this investigation. It begins by explaining its general features, how the individual circuit components were constructed and the ways in which the final

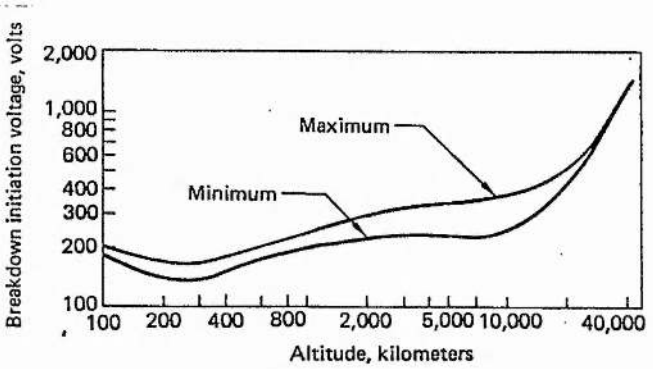

Fig 5.1.1 :- Breakdown voltages in space as a function of altitude and the sunspot cycle.

The Space Plasma.	The plasma pressure-spacing relationship is at the minimum of the Paschen curve and this means that breakdown voltages in space are extremely low, see figure 5.1.1. Relative motion betweeen the spacecraft and the plasma can cause sheaths and wakes to form and these can charge up insulating surfaces. If a flashover or bulk breakdown occurs then the resulting EMI can upset logic circuits, cause premature triggering of separate circuits or damage circuit components.
Radiation Effects	UV or x-radiation and heat can cause certain materials to polymerise and crack . This can reduce their operating life and lower their breakdown voltage. Teflon is particularly prone to radiation damage. Radiation can also charge up certain dielectric surfaces.
Atomic Oxygen Effects	Atomic oxygen can react with many dielectric materials, for example 60% mass loss can be observed in some dielectrics with only a 35 hour exposure.
The solar wind, micrometeorites and space particulates.	These can bombard surfaces and cause surface damage. Dust particles can adhere to electrode surfaces and produce field enhancement and this can induce breakdown.

Fig 5.1.2. Table showing some of the major environmental effects that influence the design of a space based pulsed power supply.

design differed from that initially conceived because of constraints imposed by engineering difficulties, the unavailability of certain materials and cost. It then describes how the system performed and discusses some a number of important points that have emerged from the project that are relevant to the design of space based pulsed power supplies.

5.2. General Overview of the 2nd TLT Pulsed Power Supply.

A circuit diagram and photograph of the pulsed power supply is shown in figures 5.2.1 and 5.2.2. It produced 200ns, 150kV voltage pulses into a 100Ω load at 10Hz and was built along the same lines as the "prototype" (i.e. it consisted of two separate sub-systems, the pulse generator and the TLT itself). The pulse generator was a pulse charged 4Ω Blumlein circuit (**A**) constructed from K2100 ceramic tiles. It was command charged to 35kV using a hydrogen thyratron charging diode and switched using 4 CX1685A hydrogen thyratrons in parallel (**B**). The stainless steel earthed wire mesh that is visible around the body of the thyratrons (see photograph) prevented the discharge from being pulled off-axis (this can occur if the ground plane is too localised) while the plastic inserts around the thyratron stems contained the Rogowski coils that were used to monitor the current flow. The TLT, **C**, was a 5-stage device. Each stage comprised four 5Ω strip transmission lines connected in series. The first stage was wound onto a perspex former and the others on 4 magnetic cores. The 100Ω copper sulphate resistive load is labeled **D**.

The complete system was built on an extensive earth plane that could be raised or lowered into an oil filled earthed metal tank by a hydraulic lift. This oil could be circulated to help remove the heat produced by the thyratron heater and

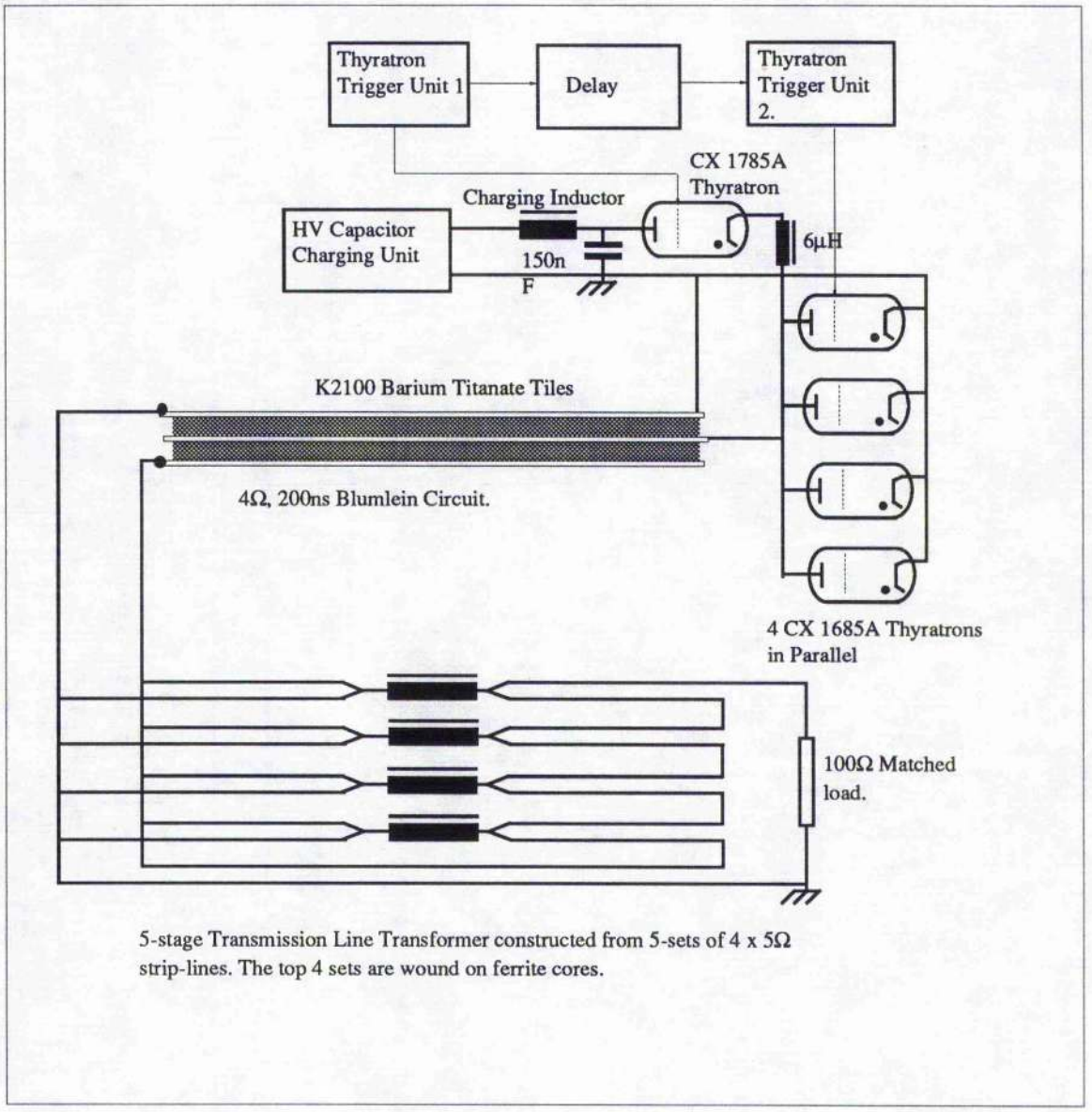

Fig 5.2.1 :- Circuit diagram of the TLT pulsed Power Supply.

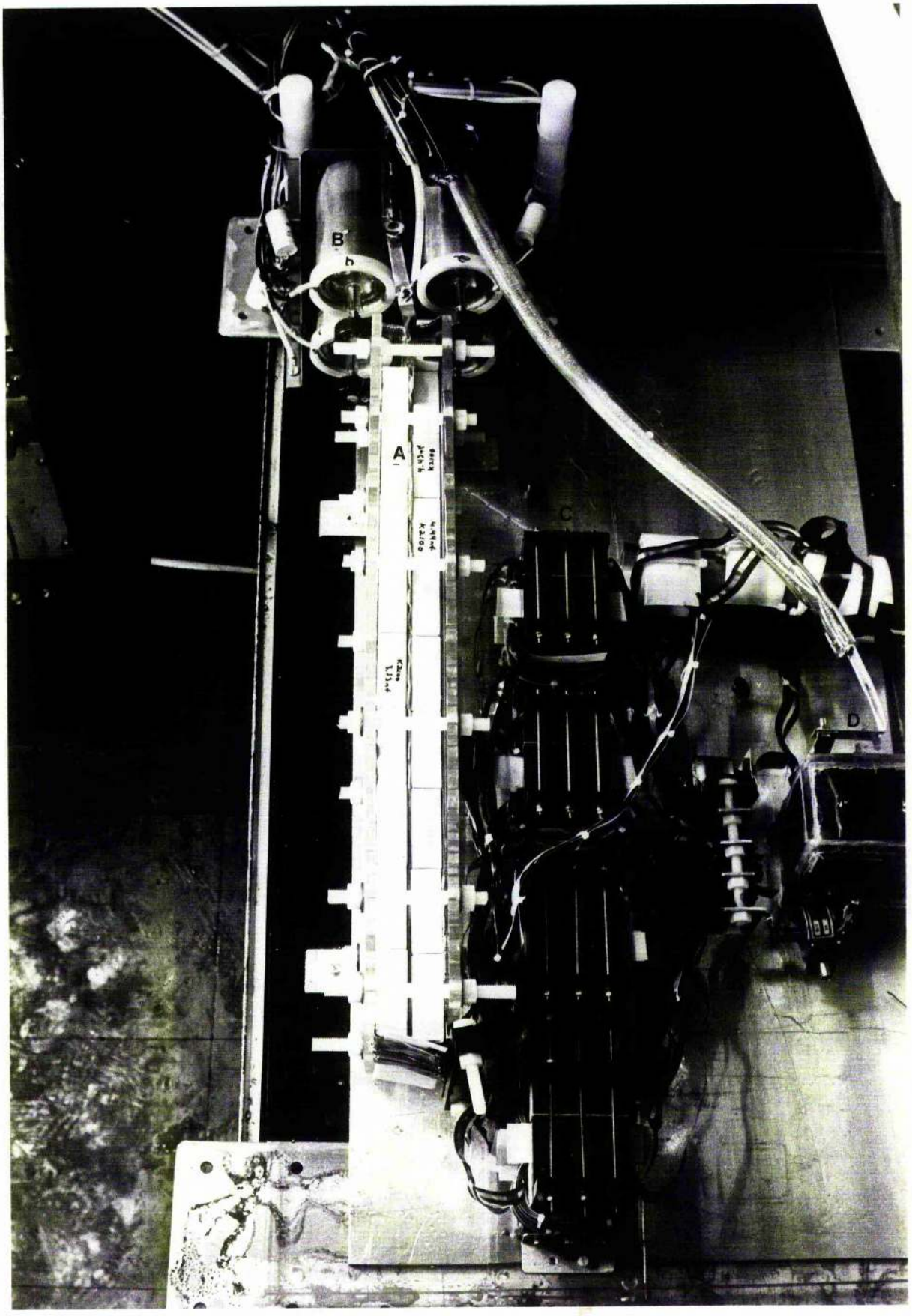

Figure 5.2.2 :- Photograph showing the completed TLT pulsed power system.

reservoir circuits, although in practice this feature was never actually used. The DC charging unit, the pulsed power supply, the pulse charging circuitry and the thyratron heater, reservoir and trigger circuits were mounted in a 19" control cabinet next to the tank but are not visible on the photograph.

5.3. Details of the Individual Circuit Components. The Blumlein Circuit.

The Blumlein circuit (**A** in photograph 5.2.2) was constructed by connecting the two transmission line sections back-to-back. This folded-configuration, which is shown schematically in figure 5.3.1, is often preferred because it is relatively compact and the high voltage electrode is well shielded. Each transmission line was constructed from 9 x 1.33 K2100 ceramic tiles each with dimensions 2.5cm x 7.5cm x 7.5cm, a characteristic impedance of 2.5Ω and propagation delay time of 11ns.

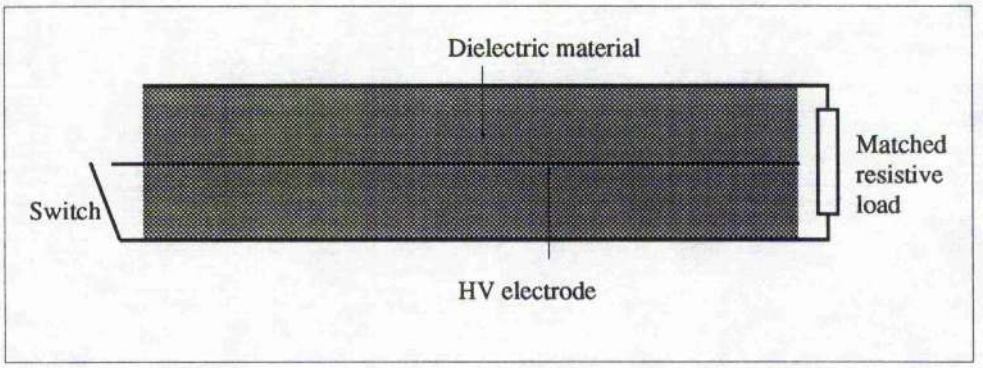

Figure 5.3.1. :- Schematic diagram of a folded Blumlein circuit.

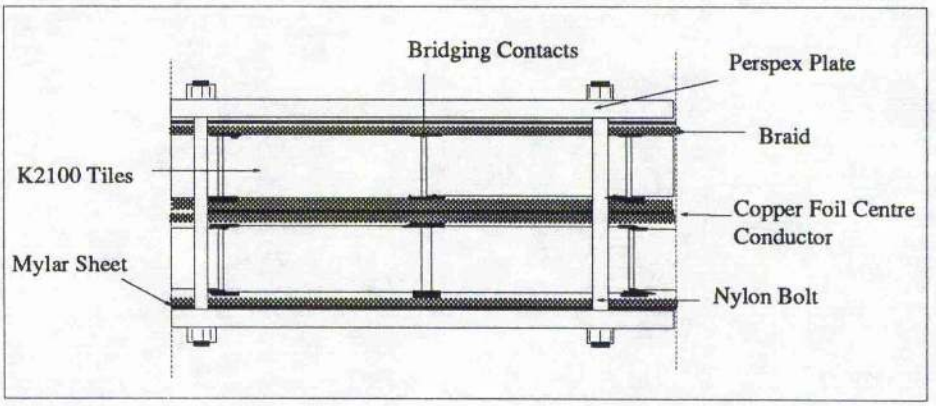

Fig 5.3.2 :- Diagram showing the construction of the ceramic tile Blumlein circuit viewed from above.

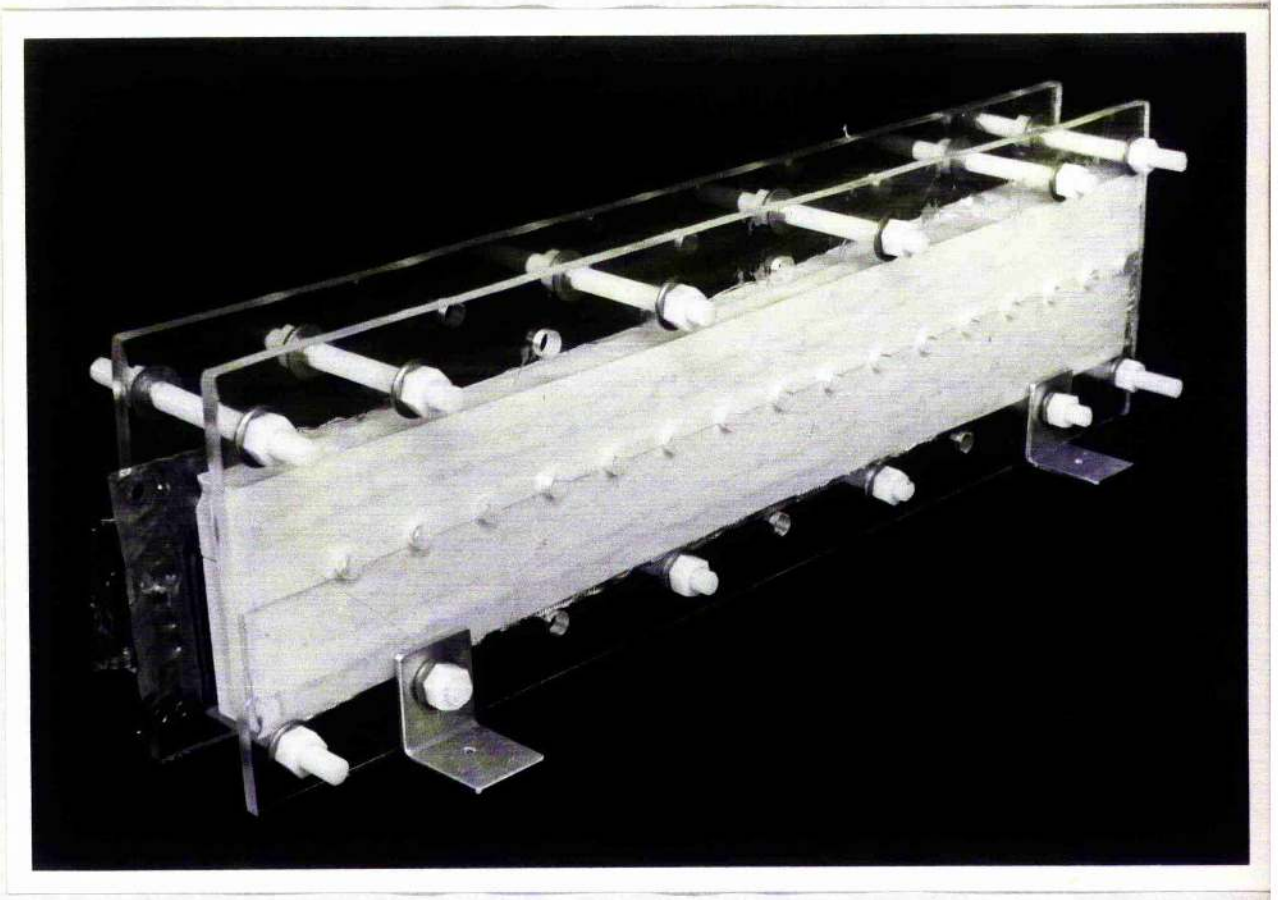

Figure 5.3.3 :- Photograph showing the ceramic tile Blumlein circuit.

The electrical connections between these tiles were made by soldering copper foil bridging contacts onto adjacent tiles using a low temperature solder. Lengths of copper braid were laid along the length of the tiles to form additional contacts. The Blumlein circuit was supported by two perspex plates that were held together using 12 M10 nylon bolts. Figure 5.3.2 highlights the construction more clearly.

When completed the Blumlein circuit (see figure 5.3.3) measured 67.5cm x 10cm x 5cm, had a total capacitance of 98.8nF and could store 54 J of energy at 35kV at an energy density of 2.8 J/kg.

5.4. The Blumlein Circuit Switch.

It is necessary to operate thyratrons in parallel when the peak and average power capability of a single device is insufficient to switch a circuit effectively (see section 3.3 of chapter 3). This section takes a more detailed look at parallel thyratron operation and then it describes the parallel thyratron switch used to discharge the Blumlein circuit.

Parallel thyratrons are usually switched using a common trigger generator. This must have a low output impedance so that it can supply enough current to initiate a discharge in each tube and, at the same time, produce a fast trigger pulse because this minimises firing jitter. This pulse is usually applied to the thyratron grid drive circuits using standard 50Ω coaxial cable. As has previously been explained, the lengths of this cable must be carefully calculated to compensate for the variation in the anode delay time, t_a, of these thyratrons. Compensation is achieved when :-

$$t_a + t_d = K. \qquad 5.4.1.$$

where K is a constant and t_d the delay time in the cable. If equation 5.4.1 is not satisfied the thyratron that conducts first lowers the anode voltage and this either prevents the other tubes from switching and/or produces an uneven current distribution.

Even when equation 5.4.1 is satisfied, this current distribution can change slowly because the anode delay time of a thyratron varies during its life. The different methods used to circumvent the problem of anode delay time drift (ADTD) provides a means of identifying different circuit designs for parallel thyratron switches. For example :-

1). The simplest parallel thyratron switch requires no variable delay control to compensate for ADTD because each thyratron is used to switch a separate circuit. This technique was used by Smith and Brown to switch up to 10 thyratrons at once in a laser modulator that was used to drive a mercury bromide laser[3]. It was also used in the TLT pulsed power supply described in chapter 3. This approach, however, requires a greater number circuit components than would otherwise be required and this makes the power supply heavy, bulky and less reliable.

2). Delay control and hence current sharing can also be produced by connecting a ballast resistor or inductor in series with the thyratron anodes, a technique that was first used by Reintjes and Godfrey[4] and Lake[5]. If one tube sinks too much current then the impedance of the ballast element is increased until

equilibrium is restored. This technique is, however, inefficient and unsuitable for fast pulse work because the ballast element limits the rate of rise of current in each thyratron.

3). Faster pulses and compact construction can be accomplished if the thyratrons are connected to a common energy source using low inductance feeds. Lake[5] has shown that it is possible to control the breakdown times of the thyratrons in these "hard-parallel arrays" by varying the negative bias on the second thyratron grid. McDuff, having found that the negative bias affects recovery, switching and jitter, developed a microprocessor controlled trigger system that operated up to 5 ceramic thyratrons at once[6]. It worked in the following way. The total charge, Q, flowing in each thyratron was determined by integrating the output from a current viewing resistor (CVR) and translating it into an 8-bit word using an A/D converter. This was averaged and compared to the total energy storage capacity of the circuit. The resulting error signal was used to adjust the delays to the thyratron drive circuits so that those that were conducting too much current were triggered later in time. The thyratron array to be described below used a simpler approach. Current regulation was obtained by first measuring the relative flow of current in each tube using a Rogowski coil and then controlling the reservoir voltage, breakdown voltage and hence the point on the rising edge of the trigger pulse that the thyratron switched. Thyratrons that were initially conducting too much current had their reservoir voltage (and hence gas pressure) reduced so they triggered at a higher voltage or later in time. This technique, it is believed, has not been demonstrated elsewhere.

Circuit description of the Blumlein Circuit Switch :- The Blumlein switch, which had to be capable of a dI/dt of about 350kA/μs in order to produce a pulse with an output risetime of 50ns, was constructed from 4 CX 1685 thyratrons (dI/dt rating of 80kA/μs each [7]). A circuit diagram of the switch is shown in figure 5.4.1 and a photograph in figure 5.4.2. Each thyratron had a separate reservoir supply that consisted of a 50VA step-down transformer and a mains variac. These were initially set to give an output of 2A at 7V, but this could be easily varied by altering the setting on the variac. The thyratrons were triggered using a trigger generator shown in figure 5.4.3. The transformer, T_1, was used to step up the mains voltage from 240V to 3kV. This voltage was rectified, smoothed and used to charge up a 500nF storage capacitor, C_1. The series resonant circuit formed by C_1, the 50nF capacitor, C_2, the two 10μH inductors and the charging diode provided the gain that was needed to charge C_2 to 8kV. The output pulse was produced when the voltage on C_2 was switched across the 4:1 step down transformer using the FX 2530 hydrogen thyratron. This was superimposed on a DC bias level of -150V, had an amplitude of 2kV, a risetime of 100ns, a FWHM of 2μs and was applied to the grid drive circuits using 50Ω coaxial cable of the appropriate length. The output impedance of the trigger unit was 4Ω.

As has been explained, the trigger pulse was applied to the thyratron grid drive circuits using pre-determined lengths of coaxial cable that compensated for the different anode delay times of the thyratrons. These grid drive circuits were the same as those used to switch the thyratrons in the Blumlein circuit of Chapter 3.

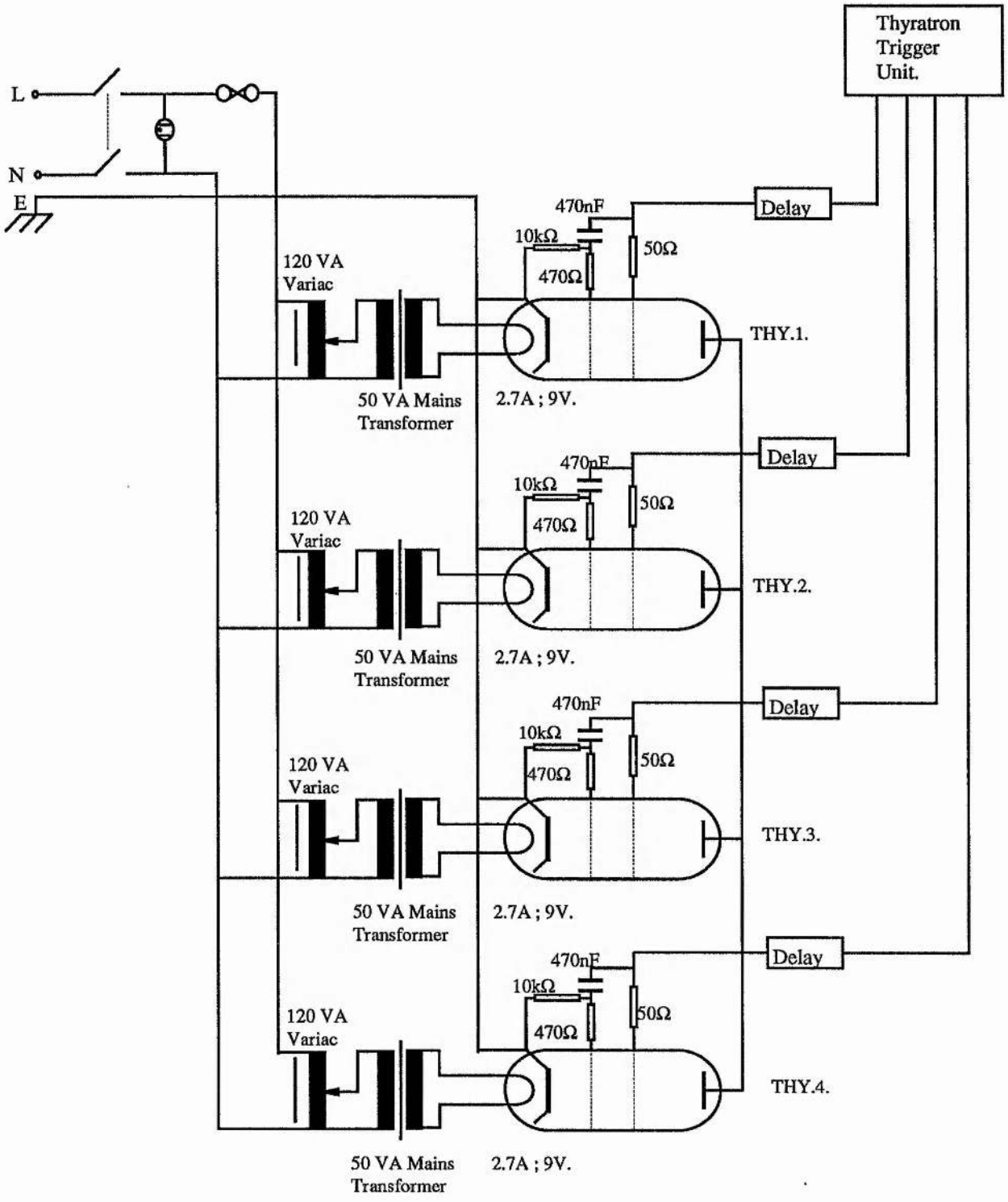

Fig 5.4.1 :- Circuit diagram of the thyratron trigger system

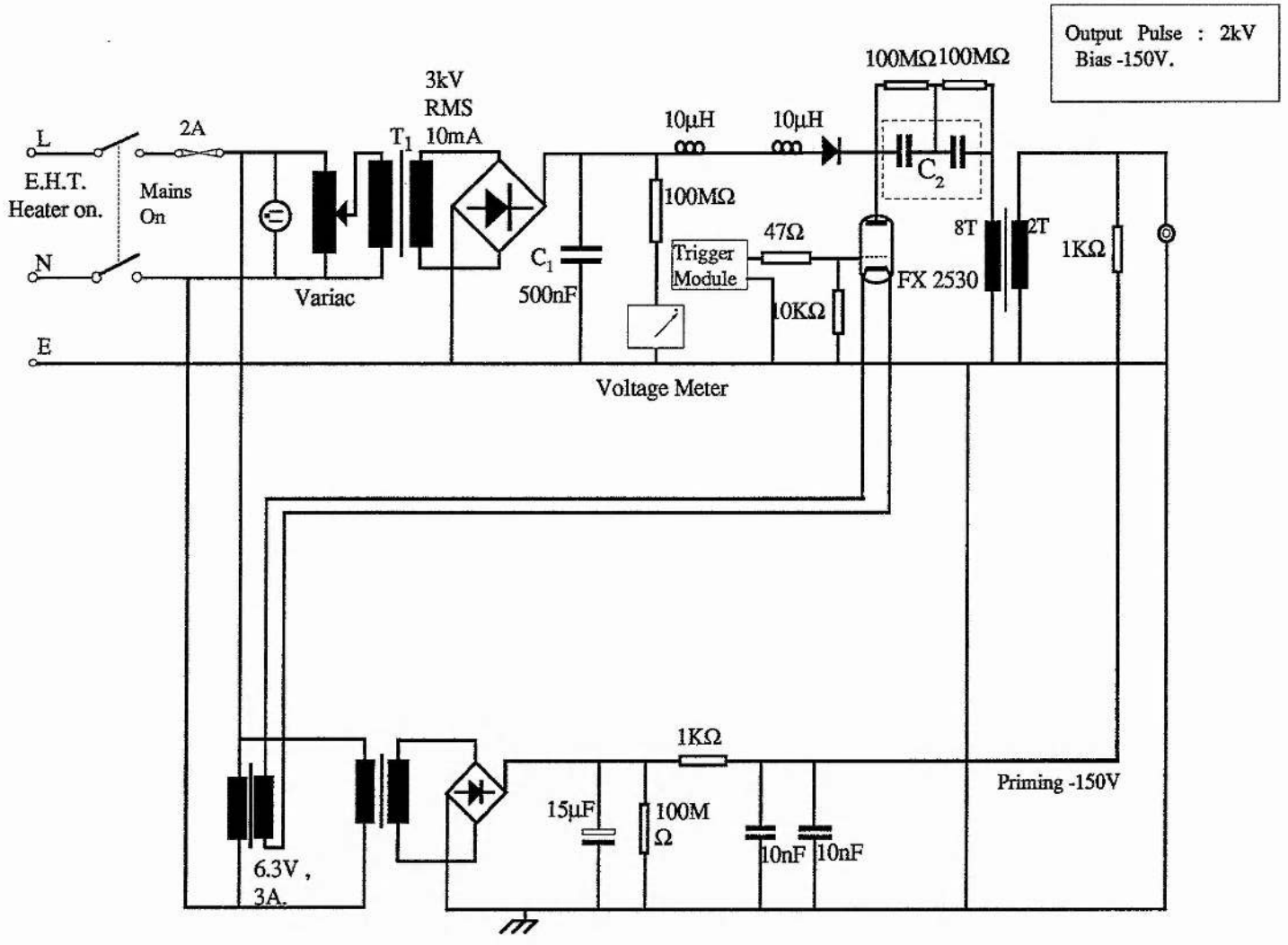

Figure 5.4.3 :- Diagram of the Thyratron Trigger Circuit for the Thyratron Array in the 2nd TLT Pulsed Power Supply.

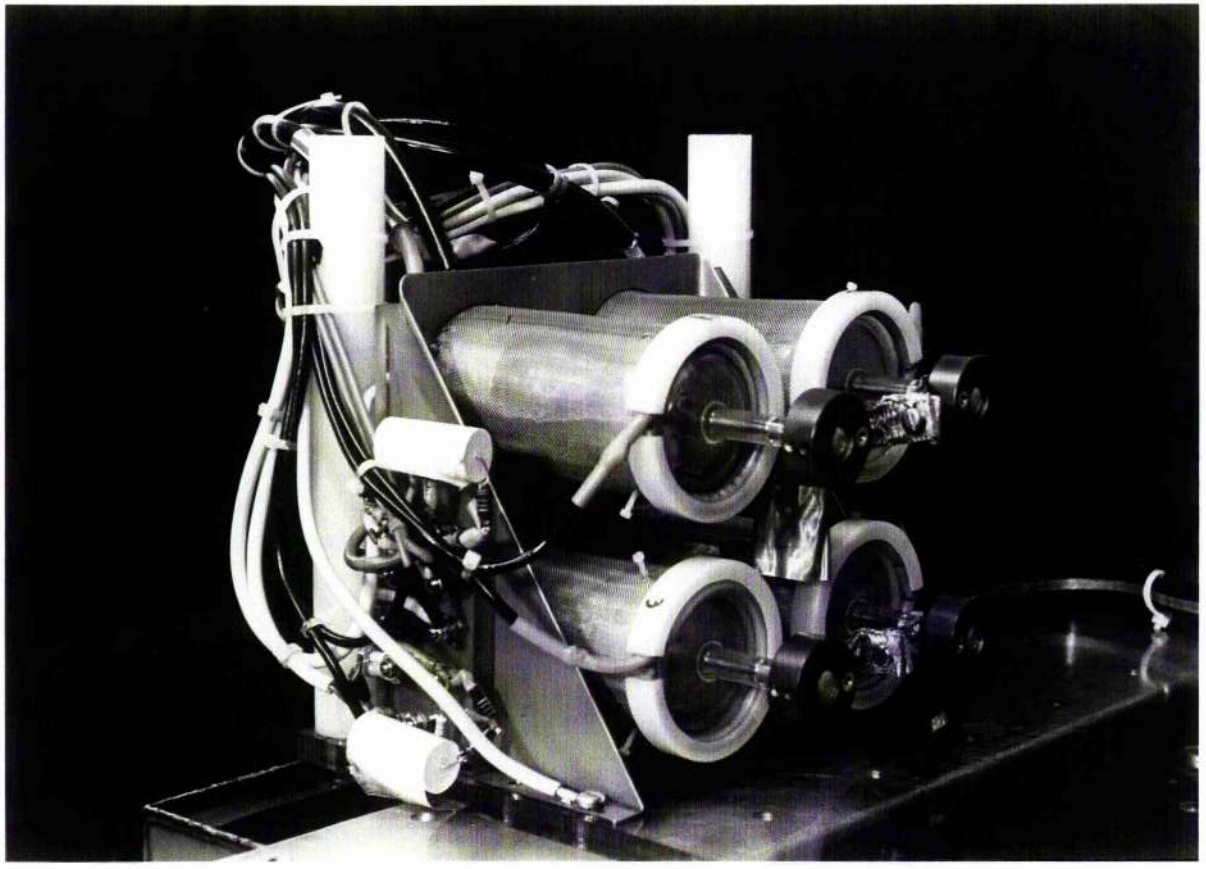

Fig 5.4.2 :- Photograph showing the thyratron array. Each thyratron is a CX 1685. They are connected to an aluminium support plate that is bolted onto an extensive earth plane. The circuit components visible on the side of this plate are part of the grid drive circuits. The earthed wire mesh that surrounds the thyratrons helps keep the discharge axial and the plastic inserts contain the Rogowski probes.

Testing the thyratron switch. :- The multi-parallel thyratron switch was tested using a pulse charged 5Ω Blumlein circuit. The current flowing in each tube was monitored by integrating the output from the Rogowski probes and viewing the resulting signal on a 519 scope. These probes had been built and cross calibrated in the laboratory so they only provided a relative measure of the current flowing in each thyratron. Each reservoir voltage was decreased/increased depending on whether the thyratron was conducting too much/too little current. The response time of the thyratrons using this method of current control is difficult to quantify because it depends on the change in reservoir voltage. However, in these tests the tubes were left for 1 minute after each setting. As the switching times converged it was found that the tubes locked in (i.e. their jitter dropped to below 2ns) a phenomenon attributed to "cross talk" by Brown and Smith. When the thyratrons had been properly set they switched at about 320kA/μs and were operated at 10Hz in burst mode and for 1Hz over a number of 2-3 hour periods. During this time, measurements of the current flow revealed that once the thyratron reservoir voltages had been set, the current distribution remained constant (i.e.to within 10% current sharing). The output waveforms produced by this test circuit are shown in fig 5.4.4. For an initial pulsed charged voltage of 25kV, the output pulse had a 10-90% risetime of 59ns (10% - 90%) and a pulse duration of approximately 150ns. The slight rounding of the leading edge shows that even with 4 thyratrons, the switch was only just capable of producing a pulse with a well defined risetime, flat top and falltime. This is further illustrated in the other traces, which show the output from the same circuit with 3, 2 and just 1 thyratron operating.

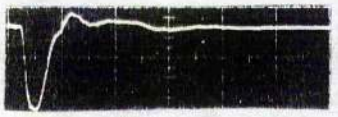

500ns.

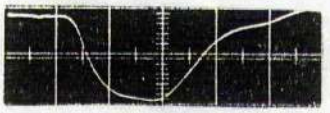

100ns

200ns.

50ns

Output into a matched 5Ω load. 12kV/div.

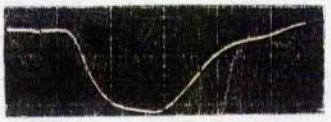

100ns

4 Thyratrons

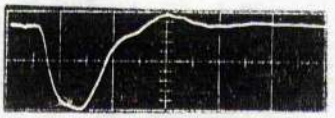

200ns.

100ns

3 Thyratrons

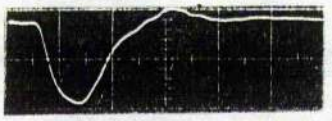

200ns.

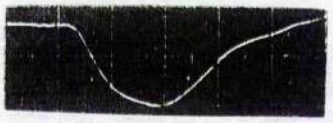

100ns

2 Thyratrons

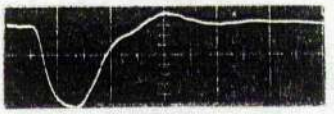

200ns.

100ns

1 Thyratron

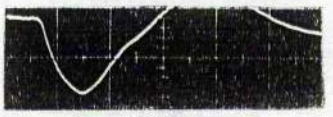

200ns.

Fig 5.4.4:- The effect of the number of parallel thyratrons on the output pulse profile for a 5Ω Blumlein circuit. 12kV/div.

5.5. Pulse Charging the Blumlein Circuit.

In a space based pulsed power system insulation, reliability and component lifetime are critical issues because breakdown voltages in space can be as low as 300V - 400V. It is therefore important that the circuit components are stressed for as short a period of time as possible. This can be achieved using a charging diode because this can switch the charge from the storage capacitor to the Blumlein circuit so that the peak of the charging waveform is coincident with the point in time when the discharge switch has to be triggered. This command charging technique was used in this second TLT system.

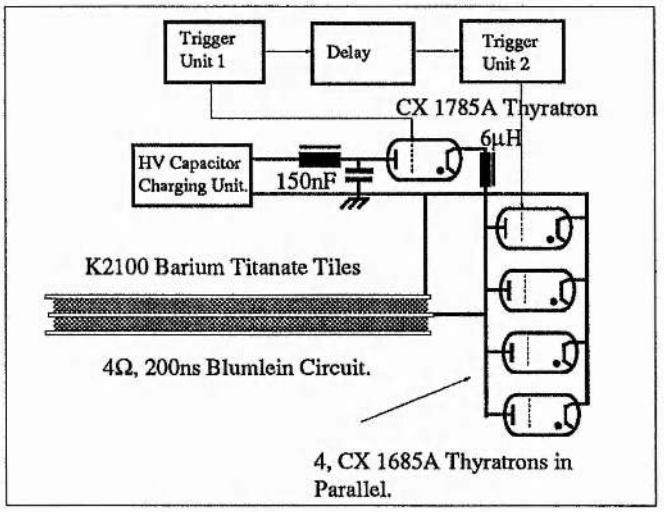

Fig 5.5.1:- Schematic diagram of the charging circuit for the Blumlein circuit.

Construction and operation of the charging circuit :- The charging circuit is shown in figure 5.5.1. The main storage capacitor, C_1, was a 150nF Maxwell rapid discharge capacitor. It was charged to 30kV via a 150nH charging inductor using a 200J/s Hartley Measurements capacitor charging unit. This limited the

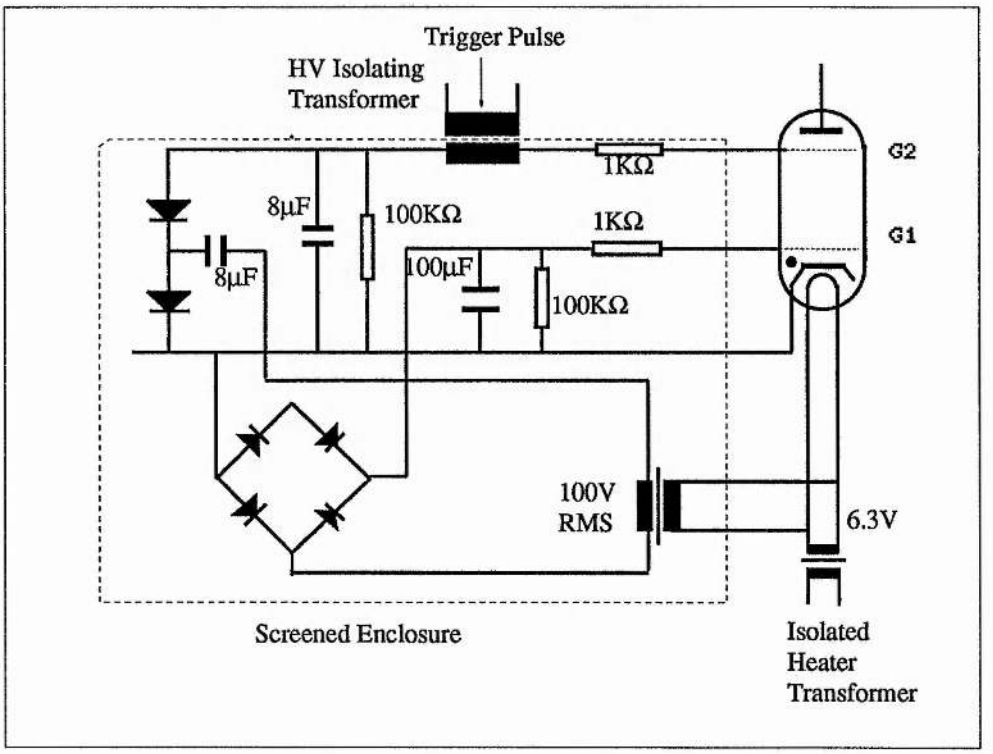

Fig 5.5.2 :- Bias circuitry for the charging diode. EEV data book.

repetition-rate of the system to about 1Hz. The charge was transferred from C_1 to the Blumlein circuit using a CX 1785 hydrogen thyratron as a charging diode.The thyratron grid electrodes, G_1, (the "keep alive" electrode) and G_2 were biased from the heater circuit which was isolated from the mains supply (see figure 5.5.2). The thyratron was switched using the trigger circuit used in the prototype TLT (see figure 3.3.1) and so it will not be described here. Switching the thyratron with this circuit produced a peak voltage of 35kV on the Blumlein circuit with a charging time of 2.4μs.

5.6. The Transmission line Transformer

The TLT was required to increase the 35kV 200ns output pulse from 4Ω Blumlein circuit to 150kV and operate into a 100Ω load. This meant that it had be a 5-stage device capable of producing a gain of at least 4.3.

Figure 5.3.1 and 5.3.2 shows the equivalent circuits of this TLT. The value of the winding inductors were 160μH, 120μH, 80μH and 40μH on the 5th, 4th, 3rd and 2nd stages respectively. These were calculated using the general low frequency response equation originally given in chapter 2 :-

$$\frac{L_N}{Z_0(N-1)} = 10t_p \qquad 5.6.1.$$

where Z_0 is the line impedance, N the stage number and t_p the pulse length.

As has been explained, the gain produced by a TLT depends primarily on the SM impedance, Z_2. In practice this varies slightly from stage to stage although it

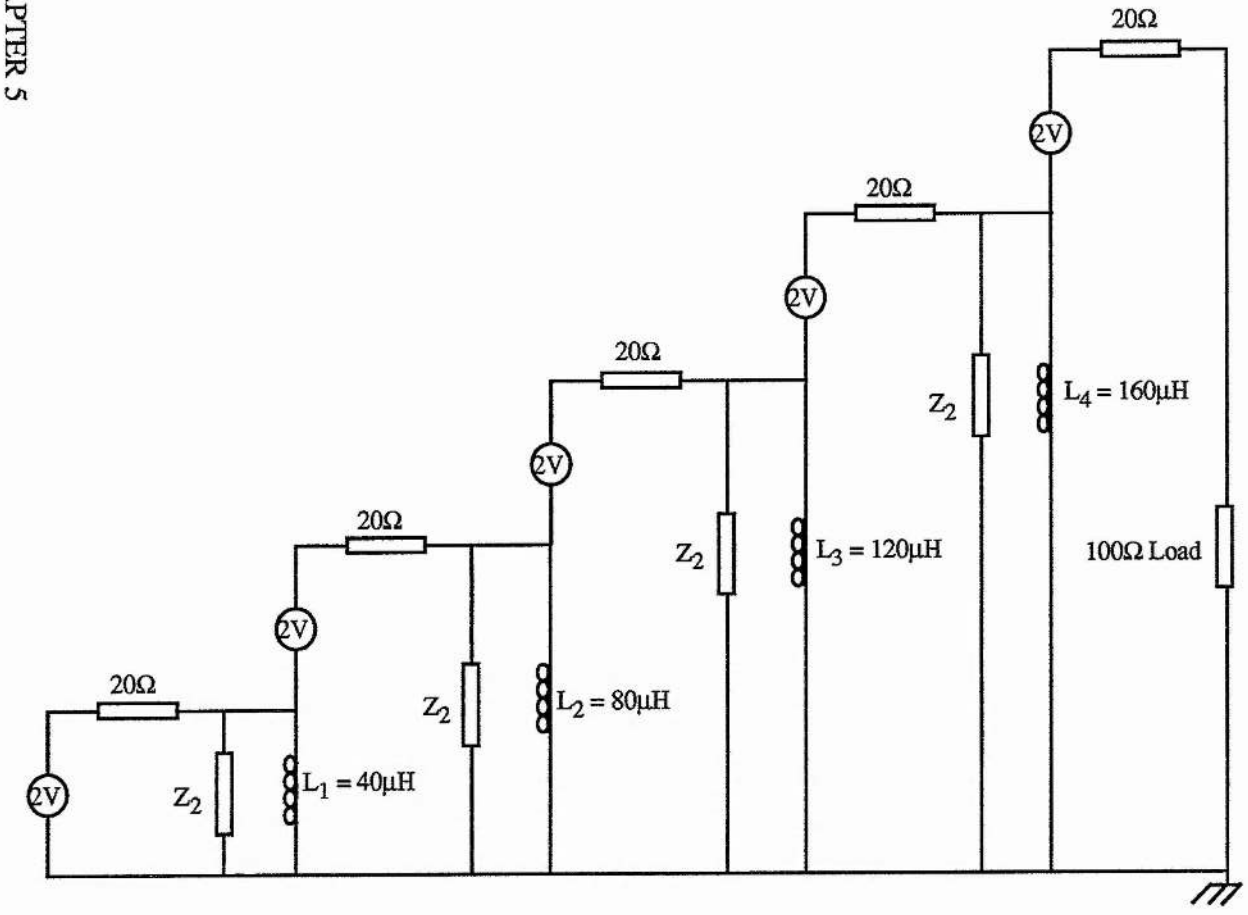

Fig 5.6.1 :- Equivalent circuit of a 5-stage TLT with 20Ω transmission lines suitable for pulse durations of 200ns.

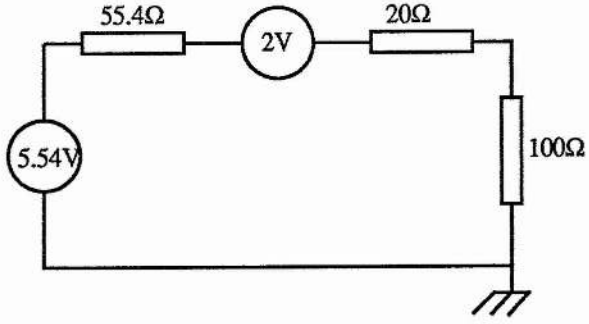

Fig 5.6.2 :- Thevenin equivalent circuit of 5.6.1.

can be taken to be a constant for design purposes. In order to construct a TLT with a specified gain G, it is necessary to raise Z_2 above some minimum level. This can be calculated from the General Gain Equation given in Appendix A. For N=5, $Z_0 = 20\Omega$ $Z_L = 100\Omega$ and G = 4.3, Z_2 must be at least 325Ω.

TLT Construction :- 20Ω coaxial cable is not available commercially and so the transmission lines had to be constructed as striplines using metallised Kapton. This is a polyimide insulating film that has a dielectric constant of 3.4, a maximum operating temperature of 400^0C and a breakdown strength of 280kV/mm. Unfortunately the maximum thickness available, 127μm, does not have the electrical strength to withstand the large fringing fields produced at an electrode edge at 35kV. This constraint meant that each stage of the TLT had to be constructed from four 5Ω lines in series (see figure 5.6.3).

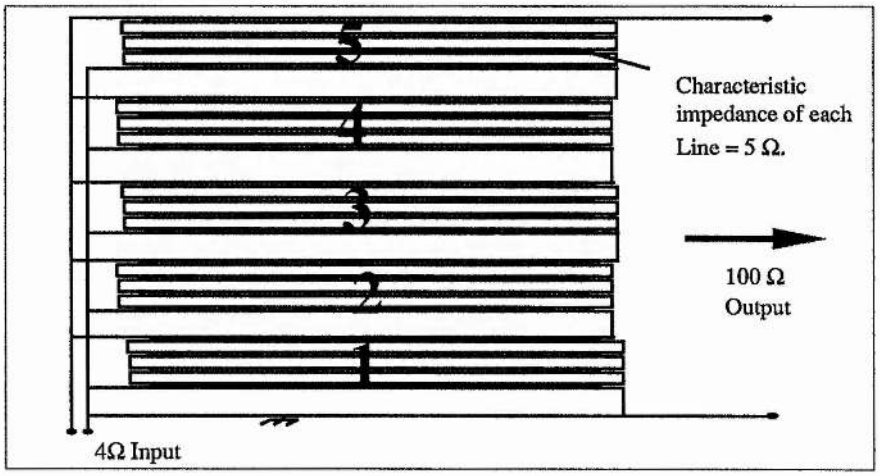

Fig 5.6.3 :- Circuit diagram of the actual TLT.

Each of these 5Ω lines were constructed by cutting the Kapton into 3cm x 3m strips, masking off a 5mm electrode on its upper and lower surfaces and etching away the residual copper using a solution of ferric chloride. Four of these lines were wound onto a single magnetic core that comprised three FX3860 and FX 3861 U and I cores (made from 3C8 magnetic material), had an area core factor of 5.19×10^{-3} m^2 and a magnetic path length of 35cm. Initial calculations, conducted using equation 5.6.5 and a value of $B_{sat} = 0.4T$, $t_p = 200ns$ revealed that 34 turns of the strip transmission line were required to prevent saturation on the upper stage of the TLT. This number of turns would have been difficult to insulate and so it was reduced to 10 by gapping the cores with 750μm of Mylar insulating film.

$$A_{CF} = \frac{Vt_p}{N B_{sat}} \qquad 5.6.5.$$

Figure 5.6.4 shows a photograph of one of the TLT stages shortly after assembly. Each of the 5Ω strip lines is clearly visible as is the 750μm thick Mylar that was required to insulate adjacent turns. The inductance of each line was measured using a Wien Kerr bridge and found to be 265μH at 10kHz, far greater than the minimum required.

5.7. Performance and Results.

The pulsed power supply was operated for several hours a day over a period of a week until a breakdown occurred in the 5th stage. The results presented below were obtained during this test period.

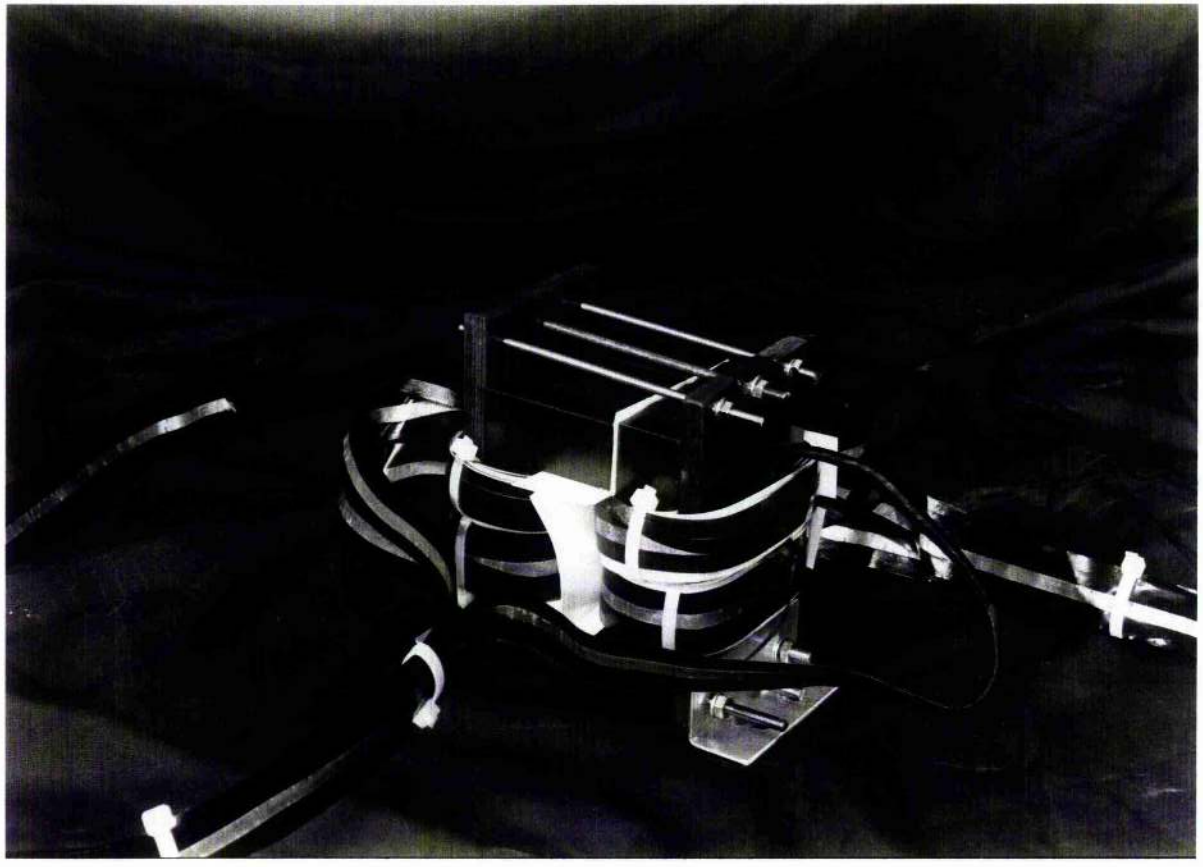

Fig 5.6.4 :- Photograph showing a single stage of the TLT. The magnetic core comprises 3 U and I cores made from 3C8 magnetic material. They are gapped with 750mm of Mylar. The four sets of strip transmission lines that make up a single stage are clearly visible.

Results :- Figure 5.7.1 shows the output voltage pulses produced from the pulsed power supply.

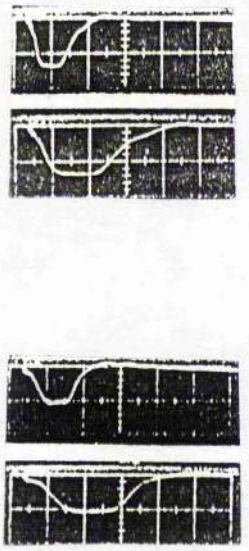

Fig 5.7.1:- Output voltage waveforms from the TLT pulsed power generator at (a) 68kV/div and (b) 168kV/div. 200ns and 100ns/div time base.

The top trace shows the output pulse produced when the Blumlein circuit was charged to 20kV. It has a risetime of 60ns, a maximum "flat-top" of 125ns and a peak amplitude of 89kV. This risetime is greater than the fall in volts at the switch, which was measured as being equal to 45ns, and suggests there was some loss in the first transmission line section. This loss is also believed to be responsible for the long falltime, t_f, or the "tailing" of the pulse. At a charge voltage of 34kV the output pulse risetime increased to 90ns and the pulse amplitude to 151kV. This increase in the risetime was due to the limited dI/dt

capability of the switch and indicates that faster risetimes can only be obtained by paralleling more glass thyratrons together, by using metal/ceramic tubes or developing pulse sharpening circuits.

For the voltage waveforms, it is possible to estimate the efficiency of the pulsed power supply which is defined here as being the amount of energy that is initially stored in the Blumlein circuit just prior to the discharge switch triggering to that discharged into the load. Calculations have shown this efficiency is of the order of 93% over 5 stages and it is believed that the 7% lost appeared as magnetic energy in the SM mode. This high efficiency is a consequence of the high value of $\xi = Z_2/Z_1$ that has been obtained using magnetics and primary lines of low impedance. It is estimated that the SM impedance in this system was approximately the minimum required, 325Ω. This gives a value of ξ of 16. Contrast this to the first TLT : there Z_2=350Ω, Z_0=50Ω , ξ=7 and the efficiency 85% over 4 stages

5.8. Assessing the Pulsed Power Supply.

This section assesses the relative merits and limitations of ceramic tile Blumlein circuit, the parallel thyratron switch and the stripline TLT. It then discusses whether they have potential in the future development of TLT systems.

Ceramic tile technology :- The Blumlein circuit generated reasonably good quality voltage pulses although they were not particularly fast. This was because first transmission line section degraded the leading edge of the voltage pulse by about 25ns or 2.5ns per tile. This degradation has been attributed to (i) dielectric loss (it takes energy to polarise a dielectric because the charged particles have a

specific mass and therefore an inertial resistance to being moved) (ii) the nonlinearity of the permittivity/electric field characteristic of the ceramic and (iii) stray capacitance between adjacent tiles. This result suggests that high permittivity tiles such as these cannot be used to produce fast voltage pulses. It has recently been shown that the optimum thickness of the tiles, when used at the 30kV - 40kV level, is about 10mm because the dielectric breakdown strength of the K2100 dielectric is 8kV/mm (at a thickness of 0.5mm). Any future ceramic tile work should therefore use tiles with this dimension because this will provide further weight and volume savings and should strengthen the case for using ceramic tiles in situations where sub-Ohm impedance levels are required. A further investigation is required to determine their lifetime and ability to operate at high repetition rates. This will be undertaken later in this research programme.

The parallel thyratron switch :- The parallel thyratron switch performed well. Switching speeds approaching 320kA/μs were obtained from 4 CX 1685 thyratrons which are individually rated at 80kA/μs. Controlling the current by regulating the thyratron gas pressure proved to be a simple and effective way to operate thyratrons in hard parallel and one that can produce a substantial cost savings because glass thyratrons are less expensive than ceramic tubes. The disappointing risetime of the output pulse produced by the Blumlein circuit was largely because of the limited switching performance of the CX 1685's and this shows the large disparity that exists between their switching capability and the performance required to measure the risetime limit of a particular TLT system. It has become apparent that the most immediate, simple and most cost effective solution to this problem is to incorporate a pulse sharpening circuit between he pulse generator and the TLT (pulse sharpening circuits can increase the risetime of

the leading edge of a voltage pulse at the expense of the fall time at the trailing edge). Research is, at the present time, focusing on their development because they will be required in high gain TLT systems. Pulse sharpening is discussed in chapters 6 and 7.

Another problem with the thyratron switch was the considerable amount of heat it generated. During tests the heater and reservoir circuits, which took several minutes to warm up, required an estimated 82 and 14 watts of heater and reservoir power and this raised the temperature of the insulating oil by some 10^0C. This brings into question the suitability of a thermionic switches for use in space because (i) most defense systems will have to be capable of operating instantaneously (ii) prime power requirements must be kept to a minimum and (iii) it is difficult to dissipate heat in the partial vacuum of space.

A cold cathode device can overcome these problems and although there are none commercially available with performance characteristics comparable to the thyratron, many are at the advanced development stage. For example, the 2.5 cm long silicon switch developed by Litz et al.[8], triggered with a 2mJ Nd:Yag laser pulse, produced a 2ns risetime voltage pulse from a 60Ω, 40kV Blumlein circuit, while Nunnelly[9] generated 1.8kA current pulses from a 25Ω 100kV PFL by triggering a 2.5cm x 0.5cm x 0.5cm silicon switch with a Q-switched Nd:Yag laser. Other power semiconducting switches such as the thyristor are also proving to be capable of operating pulsed power systems because improved fabrication techniques allows operation at several kV and hundreds of amps continuous current. Examples of series/parallel thyristor arrays can be found in the papers by Podlesak et al.[10], Hudgins et al.[11], A Schweizer and Steiner [13]. The Back of the

cathode Laser triggered Thyratron (BLT)[14-19] is probably the most promising cold cathode gas switch currently under development.

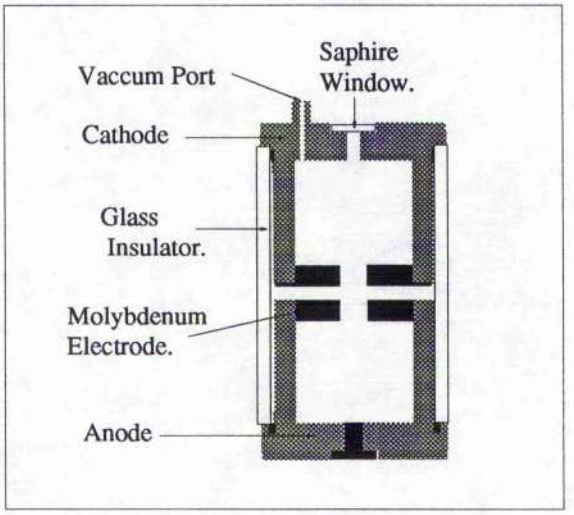

Fig 5.8.1 :- Schematic diagram of the BLT.

A schematic diagram of a BLT is shown in figure 5.8.1. It operates on the left hand side of the Paschen curve and comprises a simple anode and cathode cups separated by an insulator several mm thick. These electrodes have a central hole drilled through them. A discharge is initiated in the cathode region when the cathode is illuminated with a laser or flashlamp through that sapphire window (10mJ of energy at 222nm in a 15ns pulse has been found to be adequate). This discharge quickly extends into the hollow electrode structure at a velocity of $10^6 ms^{-1}$. There the yield of secondary electrons is increased by electron impact ionisation in the hollow cathode region. It is this multiplication of electrons that allows the BLT to be triggered with a few electrons in the cathode backspace.

Although BLTs are still at present, laboratory devices, they are probably the most promising cold-cathode switch under development because they have been extensively tested. For example, the paper by Hartmann et al. describes a BLT with dimensions 55mm x 35 mm and a 3mm electrode spacing that produced rates of rise of currents of 310 kA/μs (circuit limited) and peak currents of 17.5kA when used to switch a 25kV capacitor discharge circuit. This corresponds to a current density of $10kAcm^{-2}$ which is many orders of magnitude greater than can be achieved with hot dispensor cathodes[19].

The Stripline TLT :- Stripline appears to be able to produce efficient TLTs because it can be made with a low characteristic impedance and, being lightweight and flexible, can be wound onto a magnetic core. Each stage of the TLT comprised 4 5Ω lines in series because the 127μm thick Kapton dielectric, which was all that was available, had a breakdown strength of about 20kV. Stripline TLTs should therefore be considerably easier to build once metallised films become available with a greater electrical strength.

The main disadvantage with stripline is that it is prone to flashover because the electrode edge produces large fringing fields. This is why the TLT broke down in the 5th stage. In addition, the life span of stripline is shorter than coaxial cable because partial discharges and corona at the electrode edges degrade of the insulating properties of the dielectric. This means in applications where a high degree of reliability, a long operational lifetime and very high voltages are required, coaxial cable is best.

5.9 . Progress in the SPI Program.

Since the completion of this TLT the SPI work has continued. Darlingtons and other stacked line structures have been tested and assessed during the second phase of this research program to see if they can perform better than simple stacked line generators. These findings were briefly discussed in section 2.1 of chapter 2 and will not be repeated here. A number of pulse sharpening lines have also been developed and these are discussed in the following two chapters. At the present time a 10 stage TLT pulsed power supply is being designed. A low voltage version of the TLT has been tested together with some pulse sharpening circuits. It is hoped that these can be scaled to the appropriate voltages and the final device constructed later this year.

5.10 Summary of Chapter 5.

This chapter described a second TLT based pulsed power supply. It was built during the first phase of a three stage program which is attempting to develop a new generation of pulsed power supply for certain high repetition rate space based systems. It produced 150kV, 200ns voltage pulses into a 100Ω load and exhibited a number of new design features and construction techniques including a ceramic tile Blumlein circuit, a stripline TLT and a multi-parallel thyratron switch. It has been found that (i) high permittivity ceramic tiles can be used to produce good quality pulses (ii) striplines can produce efficient TLTs but are prone to flashover (iii) current control in a multi-parallel thyratron switch can be achieved by regulating the gas pressure (iv) thyratrons cannot switch at a rate sufficient to allow the risetime limit of many TLT systems to be determined (v) the power consumed by thyratron heater and reservoir circuits may make them unsuitable for use in space. This has lead to the conclusion that a cold-cathode

device may be a better type of switch for a space based systems and that a pulse sharpening circuit might be a simple, cost effective method of improving the risetime of the output pulse from a thyratron switched, low impedance pulse generator. Pulse sharpening is described in the following chapter.

References.

1). W. Dunbar and D. Schweickart ; "Effects of Breakdown Threshold for Power Components Exposed to the Natural and Induced space Environments", Proc 17th Power Mod. Symp. Seattle, (1986).

2). The Space Power Institute Prospectus ; Auburn Univ. USA.

3). A. Brown and P. Smith ; " A Multi-parallel Thyratron, Rep Rate Power Supply for High Power Gas Lasers" , Proc. 17th Power Mod. Symp., Seattle, (1986).

4). J.Reintjes and T. Godfrey ; "Principles of Radar", Mc-Graw-Hill Book Co., (1952).

5). R.Lake ; "The Parallel Operation of Hydrogen Thyratrons", Proc. 8th Power Mod. Symp. (1964).

6). G. McDuff ; Ph.D Thesis. Chapter 7. Univ. St. Andrews, (1989).

7). EEV Data Book, EEV Ltd, Chelmsford, England.

8). Proc. IEEE, 6th Pulsed Power Conference, p.153, Arlington, Virginia, (1987).

9). W. Nunnally and R.Hammond ; "80MW Photoconductive Power Switch", Appl. Phys. Lett., Vol 44, No.10, May, (1984).

10).T.Podlesak et al. ; " Demonstration of Compact Solid-State Opening and Closing Switches Utilising GTO's in Series", Proc. IEEE Trans. Elect. Devices, Vol. 38, No.4, April, (1991).

11). J.Hudgins et al. ; "High dI/dt Switching with Thyristors", Proc 18th Power Mod. Symp., p292, South Carolina (1988).

12). A. Schweizer and J.Steiner ; "Fast Switching Thyristor Replace Thyratrons in High Current Pulse Applications", ABB Publication No. CH-EC 1661 87 E, Power Semiconductor Division, Lenzberg, Switzerland.

13). M.A.Gunderson and G.Schafer ; "The Physica and Applications of Pseudosparks" New York, Plenum (1990).

14). K.Frank et al.: "High Rep-Rate Pseudospark switch for Laser Applications:, Proc. SPIE, Vol. 735, p 74, (1987).

15). K. Frank et al. "High Power Pseudospark and BLT Switches," IEEE trans. Plasma Sci., Vol. 16, No. 2, p. 317, (1988).

16). A. Tinschmann et al. " A High Voltage Gas Discharge Switch for High Power Applications," Jap. J. Appl. Phys., Vol. 29, No.2, p. 371, (1990).

17). G Mechtersheimer and R.Kohler ; " Multi-channel Pseudospark Switch," J.Phys. E: Sci. Instrum., Vol. 20, p.270, (1987).

18). Hartmann et al.; Proc 7th IEEE Pulsed Power Conf., Monterry, Ca., (1989).

19).———— "An Analysis of the Anomalous High Current Cathode Emission in Pseudospark and BLT Switches," J.Appl. Phys., Vol.65, No.11, p.4388, (1989).

CHAPTER 6.

Nonlinear Dielectric Pulse Sharpening in Pulsed Power.

6.0. Introduction.

It is now believed that the best way to generate a fast voltage pulse for a TLT is by sharpening the output from a pulse generator. This chapter explains how this can be achieved using conventional pulse sharpening circuits. It then introduces a new development in this area, the nonlinear dielectric (NLD) pulse sharpening line. This emerged as a spin-off from the work reported in chapter 4. To demonstrate this new technology two NLD HV pulse sharpening ladder networks are described and their performance analysed. The first demonstrates the "Catch-Up Theory", the second that solitary waves or "solitons" modulate a sharpened waveform when a pulse contains frequency components near the cut-off frequency of the line. Both show that nonlinear capacitors have excellent pulse sharpening characteristics.

6.1. Magnetic Pulse Sharpening Techniques.

In recent years magnetic pulse shaping circuits have become standard techniques in the pulsed power field, primarily because there are few alternative circuits available that can increase the rate of rise of current at a load beyond the capability of the primary switch. Probably the most familiar one of these is the

"pulse compression circuit" that was developed to drive the early magnetrons during the second world war. An example is shown in figure 6.1.1 and a comprehensive description of how it works can be found in the paper by Melville[1]. It consists of a series of LC stages, each separated by a switch and each with a shorter charging time. Pulse compression is obtained by closing these switches in sequence and transferring charge in steps to the faster stages. In the original circuits ignitrons or hydrogen thyratrons were used but today "magnetic switches" are favoured because they have a longer life, radiate less electrical noise and are capable of instantaneous operation.

Recently, the advent of the new ferrites and amorphous glasses has revived an interest in magnetic pulse compression circuits (MPC)[2] although their basic design has changed little over the years. They are capable of operating at repetition-rates of 10kHz and efficiencies of 85%[3,4] and are frequently used in laser discharge circuits, e.g. the Lambda EGM Series. They can also be scaled to high voltages. For example, the 100kV modulator by Stockton[5] called RAMESES I uses a magnetic switch to produce a 200ns pulse for a 1Ω coaxial water transmission line and Comet[6], the 6MV 400 J/pulse accelerator uses one to generate a 23ns risetime pulse into a 2.16Ω load. The problem with magnetic switches is that they cannot be used to produce output pulses with risetimes less than a few tens of nanoseconds because there is still a significant amount of inductance present in a saturated magnetic switch.

Faster risetimes can be produced using a pulse sharpening transmission line that contains a nonlinear magnetic material[7] either in the form of a distributed dielectric or as inductor cores. Pulse sharpening is caused by the amplitude dependence of

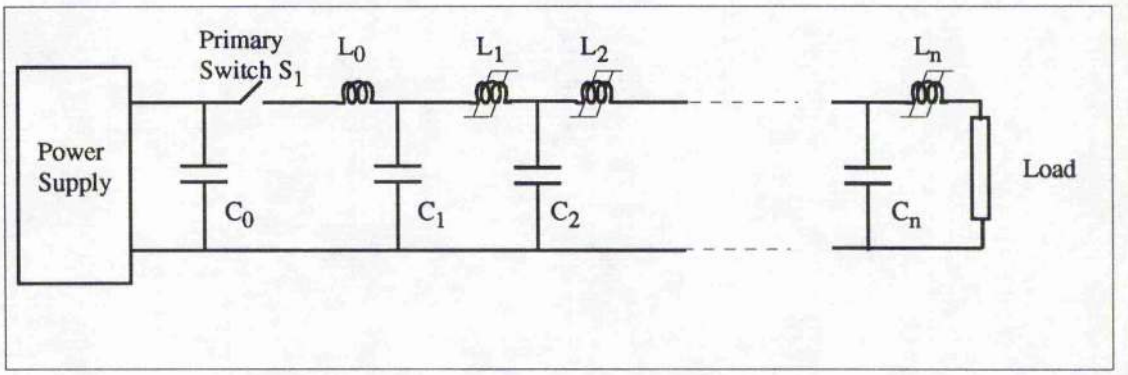

Fig 6.1.1 :- Circuit diagram of a simple magnetic pulse compression circuit. In the general case $C_0=C_1=C_2=C_n$ and $L_1>L_2>L_n$.

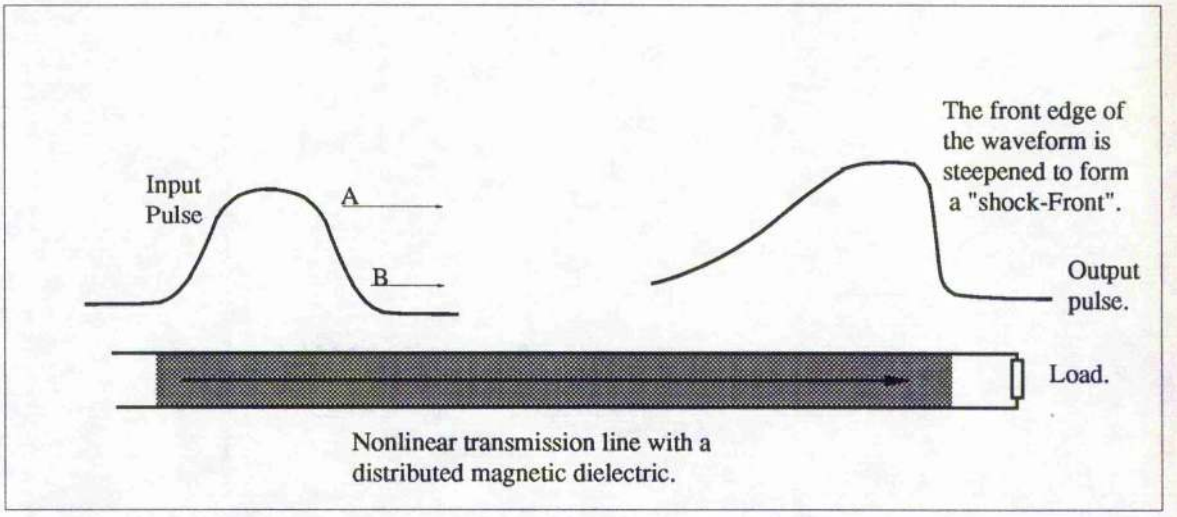

Fig 6.1.2 :- Schematic diagram showing the principle of the magnetic "shock-line".The transmission line constains a nonlinear magnetic material that is distributed throughout its length. Because the velocity of the input pulse is faster at point A than point B, the leading edge steepens to form a "shock front".

the phase velocity of the signals propagating along these lines. This increases with signal amplitude because the permeability of the magnetic material falls as it is driven into saturation; it is given by :-

$$v = \frac{1}{(\varepsilon_0 \mu_0 \varepsilon_r \mu_r(H))^{1/2}} \qquad 6.1.1.$$

where $\mu(H)$ permeability of the magnetic material. The other symbols have their usual meaning.

For example, in the distributed line shown in figure 6.2.2, point A will propagate faster than point B and sharpen up the leading edge. This will continue until the pulse sharpening process is counter balanced by dispersion due to transmission line losses. Lines such as these have enabled Xinming and Dianyuan[8] to pulse sharpen to 1.5ns at 8kV and Sneddon and Thornton[9] to produce output pulses with a risetime of 350ps at 100kV.

The main disadvantage with a magnetic pulse sharpening circuit is that it is difficult to scale because the magnetic cores are large and heavy and the windings of the inductors difficult to insulate. In addition, they must be cooled when used at high repetition rates because hysteresis and eddy current losses cause the cores to heat-up. This can easily alter the electrical characteristics of the pulsed power circuit because the magnetic permeability and hence the magnetic flux density, B, is a strong function of temperature.

The pulse sharpening circuit to be described next is analogous to magnetic pulse sharpening in that it is the fall in the permittivity with electric field that produces an amplitude dependent pulse velocity. It was first demonstrated at low voltages in the 1960s using reverse biased varactor diodes (Fallside and Bickley[10], Owens and White[11]) but never before at high voltages using nonlinear dielectrics. This is therefore thought to be a new development in pulsed power.

6.2. Pulse Sharpening Lines using Nonlinear Capacitors.

The original "proof of principal" experiment for the NLD shock-line was conducted at the 1kV level using simple "off-the-shelf" high frequency 10nF decoupling capacitors with a maximum voltage rating of 2kV and a dielectric thickness of 0.4mm (the dielectric in these capacitors has been called dielectric A).

Figure 6.2.1 shows the fall in capacitance in these capacitors as a percentage of the initial unstressed dielectric. These measurements were obtained using the same experimental procedure described in section 4.4, i.e the test capacitor was charged in series with a linear one and the combined capacitance measured using a capacitance meter. As has previously been explained, this is the "differential capacitance" because the amplitude of the signal produced by a capacitance meter is very much less than that of the applied DC voltage. From the graph, the unstressed capacitance was 10nF and the differential capacitance 25% of this value at 2 kV/mm.

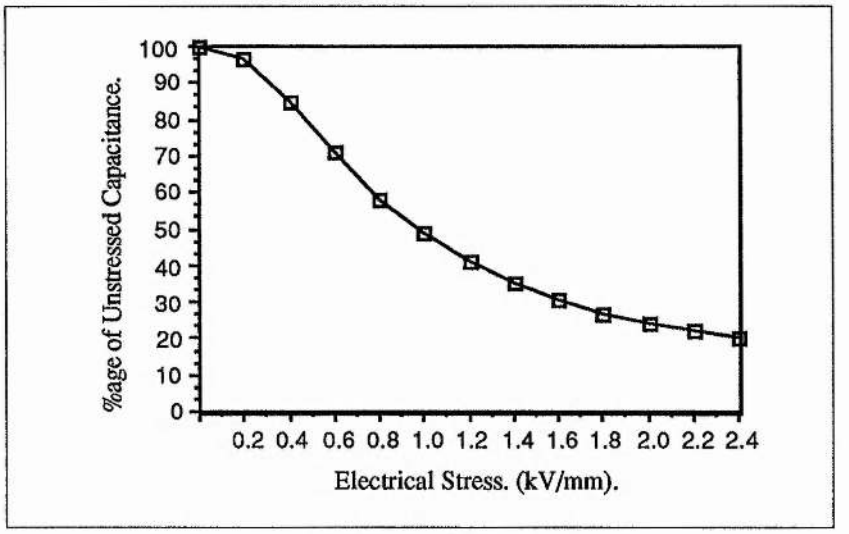

Fig 6.2.1 :- A plot of the variation of the capacitance as a percentage of the initial unstressed capacitance for the test capacitors containing "dielectric A".

The test circuit that was used to evaluate the pulse sharpening properties of these capacitors is shown in figure 6.2.2. The initial voltage waveform was produced using a simple resonant charging circuit that consisted of a 150nF and 100nF capacitor and a hydrogen thyratron discharge switch. It was injected into a 9 section LC ladder network constructed from 2μH air-core inductors and the capacitors under test. This network was terminated by the saturated line impedance, that is, the impedance at maximum signal amplitude or the minimum capacitance value. This was calculated using the value of the capacitance at an electric stress of 2.2kV/mm in the standard impedance equation :-

$$Z_{sat} = \left(\frac{L}{C_{sat}}\right)^{1/2} \qquad 6.2.1.$$

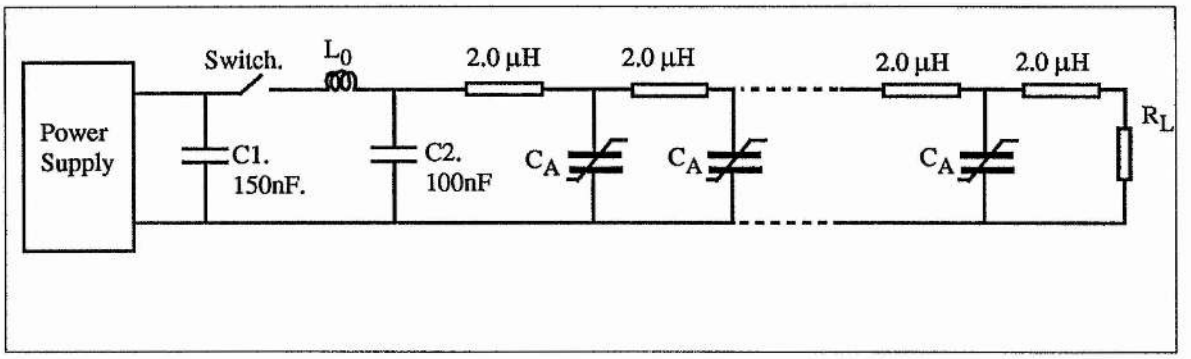

Fig 6.2.2. :- Circuit diagram of the 9-stage ladder network.

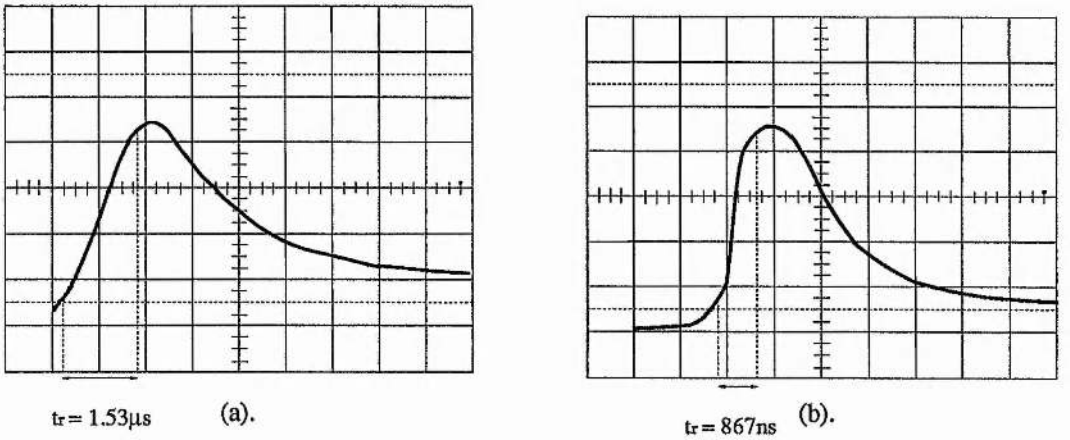

Fig: 6.2.3 :- (a) Input and (b) output waveforms from a 9 stage ladder network containing capacitors constructed from dielectric A. 1 μs/div; 200V/div.

The value of C_{sat} was 2.5nF and the saturated impedance 28Ω.

The input waveform that was produced by the resonantly charged circuit is shown in figure 6.2.3.(a). It has a risetime of approximately 1.53μs and an amplitude of 900V (or a peak electric field of 2.25 kV/mm). The output pulse is shown in figure 6.2.3.(b). Its leading edge has been sharpened to 857ns (10% - 90%) and its amplitude is approximately equal to that of the input pulse. Note that the delay, 1.3μs, is given by the unsaturated propagation delay time, $T_{(unsat)}$, calculated using the capacitance value at zero stress.

6.3. Mathematical Analysis and the "Catch-Up Theory".

It is extremely difficult, if not impossible, to obtain a simple expression for the transfer function for a nonlinear ladder network in terms of the measurable circuit parameters such as the signal amplitude and the voltage dependent capacitance, C(V) because the "nonlinear telegraphist equation" is difficult to solve.

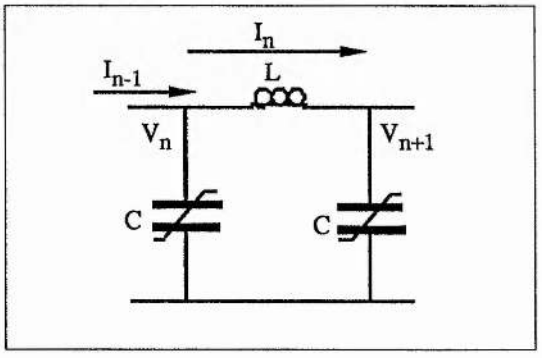

Fig 6.3.1 :- Single stage of a nonlinear ladder network.

This can be shown by considering a single stage of a ladder network (see figure 6.3.1). The usual way to solve these networks is to apply the analysis of Benson and Last[12] and use Kirchoff's laws to obtain the initial set of differential equations :-

$$C\frac{dV_n}{dt} = I_{n-1} - I_n . \qquad 6.3.1.$$

$$L\frac{dI_n}{dt} = V_n - V_{n+1}. \qquad 6.3.2.$$

These describe the change in current and voltage along the line due to the current I_n flowing in the inductor and the current $I_{n-1} - I_n$ in the nonlinear capacitor. An approximate continuous wave equation for the lumped element line can be derived from 6.3.1 and 6.3.2. This takes the form of the differential difference equation :-

$$LC\frac{d^2V_n}{dt^2} = V_{n+1} - 2V_n + V_{n-1}. \qquad 6.3.3.$$

To develop this analysis further it is necessary to obtain an approximation to $V_n(t)$ using a continuous variable function $V(x,t)$ such that $V_n(t) = V(n\,\delta x, t)$, where δx is a constant. By expressing V_{n+1} and V_{n-1} in terms of a Taylor expansion of $V(x,t)$ about $V(n\,\delta x, t)$, we get :-

$$L'C'\frac{\delta^2V}{\delta t^2} - \frac{\delta^2V}{\delta x^2} \approx \frac{\delta x^2}{12}\frac{\delta^4V}{\delta x^4} \qquad 6.3.4.$$

where L' δx = L and C' δx = C. In the case where the capacitance is nonlinear, equation 6.3.4 becomes :-

$$L\frac{\delta^2 C'(V)V}{\delta t^2} - \frac{\delta^2 V}{\delta x^2} \approx \frac{\delta x^2}{12}\frac{\delta^4 V}{\delta x^4} \qquad 6.3.5.$$

where C'(V) is the function that describes the nonlinearity of the dielectric. On the assumption that :-

$$C'(V)\ V = C_0'(V+\varepsilon f(V))$$

where C_0' is a constant, f(V) is a function representing the nonlinearity and ε a constant that determines the strength of this nonlinearity, equation 6.3.6 becomes :-

$$\frac{\delta^2 V}{\delta t^2} + \varepsilon\frac{\delta^2 f}{\delta t^2} \approx \frac{1}{L'C_0'}\left[\frac{\delta^2 V}{\delta x^2} + \frac{\delta^4 V}{12}\frac{\delta^4 V}{\delta x^4}\right] \qquad 6.3.7.$$

Following a perturbation method introduced by Washimi and Taniuti[13], V is now expressed as a power series expansion in the small parameter ε :

$$V(x,t) = \varepsilon V^{(1)}(x,t) + \varepsilon^2 V^{(2)}(x,t) \ldots\ldots\ldots\ldots \qquad 6.3.8.$$

where $V^{(1)}$ is the first order approximation, $V^{(2)}$ the second etc. Changing the cordinates of this system to one moving at a velocity c is achieved using the substitutions :

$$\xi = \varepsilon^{1/2}(x-ct) \quad \text{and} \quad \tau = \varepsilon^{1/2} ct.$$

where $c = (L'C_0')^{-1/2}$.

Collecting terms in the same power of ε, an equation for $V^{(1)}$ is obtained :-

$$2\frac{\delta^2 V^{(1)}}{\delta\xi\delta\tau} - \frac{\delta^2 f}{\delta\xi^2} + \frac{\delta x^2}{12}\frac{\delta^4 V^{(1)}}{\delta\xi^4} = 0 \qquad 6.3.9.$$

Integrating this equation once with respect to f and assuming a quadratic nonlinearity of the form $f(V) = -aV^2$ results in :-

$$\frac{\delta V^{(1)}}{\delta\tau} + \alpha V^{(1)}\frac{\delta V^{(1)}}{\delta\xi} + \frac{\delta x^2}{12}\frac{\delta V^{(1)}}{\delta\xi^3} = 0 \qquad 6.3.10.$$

This is the form of the well known Korteweg- de -Vries equation . If the input pulse has a risetime well below the cut-off frequency of the line the third term in the equation, the dispersion term, can be neglected. The velocity of the propagating pulse then becomes amplitude dependent and and pulse sharpening occurs. There appears, however, to be no simple technique available to obtain a straight forward algebraic solution for the form of the output pulse usimg

equation 6.3.10 although a solution for a *distributed* line has been developed by Peng and Landauer[14].

For design purposes it is, however, possible to estimate the pulse sharpening properties of a line by calculating the difference in the delay time at 10% and 90% of the signal amplitude using the standard network equations for the characteristic impedance, cut-off frequency and delay time. In this "catch-up" theory the reduction in risetime, t_s, produced by each section of a nonlinear network is given by :-

$$t_s = (LC(V_{10\%})^{1/2} \left(1-\left[\frac{C(V_{90\%})}{C(V_{10\%})}\right]^{1/2}\right) \qquad 6.3.11.$$

and the value of the capacitors at the appropriate signal amplitude by the curve of figure 6.2.1. Note that this theory is only applicable if the pulse risetime is greater than[15] :-

$$t_{rise,min.} = \frac{\pi}{4}\left[L\,C(V_{max})\right]^{1/2}$$

because the network equations are only applicable below the cut-off frequency of the line.

It is possible to use equation 6.3.6 to obtain a first approximation to the sharpening potential of a particular nonlinear network. It is therefore a useful design relation because it can be used to estimate the number of stages required to

produce a specified pulse risetime in a given NLD pulse sharpening circuit. It can also be used to check that a line is performing correctly. Figure 6.3.2 shows how it was applied to the pulse sharpening circuit described previously.

6.4. High Voltage Pulse Sharpening.

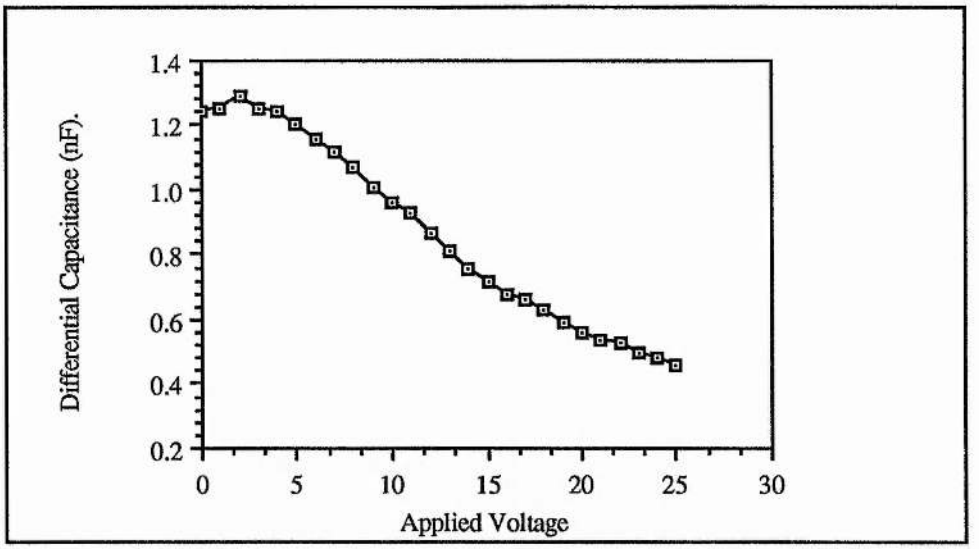

Fig 6.4.1: Differential Capacitance against DC bias voltage for dielectric B.

Extending these ideas to higher voltage levels required the use of "door knob" capacitors that could operate at the 30kV level and had a nonlinearity comparable to that of dielectric A. The dielectric that satisfied these demands has been called dielectric B and its voltage/capacitance characteristic is shown in figure 6.4.1. It

Details of the Pulse sharpening line.	Dielectric Type A.
Pulse amplitude.	900V.
Inductance per stage.	2μH.
Initial unstressed capacitance.	10nF.
Unsaturated delay time/ stage.	141ns.
Total delay time along line.	1.27μs.
Field across capacitor at 90% voltage amplitude.	2.25 kV/mm.
Capacitance at 2.25kV/mm.	2.5nF.
Saturated delay time/stage.	71ns.
Catch-up time /stage.	70 ns.
Total catch-up time of line.	630 ns.
Experimentally determined catch-up time of line (change in risetime between input and output pulse).	663 ns.

Fig 6.3.2 :- Results from the low voltage nonlinear dielectric pulse sharpening line containing dielectric type A

was made from a proprietary ceramic material based on a barium titanate formulation with a Curie temperature of 12^0C. This particular mix contained no modifying agent to depress the permittivity peak and consequently it had a strong temperature and voltage dependence.

A diagram of the circuit used to demonstrate HV pulse sharpening is shown in figure 6.4.2. The initial voltage waveform was produced using a simple capacitor discharge circuit that consisted of a 150nF rapid discharge Maxwell capacitor that had been pre-charged to 30kV with a Wallis power supply. It was discharged through a 5μH inductor with a CX1685 glass thyratron using the same triggering, heater and reservoir supply circuits discussed in section 3.4. The resulting voltage pulse, which had a risetime of 340ns and an amplitude of -28kV, was injected into a lumped element ladder network that consisted of 15 LC sections, each comprising a 1.5μH air core inductor and a nonlinear capacitors. The line was terminated with a 50Ω copper sulphate resistive load. The voltage waveforms were measured at the input, at the seventh stage and at the load resistor using copper sulphate resistive voltage probes and a Tektronix 2440 digital sampling oscilloscope.

These waveforms are shown in figures 6.4.3 - 6.4.5. The input at the first stage of the network had an amplitude of -28kV and a risetime of 340ns, corresponding to a rate of rise of current of 1.65kA/μs. At the seventh stage, this risetime was reduced to 70ns and the waveform modulated by a strong high frequency oscillation at 15MHz. The output waveform, shown in figure 6.4.5, also had an

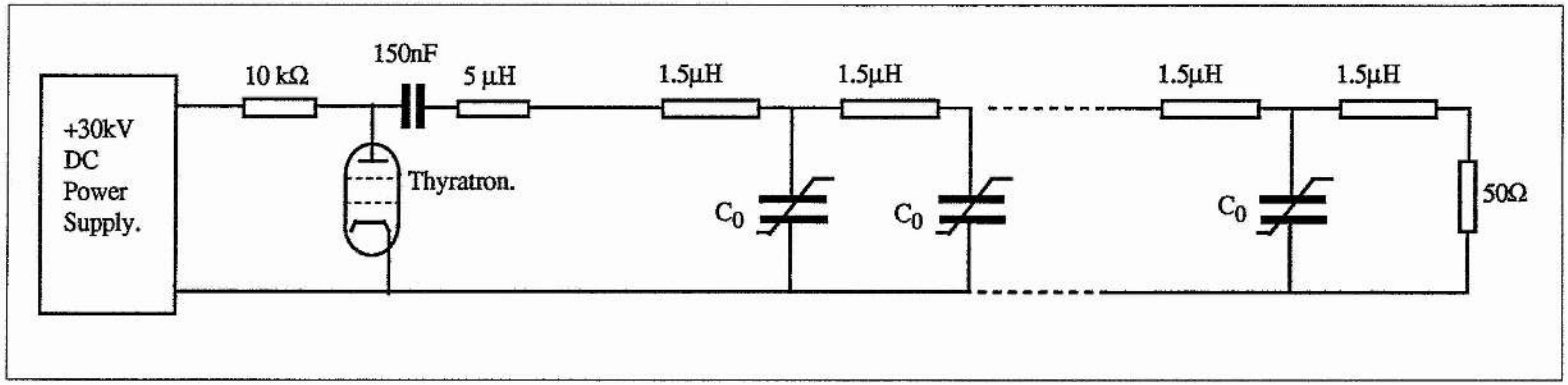

Fig 6.4.2 :-Circuit diagram of the 15-stage ladder network.

amplitude of -28kV but a risetime of under 50ns. This represents a dI/dt at the load of 11.2kA/μs, or an improvement of just under 10kA/μs along the line.

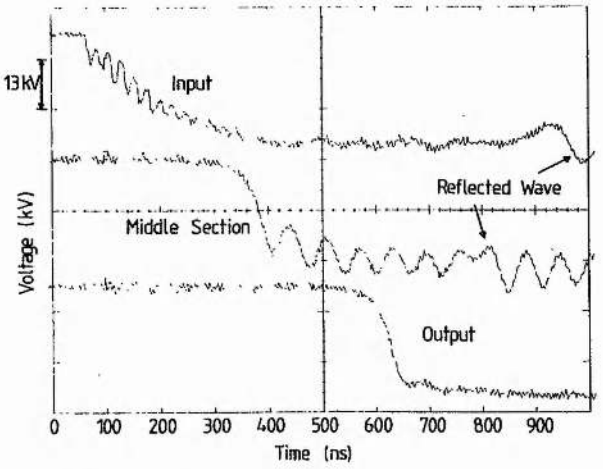

Figures 6.4.3 - 6.4.5 :- The voltage pulse for the HV shock line.

Note also that in the first 7 sections the pulse risetime was reduced by about 260ns compared to just 20ns between stages 8-15. This was because of dispersion of the high frequency components of the pulse near the cut-off frequency of the line. When dispersive effects become significant (i) the "Catch-up Theory" cannot be applied and (ii) the dispersion term in the nonlinear general wave equation 6.3.10 must be retained[16]. Physically, the dispersive term distorts and spreads the voltage pulse while the nonlinear term sharpens and steepens it. These combined effects compete with each other and when they balance they produce an oscillatory steady state solution called a soliton. These solitons appear as the high frequency oscillation on the voltage waveform in figure 6.4.3. This oscillation, which has been reported in many of the original dielectric pulse sharpening experiments using varactor diodes[17,18], modulates the power

delivered into the load. Furthermore, as a wavefront evolves into a soliton array an increasing fraction of the propagating power is present in frequencies that are close to the cut-off frequency of the line. These frequencies cannot be coupled out simultaneously because of the rapid variation of the matched value of the terminating of the line near the cut-off frequency, given by :-

$$Z_T = Z_0 \left[1 - \frac{\omega^2}{\omega_c^2} \right]^{1/2} \qquad 6.4.1.$$

for a network constructed from "T" sections with a cut-off frequency ω_c and with a low frequency characteristic impedance $Z_0=(L/C)^{1/2}$.

This means that any resistive termination will reflect a fraction of the incident power. This can be seen in the form of a reflected wave in figure 6.4.3. The implication is that there is an upper limit to the useful length of a lumped element shock-line, above which no further reduction in pulse risetime occurs and the overall pulse shape is degraded by the instability of the waveform.

The best way to model pulse sharpening lines is by computer. The line just described has been analysed using a code developed by Turner[19]. The nonlinearity of the capacitors was modelled by fitting the nonlinear curve to equation 6.3.4 and the resulting set of differential equations solved numerically using the method of Stoer and Bulirsch[20].

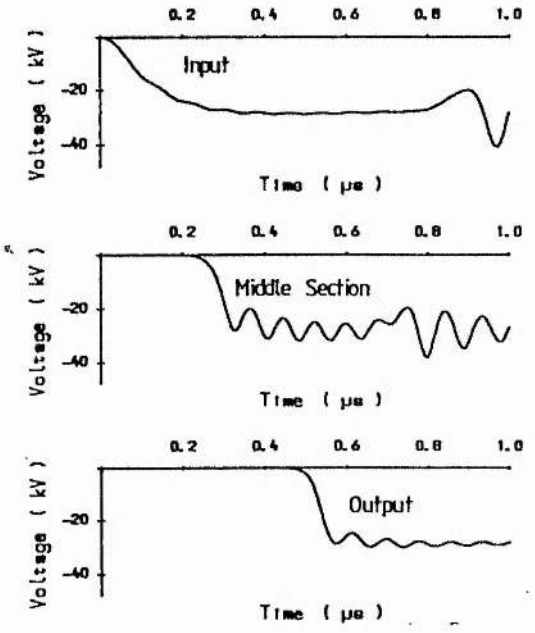

Fig 6.4.6 - 6.6.8 :- Predicted leading edge profiles that correspond to those given in figures 6.4.2 - 6.4.5.

The results are shown in figures 6.4.6 - 6.4.8. There is a remarkably close correlation between these and the experimental waveforms. It is therefore hoped that this computer model can be used to develop lines that can operate at low impedances and produce risetimes down to 20ns because these should be particularly useful in the development of high gain TLT systems.

6.5. Summary of Chapter 6.

This chapter has been concerned with the application of nonlinear dielectric materials in pulsed power. A nonlinear dielectric pulse sharpening line has been developed and the concept demonstrated at low voltage levels as a proof of principle exercise. The ideas have also been demonstrated at the 30kV level using a 15-stage pulse sharpening line. This sharpened the voltage waveform produced by a capacitor discharge circuit from 340ns down to 50ns. The response of the line has been modelled by computer and excellent agreement has been obtained

between the experiment results and the predictions of the computer model. It is thought that this model can be used to develop a NLD pulse sharpening line to sharpen up the pulse produced by low impedance pulse generators before it is injected into a TLT.

References.

1). W.S.Melville ; Proc. IEE., Vol 98. p 185. (1951).

2). Erice and Trapani ; 4th Workshop "Pulsed Power Techniques for Future Accelerators", Sicily, March (1988).

3). R.I.Okunev et al ; "Magneto Thyristor Pulse Compression Generator for Copper Vapour Lasers", Journal Tech. Phys., No.(**9**). pp 670-673, (1983).

4). T.Shimada and M.Ohara ; 5th IEEE Pulsed Power Conference Proc. Va. U.S.A. (1985).

5). M.Stockton et al ; J.Appl.Phys., 53(**3**) March (1982).

6). Neau ; "Comet, a 6MV, 400kJ Magnetically Switched Pulsed Power Module", Proc. 4th IEEE Pulsed Power Conference, p246, June, (1983).

7)."Electromagnetic Shock Waves." I.G.Katayev, London Iliffe Books Ltd. (1966).

8). Z. Xinming et al ; Chinese Physics - Lasers, No.(**13**), p483, July (1986).

9). Sneddon and Thornton ; Rev. Sci. Instru. 59, p2497, (1988).

10). A.R.Owens and G White ; "Generation of High Speed Waveforms using Nonlinear Delay Lines". Proc. IEE., Vol. 113, No.(**11**), Nov. (1966).

11). F.Fallside and D.Bickley ; Electron. Lett., Vol. 2, No. (**1**), Jan (1966).

12). F.A.Benson and J.D.Last ; "Analysis of Lumped Parameter Nonlinear Transmission Lines", Electronics Lett., Vol. 1, No.9, Nov. (1965).

13). H. Washimi and T. Taniuti ; "Propagation of Ion-Acoustic Solitary Waves of Small Amplitude ", Phys. Rev. Lett., Vol. 17, p. 996, (1966).

14). S.T. Peng and R. Landauer; "Effects of Dispersion on Steady State Electromagnetic Shock Profiles", IBM J. Res. Develop. No.(**17**), p 299, (1973).

15). M.M Turner et al ; Proc 19th Power Modulator Symposium, San Diego, July (1990).

16). G.E.Peterson "Solitons", Bell Labs Tech. Journal. Vol 63, No.(**6**), p 900, July - August (1984).

17). A.R.Owens and G.White ; Electron. Lett., Vol.2, No.(**5**), May (1966).

18). F.Fallside and D.Bickley ; Electron. Lett., Vol. 2, No. (**1**), Jan (1966).

19). M.M Turner et al ; Proc 19th Power Modulator Symposium, San Diego, July (1990).

20). J.Stoer and R Burlish; "Introduction to Numerical Analysis" Springer, New York, (1990).

CHAPTER 7.

Summary and Conclusion.

7.0 Introduction

This thesis, which has been concerned with the development of TLT pulsed power supplies, is summarised in this last chapter. Future work is also discussed, as are a number of other relevant pieces of work that have recently been completed. Some new and novel pulse sharpening circuits are also described.

7.1. Review of the TLT work and its Major Findings.

Chapter 1 introduced the concept of preionisation, described a number of preionisation techniques and discussed the pulsed power requirements of flash x-ray preionisation sources. This showed that an output pulse risetime of 6kV/ns and a peak voltage of about 100kV can produce uniform electron emission along a cold cathode field emitter. It also explained that it is difficult to produce these requirements with pulse transformers, Marx generators or pulse charged pulse generators because there is always a certain amount of stray inductance and capacitance in these circuits. Chapter 2 demonstrated that a transmission-line transformer can be used as a fast, efficient HV generator that is well suited for use in an x-ray preioniser. It also established that :-

1). The mechanism of line stacking excites a secondary mode of propagation and the performance of a TLT is directly related to how effectively this mode is suppressed. In addition, if a TLT is constructed from short lengths of HV 50Ω coaxial cable, it can have a GHz bandwidth.

2). The primary loss mechanism in a TLT is the skin-effect. Radiation and dielectric loss may also play apart but these are, in general, of secondary importance. For HV 50Ω coaxial cable, these losses are so low that it may be possible to operate a TLT at kHz repetition rates.

3). The output risetime of a TLT is principally determined by the response of the transmission line to a step excitation. For 50Ω HV coaxial cable this is given by :-

$$V_{out}(t) = V_{in}\left[1 - \mathrm{erf}\frac{1K}{4Z_0 t^{1/2}}\right]. \qquad 7.1.1.$$

where V_{in} is the amplitude of the input step, t the time after the propagation delay, l the length of the cable and :-

$$K = \frac{1}{2\pi r}\left[\frac{\mu}{\delta}\right] \qquad 7.1.2.$$

where r is the conductors radius, μ the permeability and δ the conductivity of the wire .

4). The low frequency response of an inductively isolated TLT is given by the time constant of the isolating inductance at the Nth stage and the output impedance of the previous N-1 stages, i.e.

$$L_{(Line\ N)}/(N-1)Z_0 = 10t_p \qquad 7.1.3.$$

5).The parameter $\xi = Z_2/Z_0$ can be used as a measure of how effectively the secondary mode is suppressed (Z_2 is the secondary mode impedance and Z_0 the characteristic impedance of the transmission line).

6). The TLT can be modelled as a Thevenin equivalent circuit and its initial gain calculated using the equation :-

$$V_{out} = \frac{(V_T + 2V)\, Z_L}{Z_L + Z_T + Z_0}$$

where

$$V_T = \frac{4\,VZ_2}{(\beta+1)Z_0}\ \frac{1 - \alpha^{2n-2}}{1 + \alpha^{2n-1}}$$

$$Z_T = \frac{2\,Z_2}{(\beta+1)}\ \frac{1 - \alpha^{2n-2}}{1 + \alpha^{2n-1}}$$

and

$$\alpha = \frac{(\beta - 1)}{(\beta + 1)} \quad \text{and} \quad \beta = \left[1 + \frac{4Z_2}{Z_0}\right]^{1/2}$$

where Z_L is the impedance of the load and the other symbols have their previously defined meaning.

Chapters 3 and 5 described the design, construction and performance of two HV TLT pulsed power supplies. The first of these, the "prototype", was a 4-stage device constructed using 50Ω coaxial cable. It produced good quality 100kV, 200ns output voltage pulses with risetimes of 50ns and was used to drive a flash x-ray generator that preionised a large volume discharge pumped mercury bromide laser. This produced 760mJ output pulses at efficiencies of 1.5% at 502nm; this is thought to be the second highest output energy that has been obtained with this type of laser to date[1]. The second TLT, which produced 150kV voltage pulses with durations of 200ns and risetimes of 90ns, was constructed to help assess whether TLT technology can be used in space. It was constructed by winding striplines etched from metallised Kapton onto magnetic cores and was over 93% efficient.

Important Points Arising from the TLT work :- The design and construction of the two HV TLTs has shown that stacked line technology can be scaled to moderate pulsed power levels and used to generate good quality voltage pulses efficiently. A TLT pulsed power supply should therefore prove to be useful for driving some e-beam machines, flash x-ray generators and microwave sources. The mutually wound TLT, which was made from standard HV 50Ω coaxial cable, demonstrated a design that is cheap and easy to build and best suited for the generation of short voltage pulses. This is because the cable is too inflexible to wind onto magnetic cores of any practical size and, by equation 7.1.4, the winding inductance per stage, L_N, is directly proportional to the pulse duration t_p.

$$L_N = 500t_p\,(N\text{-}1) \qquad 7.1.1.$$

It is also the best choice of line to use for very high voltage TLTs because it is less likely to flashover than stripline. The fact that it is now available in impedance values down to 15Ω is an important development because it means that future mutually wound TLTs can be constructed with lower output impedances and higher efficiencies.

In contrast, the stripline design used in the second TLT enables higher efficiencies to be achieved because magnetic cores can produce higher secondary mode impedances. It is, however, more difficult to construct because stripline has to be carefully insulated; it also has a shorter life because the large fringing fields generated at the electrode edges produce partial discharges and corona which degrade the insulating properties of the dielectric.

The pulse generator used in this second TLT demonstrated a ceramic tile Blumlein circuit and a parallel thyratron switch in which the current distribution was controlled by regulating the reservoir voltage and gas pressure. This technique, which has not been demonstrated before, is relatively simple to implement and straight forward to operate. The relatively slow output voltage risetimes and repetition-rates produced by the Blumlein circuits has shown the large disparity that exists between the performance potential of commercially available HV equipment and the requirements for TLT Blumlein circuits. For example, a dI/dt of 1500kA/μs is required to produce a 10ns pulse from a 4Ω

Blumlein circuit charged to 30kV, but the fastest thyratron available, the CX 1625, can only switch at 320kA/μs [2]. Likewise, if a 30kV, 100nF line is required to operate at 1kHz then it must be charged at 45kJ/s. However, some of the best charging units available are only capable of charging at about 4000J/s, far less than required[3]. Future TLT research must therefore concentrate on developing (i) new and novel charging systems to enable higher repetition rates to be achieved (ii) thyratrons and other switch technology (iii) pulse sharpening circuits that can sharpen up the output from a pulse generator. A number of circuit designs and systems have been devised that should enable substantial in improvements to be made in areas (i) and (ii) in the near future. More pulse sharpening circuits are discussed later in this chapter.

7.2. The Ceramic Tiles.

The ceramic tiles that have been manufactured and tested have been used to construct a PFL and Blumlein circuit which were smaller in volume and lighter in weight than comparable water dielectric PFLs or lumped element PFN type circuits. It should be possible to make them even more compact using thinner tiles (10mm appears to be the optimum for charge voltages of 30kV-40kV). The voltage pulses produced by these lines are of a reasonable quality although they are not particularly fast because stray capacitance at the interfaces between adjacent tiles, the nonlinearity between the permittivity and the electrical stress and dielectric loss degrades the risetime. Recent work at low voltages has suggested that dielectric loss is the most serious loss mechanism and there is a trade-off between the permittivity of a material and its ability to transmit fast voltage pulses. This has been observed by N.C.Jaitly et al[4]. Their 3m transmission line made from a high permittivity PVDF solid dielectrics (permittivity 10 - 12) degraded the

risetime of propagating pulses from 3-4ns to 25ns-30ns. This was not observed when lower permittivity dielectrics such as Mylar or Kapton were used.

Future ceramic tile work will concentrate on developing distributed nonlinear transmission lines for the generation of sub-nanosecond high repetition rate voltage pulses. Since success will depend on the development of new dielectric materials and ceramic tiles, such as the K3500 variety described in chapter 4, it may be necessary to collaborate with capacitor manufacturers and materials scientists to identify the causes of dielectric loss and the reasons for the nonlinear behaviour of dielectric materials[5,6,7]. This could result in the initiation of a program of work dedicated to the development of nonlinear dielectrics for pulsed power.

7.3. Pulse Sharpening

Although nonlinear dielectric materials are used extensively in the optical field[8,9], this is not the case with pulsed power. This may, however, be a situation that will change because recent work has suggested that nonlinear pulse sharpening circuits may soon produce substantial improvements in the performance of pulsed power systems. This is because they can increase the rate of rise of voltage and current beyond the switching capability of many thyratrons, operate at high repetition-rates, are cheap and easy to construct and provide a match to certain nonlinear time dependent loads such as an e-beam diode. This is because the impedance swing, $\Delta Z = Z_{sat} - Z_{unsat}$, that occurs when a propagating pulse drives a NLD line into saturation can be controlled by the choice of the

nonlinear circuit element(s). For example, ΔZ was changed from 27Ω to -150Ω* when the inductors in the NLD line of chapter 6 were wound onto F5 MnZn high power transformer cores and the input pulse risetime reduced from 250ns to 22ns with a 30Ω load (see figures 7.3.1 and 7.3.2). These circuits can also be used with a constant impedance load because it is possible to match the fall in permittivity in a dielectric with the permeability in a ferrite to produce a constant impedance pulse sharpening line.

Pulse risetimes faster than those shown in figure 7.3.2 can only be obtained using distributed lines because these have a higher cut-off frequency. For a distributed line to work, however, it is essential that the dielectric nonlinearity decreases the risetime of the pulse faster than dielectric loss can increase it. The K3500 ceramic tiles seem to have this property because they have been used in a 4Ω pulse sharpening line that successfully sharpened up a 25kV 55ns risetime voltage pulse to 35ns (see figures 7.3.3).

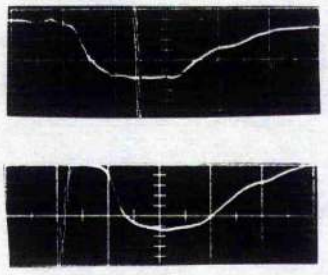

Fig 7.3.3 :- Input and output pulses from a 4Ω distributed pulse sharpening line constructed from the K3500 ceramic tiles. (pulse amplitude 25kV: time base 100ns. The leading edge has been sharpened from 55ns to 35ns.

* The negative sign means the final impedance was less than the initial unsaturated impedance

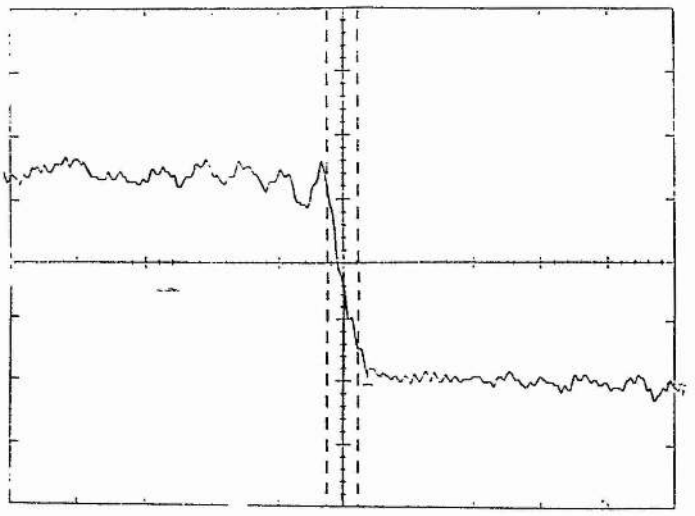

Fig 7.3.1 :- Input pulse to the nonlinear magnetic and dielectric pulse sharpening line (30kV, 50ns/div).

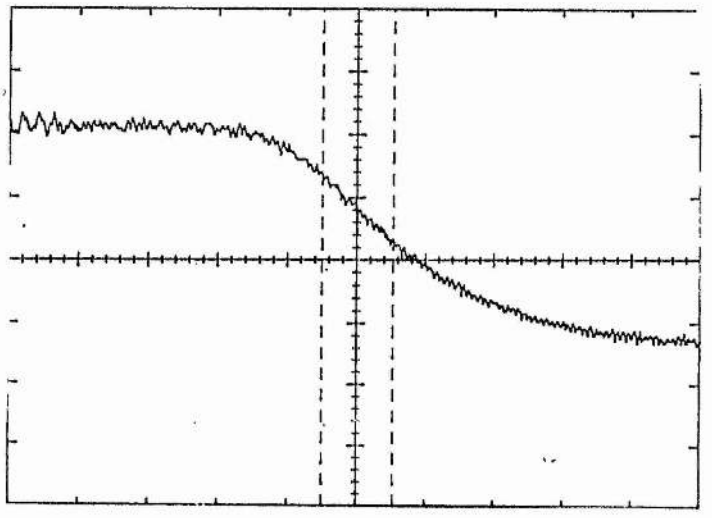

Fig 7.3.2 :- The corresponding output pulse produced at a 30 Ω load (30kV pulse amplitude, 50ns/div).

This experiment, which was conducted essentially as a "proof of principle" excercise some years ago, is now being extended under a new research programme dedicated to developing extremely fast, distributed dielectric pulse sharpening lines. This research is currently characterising a number of different dielectrics to identify those that have the largest nonlinearity and least loss and preparations being made to examine whether certain gases and polar liquids such as CS_2 [10] can be used to scale the technique to the MV level.

Probably the most interesting pulse sharpening line that has been developed so far is the self-sharpening Blumlein circuit (SSBC). It can both generate and sharpen a voltage pulse and is constructed by winding the inductors onto magnetic cores. Figure 7.3.4 shows a circuit diagram of a SSBC that was constructed for the SPI. It consisted of a single CX 1685 hydrogen thyratron and a 20LC section Blumlein circuit constructed from 2.15nF strontium titanate"linear" capacitors and saturable inductors. The inductors, which were made using Trans-Tech. 4800 magnetic material, had a unsaturated and saturated inductance of 344nH and 78nH respectively. The circuit was operated at 30kV and operated into a 12.6Ω load, that is, twice the saturated line impedance.

Figures 7.3.5 shows the current pulse produced by this circuit and it is useful to compare this with the one produced by the same line without the cores, shown in figure 7.3.6. Note that (i) the risetime of the output pulse is line limited to about 20ns, some 70ns faster than that produced by the "nonmagnetic line" (ii) the FWHM and the fall time has also been improved (ii) the amplitude is reduced from 30kV to 27kV because of hysteresis loss.

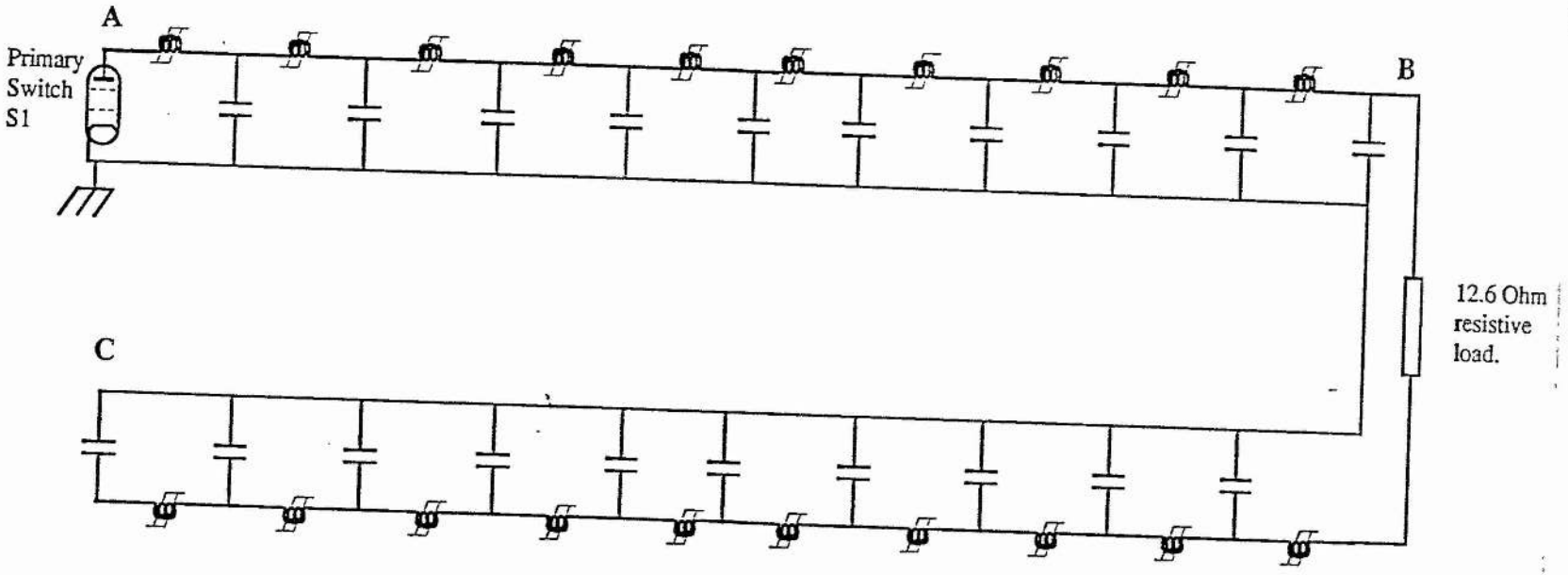

Fig 7.3.4 : Circuit diagram of the Self-Sharpening Blumlein Circuit. The primary switch, S1, was a CX 1685 thyratron and the capacitors, which were constructed from strontium titante, had a capacitance of 2.15nF. Each inductor had an unsaturated and saturated inductance of 334nH and 79nH respectively.

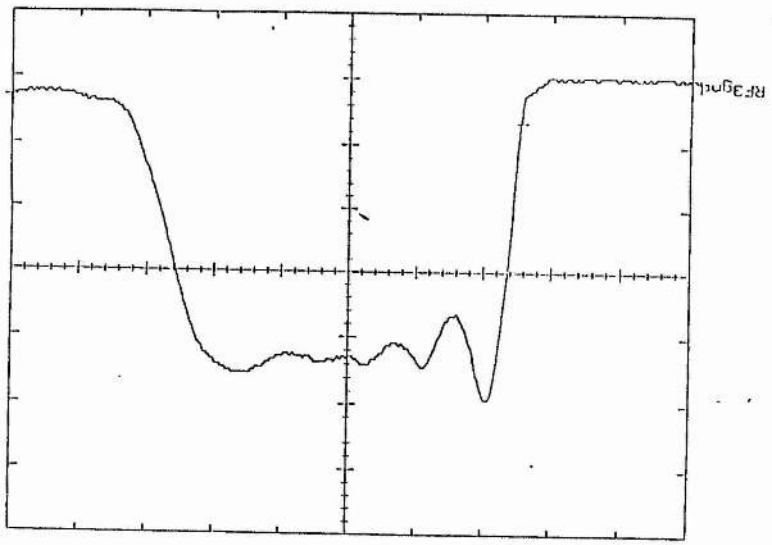

Fig 7.3.5 :- The output pulse from the SSBC into a 12.6Ω resistive load. Amplitude 30kV, time base 50ns/div.

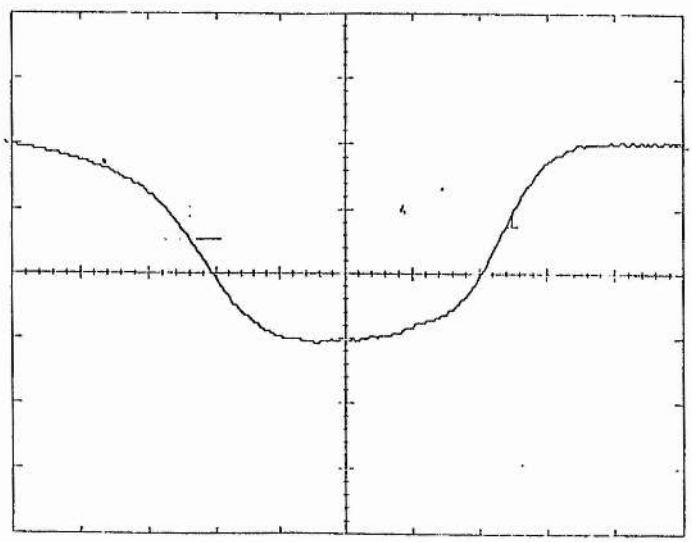

Fig 7.3.6 :- The output produced from the same line without magnetic cores. Amplitude 27kV, time base 50ns/div.

These results have suggested that the SSBC might be an attractive way to drive a TLT because it eliminates the need for a separate pulse generator and pulse sharpening circuit. It might also be possible to develop self-sharpening circuits that can produce fast, high quality voltage waveforms with risetimes limited by the natural bandwidth of the line, irrespective of the switch being used.

7.4. Concluding remarks.

This thesis has described the development of the TLT pulsed power supply. It should be capable of producing good quality, fast risetime pulses at high repetition-rates, although this performance level has yet to be demonstrated because of the limitations of commercially available HV equipment. It is thought that the development of the multi-parallel thyratron switch and the nonlinear dielectric pulse sharpening line may soon make this possible, in which case the TLT may prove to be an effective means of generating high peak and average powers for a number of devices, such as laser modulators, e-beam and microwave generators.

References.

1). A.Brown. Ph.D Thesis. Univ. St. Andrews, (1988).

2). EEV Data Book ; EEV Ltd, Chelmsford England.

3). Alrad Instrum. Technical data. A.L.E. Systems, Inc. 150 Holmer Avenue, Ashland, Ma 01721, USA.

4). N.C.Jaitly et al.; Proc. Power Modulator Symp. (1988).

5). D.Lewis ; "Research in Ceramic Composites at NRL". Nav. Res. Rev. (USA), Vol. 42, No.1, p18 - 27, (1990).

6). A.R.Hyde ; Mater. Des. (UK), Vol 11, No. 1, Feb. (1990).

7). M.J. Akdulla et al ; IEEE Trans. Elect. Insul. Vol 25., No.3, pp 605-610, June, (1990).

8). J.Armstrong ; Phys. Rev. Vol 127, p1918, (1962).

9). A.Yariv ; "Optical Electronics". Ch.5. CBS College Publishing, New York. (1985).

10). J.Armstrong ; Phys. Rev. Vol 127, p1918, (1962).

APPENDIX A.

A.1. Equivalent Circuit Analysis

To analyse TLTs it is necessary to approximate the distributed circuit elements with lumped parameter equivalents. Once this has been done the resulting circuit can give an alternative insight into how the TLT works, allow it to be to be modelled on computer using the network analysis programmes Microcap or Spice and enable the relevant network equations to be solved and the corresponding transfer function to be derived. As will be seen, these functions quickly become complicated for higher order TLTs (i.e for N>2) so it is necessary it make a number of approximations in order to obtain a General Gain Equation.

A.2. The 2-stage TLT.

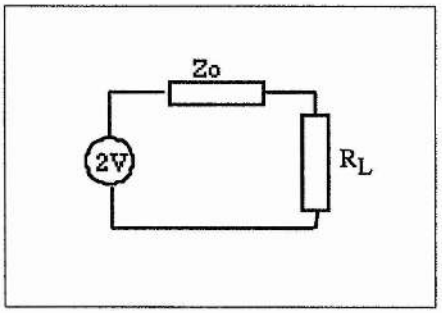

Fig A.2.1:- Equivalent circuit of a transmission line of characteristic impedance Z_0, terminated by a resistive load R_L.

The starting point and basic "building block" circuit in the TLT equivalent circuit is shown in figure A.2.1. This is the equivalent circuit of a simple transmission line of characteristic impedance Z_0 terminated by a resistive load R_L.

The equivalent circuit of the two stage TLT is obtained by simply adding two such circuits in series and terminating them with a load impedance Z_3. Loss components corresponding to the secondary mode impedance are included by placing a shunt resistance, Z_2, and an inductance, L, at the output of the 1st stage (see figure A.2.2).

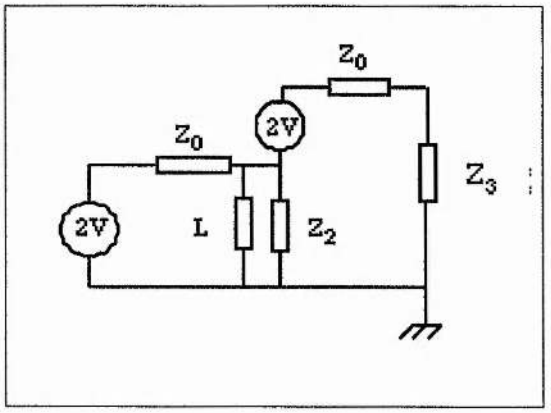

Fig A.2.2 :- Equivalent circuit for a 2-Stage TLT connected to a resistive load, Z_3

An expression for the output waveform for the 2-stage TLT follows directly from the equivalent circuit using Laplace Transforms. This is given below :-

$$V(t) = 2VZ_3\left[\frac{1}{(Z_0 + Z_3)} + \exp(-at)\left(\frac{(Z_0 + 2Z_2)}{Z_0Z_2 + (Z_0 + Z_2)(Z_0 + Z_3)} - \frac{1}{(Z_0 + Z_3)}\right)\right]$$

$$a = \frac{Z_0Z_2(Z_0 + Z_3)}{L[Z_0Z_2 + (Z_0 + Z_3)(Z_0 + Z_2)]} \qquad \text{equation A.2.1.}$$

In this equation Z_0 is the characteristic impedance of the primary transmission lines, Z_2 the secondary mode impedance, Z_3 the impedance of the load, L the isolating inductance of the second cable and the time, t. T=0 is taken to be when the voltage first appears across the load.

This equation can be simplified if it is assumed that the TLT has been wound mutually or magnetically (because then L and Z_2 can be approximated to open-circuits) and if it is evaluated at t=0. This gives :-

$$V_{out} = \frac{2VZ_3(Z_0 + 2Z_2)}{(Z_0 + Z_2 + Z_3)(Z_0 + Z_2) - Z_2^2} \qquad \text{A.2.2.}$$

This is called the initial gain equation because it allows the value of V_{out}/V to be calculated at the start of the pulse. It is useful as a design formula because the secondary mode impedance can be estimated using the formula for the characteristic impedance, Z_2, of a single cable above a ground plane, i.e :-

$$Z_2 = 138 \log D / d^* . \qquad \text{A.2.3.}$$

This equation is applicable if d<<D, where d is the diameter of the cable and D its height above the ground plane.

For coaxial cable used in the experiments in Chapter 2 d=8mm, D = 10 cm and Z_2 is 150Ω. This varies little irrespective of the position of the cable because of the logarithmic term.

To demonstrate the accuracy of equation A.2.2, consider the case of the two stage TLT discussed in section 2.2. With the values of Z_0 = 50Ω, Z_2 = 150Ω and Z_3 = 100Ω, the equation gives an expected gain of 1.86. This is in close agreement with 1.83 which was obtained experimentally.

A.3. Higher order TLTs.

The equivalent circuit of higher order TLTs can be obtained from the previous one by adding additional transmission line equivalent circuits in series (see Chadrow[1]). As an example, consider the equivalent circuit for the 4-stage TLT of section 2.3 (see figure A.3.1).

---

* Radio Data Reference Book, G.R. Jessop. RSGB Publication, London (1972).

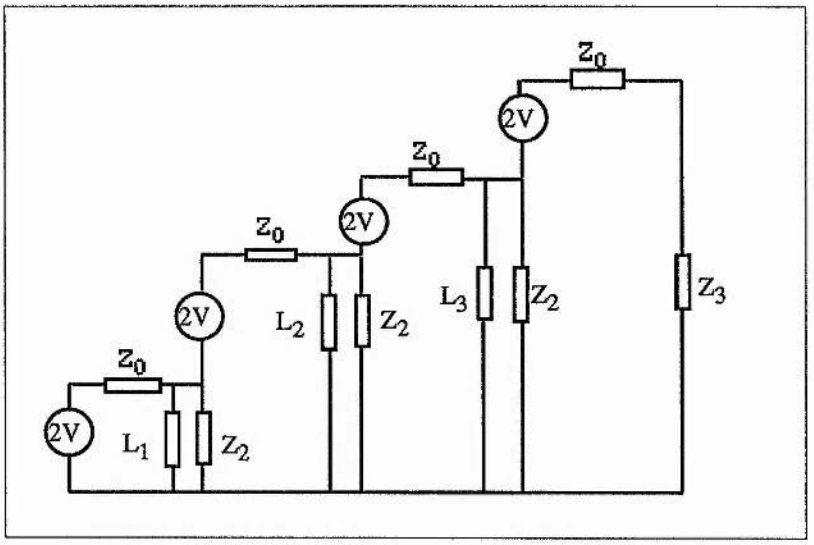

Fig A.3.1 :- The complete equivalent circuit for a four-stage TLT.

Again, if the design of the TLT satisfies the criterion :-

$$L / R = 10t_p$$

at each stage, then the initial gain equation can be shown to be given by :-

$$V_{out} = \frac{2VZ_3\,(Z_0 + 2Z_2)(Z_0^2 + 4Z_0Z_2 + 2Z_2^2)}{a_1\,((\,Z_0 + Z_2 + Z_3) - a_2Z_2^2\,)} \qquad \text{A.3.1.}$$

where $a_1 = (Z_0^3 + 5Z_0^2Z_2 + 6Z_0Z_2^2 + Z_2^3)$

and $a_2 = ((Z_0 + 2Z_2)\,(Z_0+Z_2) - Z_2^2)$.

where the symbols have their previously defined meanings.

This equation has been used to obtain an estimate of the SM impedance for the 4-stage TLT circuits discussed in section 2.3. These estimates are 350Ω for the mutually coupled TLT and 2.3kΩ for the magnetically isolated system. The higher value for the magnetically isolated TLT explains why its performance was superior.

A.4. The General Gain Equation (GGE).

While equations A.2.2 and A.3.1 give the value of the initial gain of a 2 and 4-stage TLT respectively, they are too specific to be of any real practical use. What is required is a general gain equation that can be used to estimate the initial gain of any TLT system of arbitrary design, or one that can be used to estimate the number of stages required to produce a specified gain using a TLT constructed with transmission lines with a characteristic impedance of Z_0.

Such an equation has been derived partly from a modified open circuit TLT gain equation originally published by Lewis and Wells[2] and partly by solving the equivalent circuit of a N-stage system*. The General Gain Equation (GGE) takes the form of a Thevenin equivalent circuit that is simpler than the ones described previously (see figure A.4.1).

---

* The details of this derivation can be found in Appendix B.

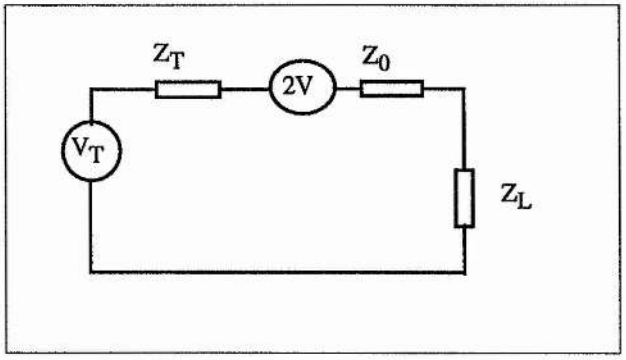

Fig A.4.1 :- Thevenin equivalent Circuit for a General TLT of order N.

The value of the Thevenin voltage source and equivalent resistance are given by the following equations :-

$$V_{out} = \frac{(V_T + 2V)\, Z_L}{Z_L + Z_T + Z_0} \qquad \text{A.4.1}$$

where :-

$$V_T = \frac{4\,VZ_2}{(\beta+1)Z_0} \; \frac{1 - \alpha^{2n-2}}{1 + \alpha^{2n-1}}$$

$$Z_T = \frac{2\,Z_2}{(\beta+1)} \; \frac{1 - \alpha^{2n-2}}{1 + \alpha^{2n-1}}$$

and

$$\alpha = \frac{(\beta - 1)}{(\beta + 1)} \quad \text{and} \quad \beta = \left[1 + \frac{4Z_2}{Z_0}\right]^{1/2}$$

The equivalent circuit of the 2 and 4-stage TLTs described in chapter 2 are shown in figure A.4.2.

When the GGE equation was derived it was assumed that the value of the SM impedance in the TLT, Z_2, remains constant for the first N-1 stages. Whilst this assumption does give fairly accurate estimates of voltage gain, a more detailed analysis of the effect of parasitic impedances on both the gain and pulse distortion has been made by Chadrow[1]. When a more rigorous analysis of a TLT is required this reference should be consulted.

The GGE is, however, sufficiently accurate for most design purposes. It also shows that the gain of a TLT is limited by the shunting effect of the secondary mode. This limit can be calculated using equation A.4.1 by letting N tend to infinity. This gives :-

$$\text{Gain limit} = 2 + [4\,\xi/(\beta+1)]. \qquad \text{A.4.2.}$$

Figure A.4.3 shows this equation plotted as a function of N for three TLTs with values of Z_0 of 200Ω, 50Ω and 10Ω and a secondary mode impedance, Z_2, of 500Ω. Note that a 10-stage device will have a gain of 3.55, 5.4 and 10 respectively. This is because the shunting effect of the SM is less for lower impedance transmission lines. This implies that (i) higher efficiencies can be obtained from lower impedance TLTs and (ii) $Z_2/Z_0 = \xi$ can be used as a measure of how effectively the SM is suppressed. In short, the most efficient TLTs are low impedance ones with a physical construction that keeps Z_2 as high as possible.

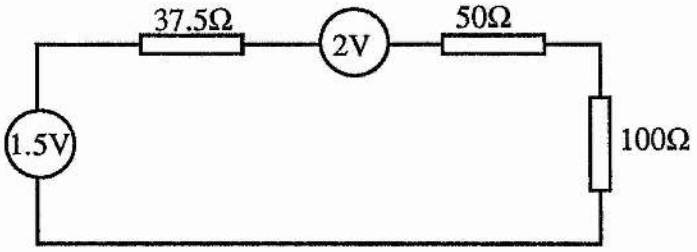

The 2-stage TLT

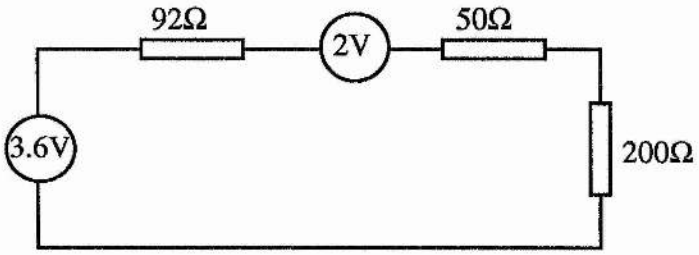

The mutually wound 4-stage TLT

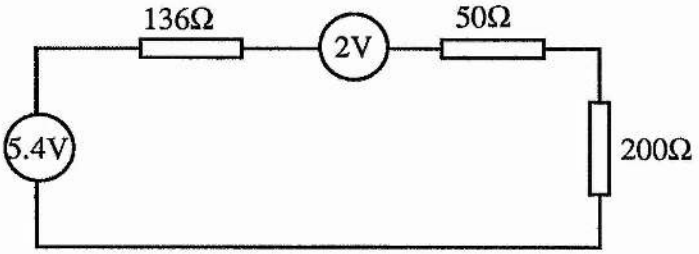

The magnetically isolated 4-stage TLT.

Fig A.4.2 :- Thevenin Equivalent circuits of the 2 and 4-stageTLTs.

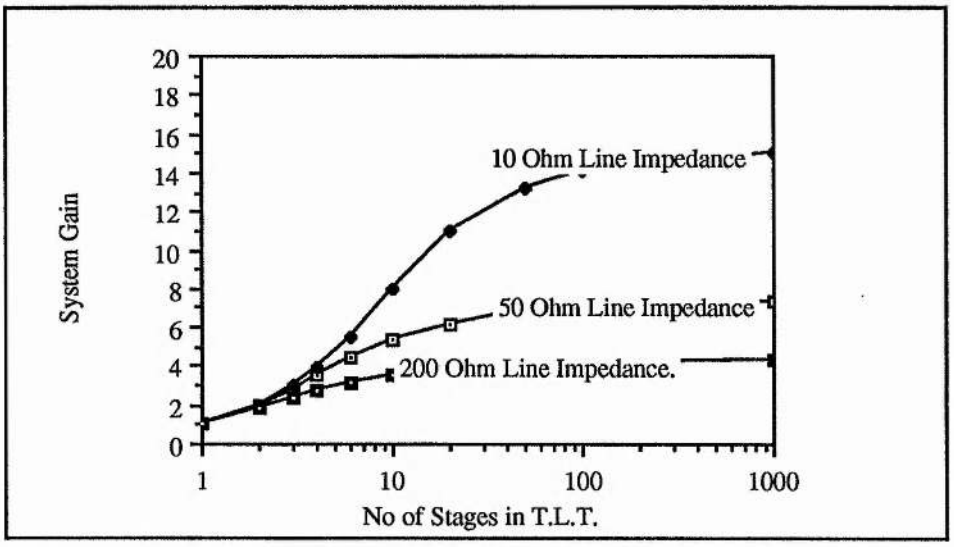

Fig A.4.3 :- TLT Gain vs No. of stages for three TLT systems each with a different transmission line impedance.

References

1). A.M.Chadrow ; "The Time Isolation High Voltage Impulse Generator". Proc. IEEE, pp. 1082 - 1084, July, (1975).

2).T.A.D.Lewis and F.H.Wells ; " Millimicrosecond Pulse Techinques", London, Pergamon, 1959, Ch.3, pp. 109 -111.

APPENDIX B.

B.1. Transfer Function of a Ladder Network.

To determine the general Transfer Function of a Ladder Network, consider the circuit shown in figure B.1. This can be solved by first applying Kirchoff's laws. These give : -

$$i_n = i_{n+1} + I_{n+1} \qquad \text{B.1.1.}$$

and

$$\frac{V_n - V_{n+1}}{Z_1} = \frac{V_{n+1} - V_{n+2}}{Z_1} + \frac{V_{n+1}}{Z_2} \qquad \text{B.1.2.}$$

for n = 1, 2, 3 ..... N-2.

These equations can be used to develop the difference equation B.1.3 :-

$$\left\{ E^2 - \left\{ 2 + \frac{Z_1}{Z_2} \right\} E + 1 \right\} V_n = 0 \qquad \text{B.1.3.}$$

To obtain the required solution, this equation must be solved subject to the boundary conditions :-

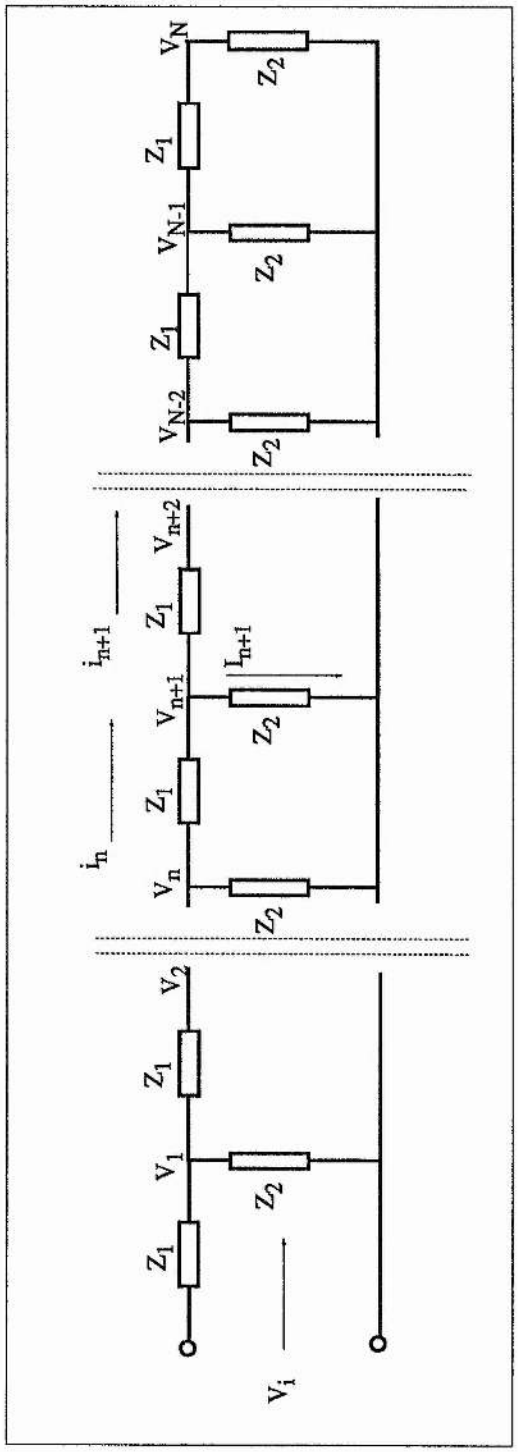

Fig. B.1 :- General Ladder Network. For a Transmission line Z_1=sL and Z_2 = 1/sC.

$$V_0 = V_i \qquad \text{B.1.4.}$$

and

$$V_n = V_{N-1}\frac{Z_2}{Z_1 + Z_2} \qquad \text{B.1.5.}$$

To simplify the mathematics it is convenient to make the following change in variables:-

$$2 + \frac{Z_1}{Z_2} = 2\lambda \quad \text{i.e.} \quad \lambda = 1 + \frac{Z_1}{2Z_2}$$

The Characteristic Equation then becomes :-

$$M^2 - 2\lambda M + 1 = 0 \qquad \text{B.1.6.}$$

with roots :-

$$M_1, M_2, = \lambda \pm [\lambda^2 - 1] \qquad \text{B.1.7.}$$

Assuming M_1 and M_2 to be real and unequal the solution to B.1.3 is :-

$$V_n = A\, M_1^n + B\, M_2^n. \qquad \text{B.1.8.}$$

Now, using the change of variable :-

$$\lambda = \frac{\beta^2 + 1}{\beta^2 - 1}$$

M_1 and M_2 can be shown to be equal to :-

$$M_1 = \frac{\beta + 1}{\beta - 1} \qquad \text{and} \qquad M_2 = \frac{\beta - 1}{\beta + 1}$$

Equation B.1.8 therefore becomes :-

$$V_n = A \left(\frac{\beta + 1}{\beta - 1}\right)^n + B \left(\frac{\beta - 1}{\beta + 1}\right)^n \qquad \text{B.1.9.}$$

A and B can be determined by substituting the Boundary conditions into B.1.9. This gives :-

$$V_n = V_i \left[\Phi^n \left\{ \frac{(\beta - 1)^{2n+1}}{(\beta + 1)^{2n+1} + (\beta + 1)^{2n+1}} \right\} \Sigma^n \left\{ \frac{(\beta + 1)^{2n+1}}{(\beta + 1)^{2n+1} + (\beta - 1)^{2n+1}} \right\} \right]$$

where $\Phi = \left(\frac{\beta+1}{\beta-1}\right)$ and $\Sigma = \left(\frac{\beta - 1}{\beta + 1}\right)$

$$T(s) = \frac{V_N}{V_i} = \frac{2\beta \dfrac{(\beta-1)^n}{(\beta+1)^{n+1}}}{1 + \left(\dfrac{\beta-1}{\beta+1}\right)^{2n+1}} \qquad \text{B.1.10}$$

This is the Transfer Function of the ladder network shown in figure B.1.

B.2. Derivation of the Thevenin Equivalent Voltage in the GGE.

The derivation for the GGE of the TLT begins with equation B.1.10 and the TLT equivalent circuit, shown in figure B.2.

Again, using Kirchoff's law, $i_n = i_{n+1} + I_{n+1}$ and :-

$$\frac{V_n + 2V - V_{n+1}}{Z_1} = \frac{V_{n+1} + 2V - V_{n+2}}{Z_1} + \frac{V_{n+1}}{Z_2} \qquad \text{B.2.1.}$$

the difference equation is obtained in the usual way. This is :-

$$V_{n+2} - V_{n+1}\left[2 + \frac{Z_1}{Z_2}\right] + V_n = 0 \qquad \text{B.2.2.}$$

for n = 1, 2, 3 ..... N-2.

As before, the characteristic equation is :-

$$\left[E^2 - \left[2 + \frac{Z_1}{Z_2}\right] E + 1\right] V_n = 0 \qquad \text{B.2.3.}$$

but this time the initial conditions are :-

$$V_0 = 0 \qquad \text{B.2.4.}$$

and

$$V_N = (V_{N-1} + 2V) \frac{Z_2}{Z_1 + Z_2}. \qquad \text{B.2.5.}$$

As in the previous derivation :-

$$V_n = AM_1^n + BM_2^n$$

$$\text{where} \quad M_1 = \frac{\beta + 1}{\beta - 1} \quad \text{and} \quad M_2 = \frac{\beta - 1}{\beta + 1}$$

and values for A and B :-

$$A = \frac{V_i (\beta - 1)^{N+1} (\beta + 1)^{N+1}}{(\beta + 1)^{2N+1} + (\beta - 1)^{2N+1}} \qquad \text{B.2.6.}$$

$$B = \frac{- V_i (\beta + 1)^{N+1} (\beta + 1)^{N+1}}{(\beta + 1)^{2N+1} + (\beta - 1)^{2N+1}} \qquad \text{B.2.7.}$$

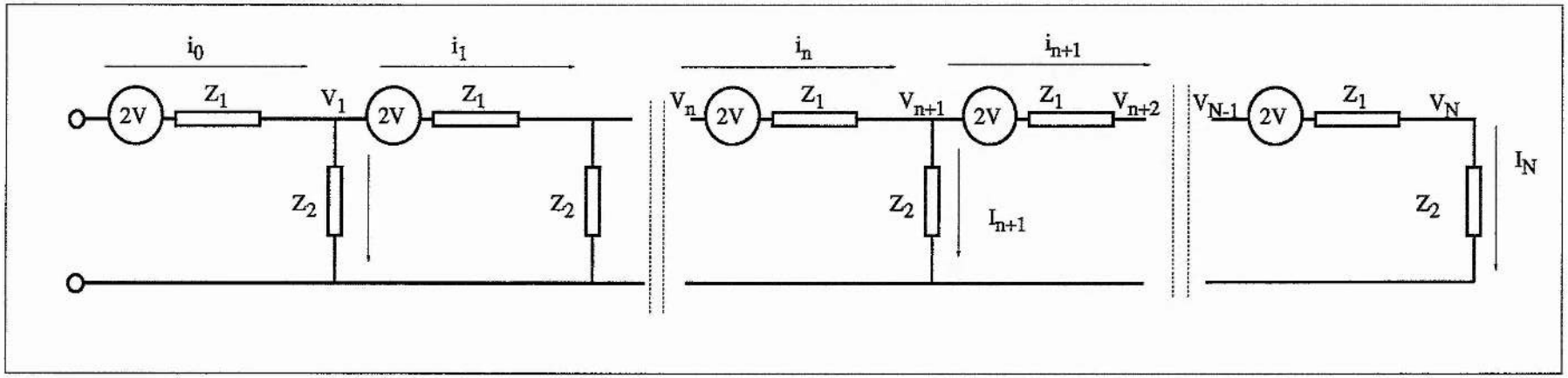

Fig B.2 :- General TLT Equivalent Circuit.

The GGE is then obtained by substituting A and B back into the original equation which, after simplifying gives :-

$$V_n = \frac{4VZ_2}{(\beta+1)Z_1} \quad \frac{1 - \alpha^{2n}}{1 - \alpha^{2n+1}} \qquad \text{B.2.8.}$$

where :-

$$\alpha = \frac{\beta - 1}{\beta + 1}$$

This is the form of the Thevenin Equivalent voltage in GGE equation given in chapter 2.

APPENDIX C.

Details of the CX 1685 Hydrogen Thyratron* .

The data to be read in conjunction with the Hydrogen Thyratron Preamble.

ABRIDGED DATA

Deuterium-filled, flange mounted tetrode thyratron featuring low jitter and low anode delay time drift. It is designed for applications requiring high rate of rise of current and a high ampere-second capability. It is suitable for use in the low inductance circuits associated with CO_2 lasers. It has a rugged reservoir, capable of being operated from a separate heater supply, and an internal X-ray shield to minimize X-ray emission from the region of the anode.

The reservoir heater voltage can be adjusted to a value consistent with anode voltage hold-off in order to achieve the fastest rate of rise of current possible from the tube in the circuit.

Peak forward anode voltage	40	kV max
Peak anode current	5.0	kA max
Average anode current	0.6	A max
Rate of rise of current	50	kA/μs max
Pulse repetition rate	50	p.p.s. max

GENERAL

Electrical

Cathode (connected internally to one end of heater)	oxide coated	
Cathode heater voltage	6.8 ± 5%	V
Cathode heater current	12	A
Reservoir heater voltage (see note 1)	5.0 to 7.0	V
Reservoir heater current at 6.3 V	2.0	A
Tube heating time (minimum)	5.0	min

Mechanical

Seated height	9.562 inches (242.9 mm) max	★
Clearance required below mounting flange	1.250 inches (31.75 mm) min	
Overall diameter (mounting flange)	3.500 inches (88.9 mm) nom	
Net weight	1 pound (450 g) approx	
Mounting position (see note 2)	any	
Tube connections	see outline	
Top cap connector (see note 3)	MA359 or MA360A	

★ Indicates a change.

* Extract from EEV Data book, EEV, Chelmsford, England.

MAXIMUM AND MINIMUM RATINGS – continued

	Min	Max	
Grid 1 – D.C. Primed (See note 13)			
D.C. grid 1 unloaded priming voltage	75	150	V
D.C. grid 1 priming current	50	100	mA
Heaters			
Cathode heater voltage	6.8 ± 5%		V
Reservoir heater voltage	5.0	7.0	V
Tube heating time	5.0	–	min
Environmental			
Ambient temperature	−50	+90	°C
Altitude	–	10 000	ft
	–	3	km

CHARACTERISTICS

	Min	Typical	Max	
Critical d.c. anode voltage for conduction (see note 14)	–	0.3	1.0	kV
Anode delay time (see notes 14 and 15)	–	0.1	0.25	µs
Anode delay time drift (see notes 14 and 16)	–	20	50	ns
Time jitter (see note 14)	–	1.0	5.0	ns
Cathode heater current (at 6.8 V)	9.5	12	14.5	A
Reservoir heater current (at 6.3 V)	1.5	2.0	2.5	A

RATINGS FOR SINGLE SHOT OR CROWBAR SERVICE (See note 13)

D.C. forward anode voltage	30	kV max
Peak anode current	5.0	kA max
Product of peak current and pulse duration	0.3	A.s max
Repetition frequency	1 pulse per 10s	max

Cooling (See note 4) . . . . . natural or forced-air

PULSE LASER SERVICE

MAXIMUM AND MINIMUM RATINGS (Absolute values)

	Min	Max	
Anode			
Peak forward anode voltage (see note 5)	–	40	kV
Peak inverse anode voltage (see note 6)	–	25	kV
Peak anode current	–	5.0	kA
Average anode current	–	0.6	A
Rate of rise of anode current (see note 7)	–	50	kA/μs
Pulse repetition rate	–	50	p.p.s.
Grid 2 (Voltage driven)			
Unloaded grid 2 drive pulse voltage (see note 8)	600	2000	V
Grid 2 pulse duration	0.5	–	μs
Rate of rise of grid 2 pulse (see notes 7 and 9)	1.0	–	kV/μs
Grid 2 pulse delay (see note 10)	0.2	3.0	μs
Peak inverse grid 2 voltage	–	450	V
Loaded grid 2 bias voltage	−100	−300	V
Forward impedance of grid 2 drive circuit (see note 11)	50	500	Ω
Grid 1 – Pulsed (Current driven)			
Peak grid 1 drive current	1.0	10	A
Unloaded grid 1 drive pulse voltage (see note 8)	300	2000	V
Grid 1 pulse duration	2.0	–	μs
Rate of rise of grid 1 pulse	200	–	V/μs
Peak inverse grid 1 voltage	–	450	V
Loaded grid 1 bias voltage			see note 12

NOTES

1. The reservoir heater supply must be obtained either from the cathode heater supply or if a separate supply is used it must be decoupled with suitable capacitors (for example a 1 μF capacitor in parallel with a low inductance 1000 pF capacitor) to avoid damage to the reservoir. The nominal reservoir voltage is 6.3 V; for maximum rate of rise of current the reservoir voltage should be set to the highest level compatible with the tube hold-off voltage being maintained.

   Permanent damage to the tube will result if it is operated below the minimum recommended reservoir voltage.
2. The tube must be fitted by means of its mounting flange.
3. A large area anode connector, EEV type MA360A, is recommended for high average currents.
4. Cooling is necessary under conditions of high voltage and high anode dissipation in order to avoid puncture of the glass and consequent loss of voltage hold-off.
5. The maximum permissible peak forward voltage for instantaneous starting is 30 kV and there must be no overshoot.
6. The peak inverse voltage including spike must not exceed 10 kV for the first 25 μs after the anode pulse. Amplitude and rate of rise of inverse voltage contribute greatly to tube dissipation and electrode damage; if these are not minimized in the circuit, tube life will be shortened considerably. The aim should be for an inverse voltage of 3–5 kV peak with a rise time of not less than 0.5 μs.
7. This rate of rise refers to that part of the leading edge of the pulse between 10% and 90% of the pulse amplitude. The maximum rate of rise of current obtained will depend on the circuit parameters.
8. Measured with respect to cathode.
9. A lower rate of rise may be used, but this may result in the anode delay time, delay time drift and jitter exceeding the limits quoted.
10. The last 0.25 μs of the top of the grid 1 pulse must overlap the corresponding first 0.25 μs of the top of the delayed grid 2 pulse.
11. During the drive pulse period and during recovery when the current flow is reversed.

12. D.C. negative bias voltages must not be applied to grid 1. The potential of grid 1 may vary between −10 V and +5 V with respect to cathode potential during the period between the completion of recovery and the commencement of the succeeding grid pulse.
13. When d.c. priming is used on grid 1, a negative bias of 100 V to 200 V must be applied to grid 2 to ensure anode voltage hold-off. D.C. priming is recommended for crowbar service.
14. Typical figures are obtained on test using conditions of minimum grid drive. Improved performance can be expected by increasing grid drive.
15. The time interval between the instant at which the rising unloaded grid 2 pulse reaches 25% of its pulse amplitude and the instant when anode conduction takes place.
16. The drift in delay time over a period from 10 seconds to 10 minutes after reaching full voltage.

HEALTH AND SAFETY HAZARDS

EEV hydrogen thyratrons are safe to handle and operate, provided that the relevant precautions stated herein are observed. EEV does not accept responsibility for damage or injury resulting from the use of electronic devices it produces. Equipment manufacturers and users must ensure that adequate precautions are taken. Appropriate warning labels and notices must be provided on equipments incorporating EEV devices and in operating manuals.

High Voltage

Equipment must be designed so that personnel cannot come into contact with high voltage circuits. All high voltage circuits and terminals must be enclosed and fail-safe interlock switches must be fitted to disconnect the primary power supply and discharge all high voltage capacitors and other stored charges before allowing access. Interlock switches must not be bypassed to allow operation with access doors open.

X-Ray Radiation

All high voltage devices produce X-rays during operation and may require shielding. The X-ray radiation from hydrogen thyratrons is usually reduced to a safe level by enclosing the equipment with metal panels.

OUTLINE

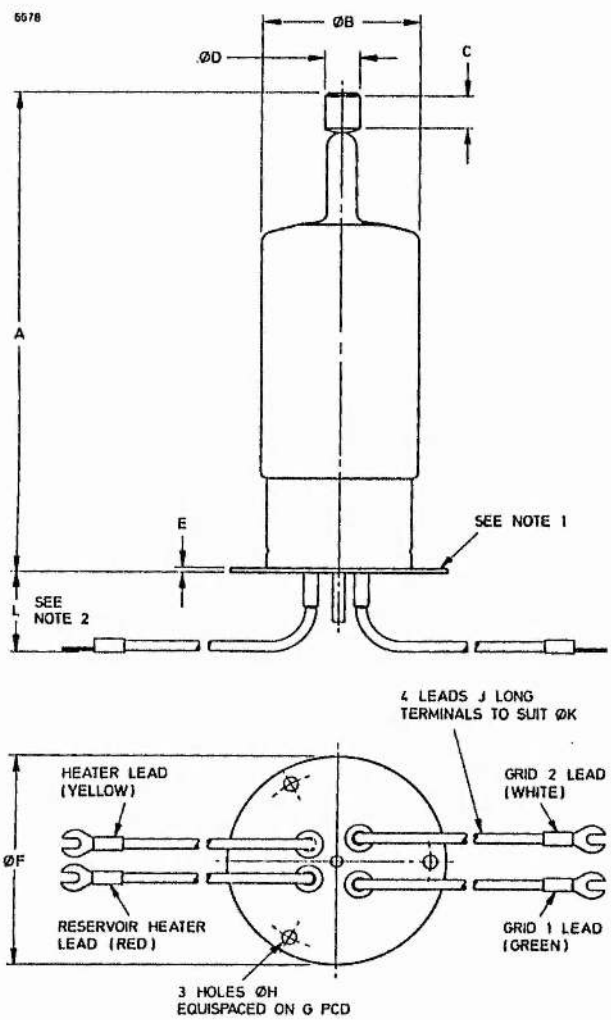
5678
ØB
ØD
C
A
E
SEE NOTE 1
L
SEE NOTE 2
4 LEADS J LONG
TERMINALS TO SUIT ØK
HEATER LEAD
(YELLOW)
GRID 2 LEAD
(WHITE)
ØF
RESERVOIR HEATER
LEAD (RED)
GRID 1 LEAD
(GREEN)
3 HOLES ØH
EQUISPACED ON G PCD

Outline Dimensions (All dimensions without limits are nominal)

Ref	Inches	Millimetres	
A	9.312 ± 0.250	236.53± 6.35	★
B	2.562 max	65.07 max	
C	0.500 min	12.70 min	
D	0.566 ± 0.007	14.38 ± 0.18	
E	0.063	1.60	
F	3.500	88.90	
G	3.000	76.20	
H*	0.197	5.00	
J	6.000 min	152.4 min	
K*	0.236	6.00	
L	1.250 min	31.75 min	

Millimetre dimensions have been derived from inches except where indicated thus *.

Outline Notes

1. The mounting flange is the connection for the cathode, cathode heater return and reservoir heater return.
2. A minimum clearance of 1.250 inches (31.75 mm) must be allowed below the mounting flange.

APPENDIX D.

D.1. The Pulse Forming Line (PFL).

A PFL is a single length of transmission line of characteristic impedance, Z_0, that is charged to a voltage V_0 and then discharged across a load, R_L, by closing a switch (see figure D.1).

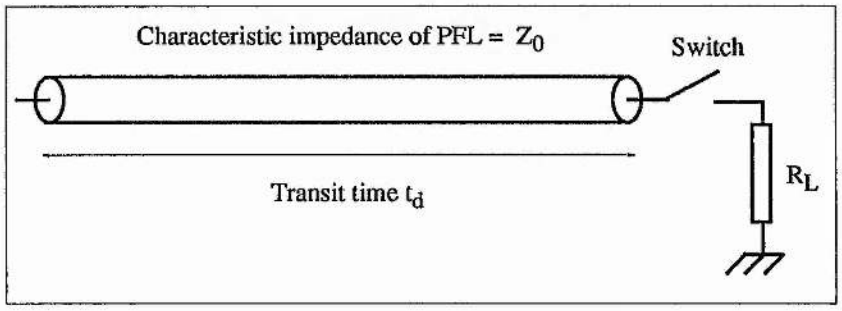

Fig. D.1 :- Diagram of a coaxial cable PFL.

The voltage across the load, V_{out}, can be determined using a lattice diagram or reflection chart. This is a graph that shows the line voltage as a function of time (see fig D.2) :-

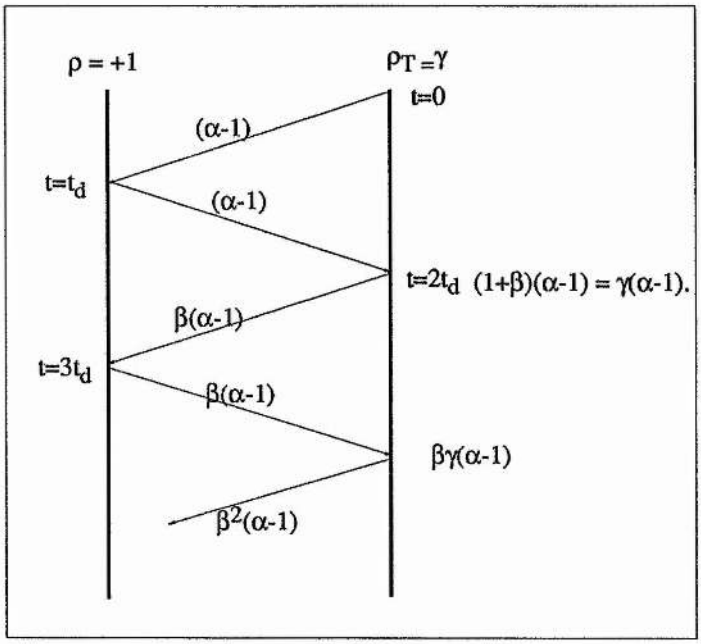

Figure D.2 :- Lattice diagram for a general PFL circuit.

Summing the terms on the RHS gives the voltage across the load, V_{out} :-

$$V_{out} = V_0 [\ \alpha + (\alpha-1)\gamma\ (1 + \beta + \beta^2 + ...)] \qquad D.1.$$

where β is the reflection coefficient from the line to the load :-

$$\beta = \frac{R_L - Z_0}{R_L + Z_0} \qquad D.2.$$

α is :-

$$\alpha = \frac{R_L}{R_L + Z_0} \qquad D.3.$$

and $\gamma = 2\alpha$.

Note that each successive term in equation D.1 is delayed in time by t_d because this is the time it takes for a voltage wave to return to the load after it has propagated twice the length of the line; note also that V_{out} can take on three distinct forms depending on the value of R_L. For example :-

1). If $R_L > Z_0$ then the line is overmatched and V_{out} has an initial amplitude αV_0. This decreases in a series of discrete steps, each lasting for the two way transit time of the line, $2t_d$. The polarity of these steps is always the same as the charge voltage.

2). If if $R_L < Z_0$ then the line is undermatched and the steps alternate in polarity.

3). If $R_L = Z_0$ then the PFL is matched and a single voltage pulse with a duration $2t_d$ and amplitude $V_0/2$ is produced.

The fact that the nature of the output waveform varies with load impedance is useful because it enables a PFL to be characterised by varying the load impedance and monitoring the output voltage until matched conditions are reached. The characteristic impedance and transit time of the line is then given by R_L and t_d respectively, where $2t_d$ is the duration of the output pulse.

Publications.

1). C.R.Wilson and P.W. Smith ; "Transmission Line Transformers for High Voltage Pulsed Power Generation". Proc. 17th Power Modulator Symposium. Seattle. (1986).

2). C.R.Wilson, A. Erickson and P.W. Smith ; "Transmission Line Transformers for Compact, Repetitive Pulsed Power Generation". Proc 8th IEEE Pulsed Power Conference. (1989).

3). C.R.Wilson, M.M.Turner and P.W.Smith ; "Electromagnetic Shock Wave Generation in a Lumped Element Delay Line Containing Nonlinear Ferroelectric Capacitors". Appl. Phys. Letts. 56(**24**). June (1990).

4). C.R. Wilson, M.M.Turner and P.W.Smith ; "Pulse Sharpening in a Uniform LC Ladder Network Containing Nonlinear Ferroelectric Capacitors". Proc 18th Power Modulator Symposium. San Diego. (1990).

5). C.R. Wilson, M.M.Turner and P.W.Smith ; "Pulse Sharpening in a Uniform LC Ladder Network Containing Nonlinear Ferroelectric Capacitors". IEEE Transactions on Electron Devices.Vol 38, No.**4**, P767. April. (1991).

6). GEC Patent No. 8919814.7. "Dielectric Pulse Sharpening".